View metadata, citation and similar papers at core.ac.uk
brought to you by CORE
provided by Caltech Theses and Dissertations

Control Theoretic Analysis of Autocatalytic Networks in Biology With Applications to Glycolysis

Thesis by

Gentian Buzi

In Partial Fulfillment of the Requirements

for the Degree of

Doctor of Philosophy

California Institute of Technology

Pasadena, California

2010

(Defended August 18, 2009)

© 2010
Gentian Buzi
All Rights Reserved

To my parents

Acknowledgments

I would like to express my deep gratitude and appreciation to my advisor, Professor John Doyle, for his guidance and support. His unique vision and approach to science and engineering have had a profound impact on me. I am very thankful to John for the opportunity and for providing a rich academic environment that helped me mature professionally. My gratitude extends also to the other members of my committee: Professors Richard Murray, Jerry Marsden and Hana El-Samad, for their help, constructive feedback, advice and encouragement.

I would also like to thank Professor Yaser Abu-Mostafa for his invaluable insight in machine learning; Professor Barbara Wold for the opportunity to work with her and learn from her biological intuition and knowledge; Professor Ellen Rothenberg and Elizabeth-Sharon Fung for their help, advice and for introducing me to a new area of biology.

I am very grateful for the many people at Caltech that have made my time here that much more pleasant and fruitful. I would like to thank Andy Lamperski, Dennice Gayme and Ufuk Topcu for their friendship, help, encouragement and the many stimulating discussions; Fiona Chandra for her friendship and the many insights and perspective on glycolysis; Gloria Bain, Wendy McKay and rest of the administrative staff in CDS for their invaluable help; and all the people in CDS for their friendship, patience and support.

I would like to thank my friends and family for the unconditional love and support they have shown me; my friends Jimmy Fung, John Choi, Frederick Balagadde, Amos Anderson, Tim Stranske, Jeremie Vaubaillon, Jonathan Mueller, Sarah Hill, Tania Abou-ezzeddine, Danny Elder and the rest of the TBC family; my grandmother; my

brother Klevis; my sister Suela and my brother-in-law Lenci. A special thank you goes to my wonderful niece Eya for always brightening up my day.

To my parents, Shpresa and Ramadan, I would like to say thank you for your unconditional love, unwavering support, patience, encouragement and the many sleepless nights and sacrifices. I have been truly blessed to have such wonderful and dedicated parents. Mom, dad, I love you and I dedicate this thesis to you.

Finally and most importantly I would like to thank my Lord and Savior Jesus Christ. Through the many ups and downs of graduate student life, it was my relationship with Him that sustained me.

Abstract

Autocatalytic networks (pathways) are a necessary part of core metabolism. In every cell, food and resources are broken down to create energy and components via processes that also require the use of those same components and energy. Indeed at a certain level all biological networks are massively autocatalytic. The simplest and most widely studied autocatalytic network is the glycolytic pathway. This metabolic pathway is used by the cell to produce energy anaerobically (without oxygen) by breaking down glucose. It is probably the most common autocatalytic pathway on the planet, found in every cell of living organisms, from bacteria to humans. Its special autocatalytic structure, like the structure of many similar autocatalytic networks, can lead to instabilities and makes it particularly hard to control.

In this thesis, we study autocatalytic metabolic networks, and specifically glycolysis, to investigate fundamental performance tradeoffs in these network topologies. Using classical linear control theory, we hypothesize that the instabilities in glycolysis, which are exhibited in the form of oscillation are a result of performance tradeoffs that stem from the structure of the pathways and a conservation law mathematically described by a special form of the Bode Sensitivity Integral. We show that the size of the pathway and the consumption of the intermediate metabolites by other processes in the cell adversely affect the performance of the pathway, while reversibility of chemical reactions improves performance. We also establish tight stability bounds for the feedback control gains, which guarantee stability of pathways of arbitrary size and arbitrary parameter values of the intermediate reactions.

In addition changes in the concentration of metabolites and catalyzing enzymes during the lifetime of the cell can perturb the system from the nominal operating point

of the pathway. We address the question of whether the controller can restore the system to normal operating conditions from these perturbations, and the maximum perturbations a cell can sustain before it dies. We investigate effects of such perturbations through the estimation of invariant subsets of the region of attraction around nominal operating conditions (i.e., a measure of the set of perturbations from which the cell recovers). The numerical procedure for estimating the region of attraction is composed of system theoretic characterizations and optimization-based formulations. For large, computationally intractable systems we employ a different technique based on the underlying biological structure, which offers a natural decomposition of the system into a feedback interconnection of two input-output subsystems: a small subsystem with complicating nonlinearities and a large subsystem with simple dynamics. This decomposition simplifies the analysis and leads to analytical construction of Lyapunov functions for a large family of autocatalytic pathways.

The results of our analysis of these autocatalytic networks reveal fundamental tradeoffs between performance and robustness, energy efficiency, evolvability of the pathway, and computational complexity.

Contents

List of Figures

List of Tables

Chapter 1

Introduction

I learned very early the difference between knowing
the name of something and knowing something
Richard Feynman

Metabolism is the collection of chemical reactions that take place in the cell to sustain life. It is comprised of *metabolic reaction networks (pathways)*, which are sequences of chemical reactions usually connected in series. The products of these chemical reactions are called *metabolites*. Metabolism is divided into two categories, catabolism and biosynthesis. Catabolism breaks down complex molecules in food to generate energy and some of the small molecules that the cell uses as building blocks, while biosynthesis uses the energy generated by catabolism to construct the components that make up the cell. The chemical reactions that comprise the metabolic pathways are catalyzed by specialized proteins called *enzymes*, which speed up (catalyze) the reactions [1]. The cell uses these enzymes to regulate (control) the metabolic pathways via two distinct mechanisms, transcriptional regulation and allosteric regulation (Figure 1.1). *Transcriptional regulation* changes the concentration levels of the enzymes by controlling gene expression, thus speeding up or slowing down the corresponding reactions. The slow events of transcription and translation dominate this mechanism making the entire process operate at a slow time-scale. *Allosteric regulation* is the process by which a molecule binds to an enzyme causing the enzyme to change shape and become more effective (activation) or less effective (inhibition).

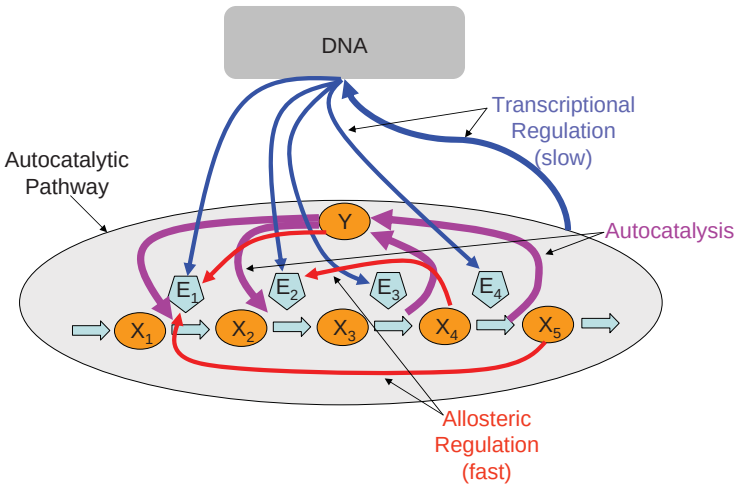

Figure 1.1: The cell regulates a pathway in two basic ways, transcriptional regulation and allosteric regulation of the enzymes. Transcriptional regulation changes the concentration levels of the enzymes by controlling gene expression, thus speeding up or slowing down the corresponding reactions. Allosteric regulation is the process by which a molecule binds to an enzyme causing the enzyme to change shape and become more effective (activation) or less effective (inhibition).

It happens at a much faster time-scale than transcriptional regulation because the effects of binding are immediate.

Some metabolic pathways contain reactions that require the use (consumption) of one of their own products, thus creating a positive feedback loop. Such pathways are called *autocatalytic pathways*. They are very common in biology; indeed at a certain level all biological networks are massively autocatalytic, since in every cell, food and resources are broken down to create energy and components via processes that also require the use of those same components and energy. In addition, these metabolic pathways, as an integral part of the whole cell activity, are also coupled with other networks through their intermediate products which are consumed by other processes in the cell. Many of these pathways contain *reversible reactions* (i.e. both the reaction that converts A to B and the reverse one that converts B to A occur) in addition to the irreversible ones.

The simplest and most widely studied autocatalytic pathway is glycolysis. The cell relies on this metabolic pathway to produce energy anaerobically (without oxygen) by breaking down glucose. It is coupled to other pathways through the provision

of many of its intermediates for the production of amino acids, lipids, nucleotides, and other organic molecules essential to the function of the cell. In glycolysis, the autocatalysis happens when two ATP molecules (energy carriers) are consumed early in the pathway (in this process Hexokinase (HK) and Phosphofructokinase (PFK) act as the catalyzing enzymes). Four ATP molecules are generated later in the pathway, for a net return of two ATP molecules.

Autocatalysis in metabolic pathways, and specifically glycolysis, can cause instability and aggravate control performance [8]. The instability of the glycolytic pathway has been experimentally observed since the 1960s when oscillations of glycolytic intermediates were seen in continuous flow experiments on yeast extracts. Since then, glycolytic oscillations have been studied extensively both experimentally and theoretically [9, 14, 24]. The oscillations appeared when precursors to the PFK catalyzed reaction (or PFK itself) were added to the system [14]. These studies led to the hypothesis that oscillations are caused by PFK activity. The effect of different enzymes on the period and amplitude of these oscillations has been investigated [6, 38] and temperature dependence has also been observed [33]. A nice review of the experimental history of yeast glycolytic oscillations can be found in [31]. Many of the mathematical models developed for glycolysis attempt to capture in detail the full mechanism of glycolysis [18]. These models have high fidelity but result in large models that are not amenable to theoretical analysis and can thus obscure fundamental tradeoffs.

In the present work, we study autocatalytic metabolic pathways, and specifically glycolysis, to investigate fundamental performance tradeoffs in these networks, and the hard limits imposed on performance by autocatalysis. We want to understand the underlying principles behind the set of nominal operating parameters for these networks and if these principles can be generalized to other networks in biology. A second goal is to use these networks as a benchmark to better understand the applicability of many available tools in control and optimization to biological system analysis. In this thesis we study a special case of the metabolic networks pictorially represented in Figure 1.1, specifically the metabolic network with the topology of

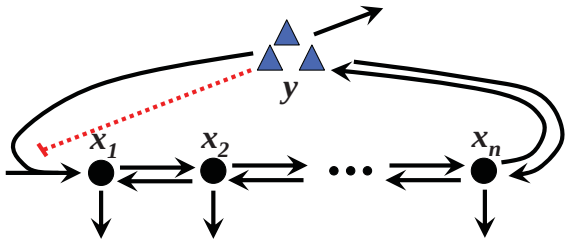

Figure 1.2: The autocatalytic network is composed of a chain of reversible reactions (black arrows) that convert one metabolite x_i to another, ultimately producing $a+b$ copies of the final product y of the pathway (blue triangles, ATP in the case of glycolysis). The pathway also requires the consumption of a copies of the final product y to convert the input of the pathway into the first metabolite x_1. The intermediate metabolites and the final product of the pathway are consumed by other processes in the cell. All the reactions are catalyzed by enzymes. Additionally, the product of the pathway inhibits (dotted red line) the enzyme (PFK in glycolysis) that catalyzes the autocatalytic reaction.

Figure 1.2, with glycolysis serving as a prime example. This network is composed of a chain of reversible reactions that convert one metabolite to another, ultimately producing $a + b$ copies of the final product of the pathway (ATP in the case of glycolysis). The pathway also requires the consumption of a copies of the final product to convert its input into the first metabolite. The intermediate metabolites and the final product of the pathway are used (consumed) by other processes in the cell. All the reactions are catalyzed by enzymes. Additionally, the product of the pathway inhibits the enzyme (PFK in glycolysis) that catalyzes the autocatalytic (first) reaction. The set of these reactions is shown below

$$\begin{array}{lccccccccc} u + ay \overset{f}{\rightharpoonup} & x_1 & \underset{h_2}{\overset{g_1}{\rightleftharpoons}} & x_2 & \underset{h_3}{\overset{g_2}{\rightleftharpoons}} & \cdots & \underset{h_n}{\overset{g_{n-1}}{\rightleftharpoons}} & x_n & \underset{h_y}{\overset{g_n}{\rightleftharpoons}} (a+b)\, y \overset{g_y}{\rightharpoonup} \varphi \\ & \downarrow_{d_1} & & \downarrow_{d_2} & & & & \downarrow_{d_n} & & \\ & \varphi & & \varphi & & & & \varphi & & \end{array} \tag{1.1}$$

where arrows signify a chemical reaction with the rate shown in the superscript (subscript for the reversible reactions) and x_i, for $i = 1, \ldots, n$, are the intermediate metabolites, u is the input, y is the output, and φ is a null state representing the consumption of the reactants by other processes in the cell. The enzymes that catalyze these reactions are not shown. We are interested in the fast allosteric regulation of

the pathway, and assume that at this time-scale the pathway's output is constant.

Biochemical networks with different topologies and different reaction rate constraints have been an object of study for many decades. General results regarding the number of the possible steady states and the convergence properties to these states for certain rather general networks with mass-action kinetics (the so-called networks of deficiency zero and one) have been established [12, 11, 16]. The theory of monotone dynamical systems [36] has proven to be a powerful tool for understanding the behavior of biological systems. Using this theory, certain network topologies have been shown to globally converge to steady states for quite general reaction rates [22]. The theory of monotone systems is directly applicable to topologies that have net positive feedback loops, but might also be useful to study more general systems. For example, the authors of [45] use singularly perturbed monotone systems to show global asymptotic stability for topologies with negative feedback, under certain time-scale assumptions. Cyclic interconnection networks are closer to the topology shown in Figure 1.2 and for these networks a sufficient local stability criterion for cyclic interconnection with inhibition of the first reaction by the end product of the network has been established [39, 43]. These results are extended to prove global asymptotic stability (using passivity of subsystems) if certain criteria are satisfied by the reaction rates [2, 3].

In most cases the difficulty associated with analyzing autocatalytic networks, with the topology and feedback structure of Figure 1.2, is that they do not exhibit such global properties. These networks can have multiple equilibrium points, each with large regions of attraction. The nonlinear nature of the autocatalytic reaction rate makes the analysis of non-local properties, such as estimating the region of attraction, difficult. This nonlinearity is caused by the coupling of positive and negative feedback, which induces many of the interesting properties in these networks. Depending on the feedback gain, the (stable) dynamics near the equilibrium points can be dominated by either positive or negative feedback. The fact that the end product of such networks is consumed by the reaction it controls, implies that the initial response to the regulatory negative feedback will yield the opposite of the desired effect (i.e., an error in the

response will initially increase before it decreases). This property is intrinsic to their structure and makes them inherently difficult to control. We investigate the control structure of these autocatalytic networks with its limitations and benefits, as well as the tradeoffs that arise from both their structure and biologically imposed constraints. We attempt to understand the cause of certain behaviors that are commonly exhibited in real biological pathways and to address the "synthesis" question of why certain feedback gains are chosen.

1.1 Biological Preliminaries

A *chemical reaction* that converts the collection of a_i copies of chemical species X_i, $1 \leq i \leq n$ into the collection of b_j copies of chemical species Y_j, $1 \leq j \leq m$ at rate k will be denoted by

$$a_1 X_1 + \cdots + a_n X_n \rightharpoonup^k b_1 Y_1 + \cdots + b_m Y_m. \tag{1.2}$$

X_i's are called the *substrates* and Y_j's are called the *products* of the reaction. The *rate k of the reaction* determines how fast the chemical reaction takes place and usually depends on the *concentration* of the substrates X_i, denoted by $[X_i]$ and their *copy number* a_i (the number of the molecules involved in the reaction), but not on the products. In the reaction given by (1.2), reaction species X_i is loosing a_i copies at rate k, so $[X_i]$ changes at a rate of $\frac{d}{dt}[X_i] = -a_i k$, and similarly Y_j is gaining b_j copies therefore $\frac{d}{dt}[Y_j] = b_j k$.

There are many different kinetics models used to determine the reaction rate k, but here we limit our discussion to the two most common ones; *mass-action kinetics* and *Michaelis-Menten kinetics*. In mass-action kinetics, the reaction rate k is modeled to be proportional to the product of the substrates, i.e.

$$k = \alpha [X_1]^{a_1} \cdot [X_2]^{a_2} \cdot \ldots \cdot [X_n]^{a_n}.$$

Michaelis-Menten kinetics models the kinetics of reactions catalyzed by enzymes, and

state that for a simple reaction that converts X into Y using enzyme E, the reaction rate κ is given by

$$\kappa = \frac{C_0[X]}{k_0 + [X]},$$

for some positive constants C_0 and k_0, where C_0 is proportional to the concentration of the available enzyme E.

Remark 1.1: *For convenience of notation, from now on we will use A to denote both the chemical species A and its concentration $[A]$, and clarify when the distinction is important.*

Let $\mathcal{X} = \{X_1, X_2, \ldots, X_m\}$ be a set of chemical species and $\mathcal{R} = \{R_1, R_2, \ldots, R_n\}$ a set of chemical reactions that involves species $\mathcal{X}$, with corresponding reaction rates $\{v_1, v_2, \ldots, v_n\}$. The vector $v = [v_1, v_2, \ldots, v_n]^T$ is known as the *reaction rate vector.* The $m \times n$ matrix $\mathcal{S}$ whose entry $s_{i,j}$ is the net gain/loss of species X_i when reaction R_j happens, is called the *stoichiometry matrix* for the set of reactions $\mathcal{R}$ on species $\mathcal{X}$. Then for $\mathbf{X} := [X_1, X_2, \ldots, X_m]^T$ (i.e., the vector of the concentrations of the species $\mathcal{X}$ in the system),

$$\frac{d}{dt}\mathbf{X} = \mathcal{S}v$$

Example 1.1: *Let $\mathcal{X} = \{X_1, X_2, X_3, X_4\}$, $\mathcal{R} = \{R_1, R_2, R_3\}$ with*

$$\begin{aligned} R_1: &\quad 2X_1 + X_2 &\rightharpoonup &\quad X_3 + X_2 \\ R_2: &\quad X_3 &\rightharpoonup &\quad X_4 \\ R_3: &\quad X_4 &\rightharpoonup &\quad X_3 \end{aligned}$$

and corresponding reaction rate vector given by $v(\mathbf{X}) = [\alpha_1 X_1^2 X_2,\ \alpha_2 X_3,\ \alpha_3 X_4]^T$. The net loss/gain of the chemical species from the reaction $\mathcal{R}$ is given by the following table

	R_1	R_2	R_3
X_1	-2	0	0
X_2	0	0	0
X_3	1	-1	1
X_4	0	1	-1

and therefore the stoichiometry matrix is

$$\mathcal{S} = \begin{bmatrix} -2 & 0 & 0 \\ 0 & 0 & 0 \\ 1 & -1 & 1 \\ 0 & 1 & -1 \end{bmatrix}.$$

Consequently,

$$\tfrac{d}{dt}\begin{bmatrix} X_1 \\ X_2 \\ X_3 \\ X_4 \end{bmatrix} = \begin{bmatrix} -2 & 0 & 0 \\ 0 & 0 & 0 \\ 1 & -1 & 1 \\ 0 & 1 & -1 \end{bmatrix} \begin{bmatrix} \alpha_1 X_1^2 X_2 \\ \alpha_2 X_3 \\ \alpha_3 X_4 \end{bmatrix}.$$

Using this formulation, the ODE for the set of chemical reactions in (1.1) is given by

$$\begin{aligned}
\dot{x}_1 &= f(y) + h_2(x_2) - g_1(x_1) - d_1(x_1) \\
\dot{x}_2 &= g_1(x_1) + h_3(x_3) - g_2(x_2) - h_2(x_2) - d_2(x_2) \\
&\vdots \quad \vdots \\
\dot{x}_{n-1} &= g_{n-2}(x_{n-2}) + h_n(x_n) - g_{n-1}(x_{n-1}) - h_{n-1}(x_{n-1}) - d_n(x_{n-1}) \\
\dot{x}_n &= g_{n-1}(x_{n-1}) + h_y(y) - g_n(x_n) - h_n(x_n) - d_n(x_n) \\
\dot{y} &= (a+b)\, g_n(x_n) - a f(y) - 2h_y(y) - g_y(y),
\end{aligned}$$

1.2 Outline and Contributions

The three main objectives of this thesis are:

- To analyze the glycolytic pathway and the various performance tradeoffs that arise by the structure of the chemical reactions in the pathway.
- To analyze autocatalytic networks of similar topology as the glycolytic pathway, and establish the various topological tradeoffs.
- To develop scalable tools to study nonlinear properties of such networks.

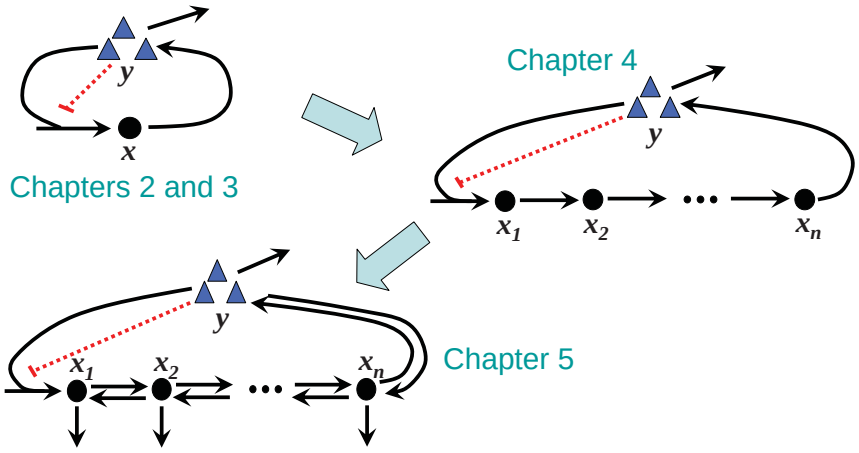

Figure 1.3: Thesis outline.

Essentially, in the context of the special structure of autocatalytic networks, we try to shed some light to the question of why biological networks are the way they are.

To address the above objectives we study progressively more complex autocatalytic networks. Figure 1.3 shows an outline of how networks of different topologies are covered in this thesis. Here we give an outline of each chapter highlighting the main contributions.

- In Chapters 2 and 3, we use a 2D model of the glycolytic pathway (incorporating both autocatalysis and feedback inhibition) that captures the essential dynamics of glycolysis. In Chapter 2 we use classical linear control theory to answer the question of why glycolysis exhibits instabilities. We then explore the many tradeoffs and hard limits that the structure of the pathway imposes on performance. In Chapter 3 we analyze the nonlinear properties of the 2D model, and answer the questions if, why and when glycolysis becomes unstable or whether or not it ever crashes (i.e., exhibits a complete loss of ATP concentration). In both these chapters, we use the 2D model to build intuition and illustrate concepts that are more easily explainable in 2D (using pictures and simple plots), but we also develop ideas and analysis techniques that generalize to higher dimensional models. This model also serves as a good benchmark to test the efficacy of certain semidefinite programming and optimization tools in

analyzing these types of biological systems.

Using the 2D model, we establish hard limits on achievable performance and provide evidence that the cause of the oscillations in glycolysis could be the result of tradeoffs in performance stemming from the structure of autocatalysis. Overall we confirm that oscillations and crashes in glycolysis are not caused by perturbations in state space (i.e., perturbations in the concentrations of the products and reactants), but rather perturbations in the parameter space (i.e., catalytic enzyme concentrations, precursors to the pathway, ATP demand, or temperature).

Additionally estimation of the region of attraction of fixed points using optimization-based formulations reveals that for this model, complex systems (measured by the complexity of the vector field near the fixed point) are fragile, i.e. they are very close to instability in parameter space.

- In Chapter 4 we extend the 2D model to incorporate multiple intermediate reactions, and study the effect of pathway size on its stability and performance. We use a natural decomposition of the system into a feedback interconnection of two input-output subsystems to reduce the complexity of the problem which allows us to obtain nice characterization of the behavior. We also explore the effects of performance and pathway size on computational complexity.

  We establish bounds on the stability of the pathway, that are independent of the pathway size and intermediate reactions. We show that the achievable performance of the pathway decreases with the size of the pathway, and that longer pathways are harder to control.

  We use the above decomposition to analytically construct Lyapunov functions for a large range of feedback gains. Furthermore, we establish a scalable method for construction of block diagonal Lyapunov functions for large pathways. We show that realizations that are more (computationally) complex can only arise from those realizations with high gains.

- In Chapter 5 we extend the model to include reversible reactions and con-

sumption of the intermediate metabolites, and explore the effects of these on performance, stability and computational complexity. We show that the presence of reversible reactions makes the pathway easier to control and improves the bounds of achievable performance, while the consumption of intermediate metabolites has the opposite effect. We establish a scalable method for construction of block diagonal Lyapunov functions using a decomposition similar to that of Chapter 4.

- Chapter 6 concludes the thesis with a summary and future research directions.

Chapter 2

Linear Aspects of Glycolysis in Two Dimensions

2.1 Introduction

Autocatalytic processes generally lead to instability but are unavoidable in cell metabolism. The cell uses external food/resources to create usable components and energy. At the same time it needs to use those same parts and energy in the process. The cell uses mechanisms such as transcriptional regulation of enzymes and product inhibition of enzymes, to stabilize such pathways and minimize the effects of the instabilities. Transcriptional regulation changes the concentration levels of the enzymes by controlling gene expression, thus speeding up or slowing down the corresponding reactions. The slow events of transcription and translation dominate this mechanism making the entire process operate at a slow time-scale. Allosteric regulation is the process by which a molecule binds to an enzyme causing the enzyme to change shape and become more effective (activation) or less effective (inhibition). It happens at a much faster time-scale than transcriptional regulation because the effects of binding are immediate.

Glycolysis is probably the most common autocatalytic pathway on the planet, since it is found in every cell of living organisms, from bacteria to humans. The cell relies on this metabolic pathway to produce energy anaerobically (no involvement oxygen) by breaking down glucose. It is composed of a chain of ten reactions cat-

alyzed by enzymes[1]. The autocatalysis happens when two ATP molecules (energy carriers) are consumed early in the pathway (Hexokinase (HK) and Phosphofructokinase (PFK) are the catalyzing enzymes). Four ATP molecules are generated later in the pathway (for a net return of two ATP molecules) (Figure 2.1A). One of the catalyzing enzymes, PFK, plays a crucial role since it is regulated by ATP (the output of the pathway). PFK is inactive when ATP concentration is high [4], and this form of inhibition is the mechanism used to stabilize the pathway on the fast time-scale. Most intermediate reactions are catalyzed by enzymes, and transcription regulation of those enzymes could be used to stabilize the pathway, but on a much slower time-scale.

We study glycolysis to investigate the tradeoffs between performance and stability in autocatalytic networks, and the hard limits imposed on performance by autocatalysis. Glycolysis is one of the main sources of energy production (ATP), and as such is vital in the control ATP production and concentration. The cell tries to keep the concentration of ATP constant in spite of high variability in both supply and demand. This is important task since many parts of the cell both use and depend on ATP.

As previously described, the instability of the glycolytic pathway appears in the form of oscillations of glycolytic intermediates. Although the details of the mechanisms of glycolysis as well as the physical components responsible for causing instabilities are very well understood, there is no good understanding of what fundamentally causes these oscillations. There are suggestions that they potentially minimize the dissipation of free energy [32], while most argue that they could be detrimental to the cell [25, 29]. Are these oscillations the result of a frozen accident in history? Are the enzymes doing something they were not intended to do? Is it bad design? Is it possible to design a better enzyme that would have better performance and eliminate these oscillations? In this chapter we will investigate these very questions. The oscillations are shown to be an unavoidable consequence of the structure of the autocatalytic pathways and a result of a performance tradeoffs.

2.2 A Two Dimensional Model of Glycolysis

We look at the inner autocatalytic loop of glycolysis, highlighted in Figure 2.1A. Other autocatalytic pathways have similar properties. A general representation of this pathway would be

$$\begin{aligned} u + ay &\rightharpoonup x_1 + a\tilde{y} \\ x_1 &\rightharpoonup x_2 \cdots \rightharpoonup x_n \\ x_n + (a+b)\tilde{y} &\rightharpoonup (a+b)y + x_{n+1} \\ y &\rightharpoonup \varphi \end{aligned} \tag{2.1}$$

where u is the concentration of some precursor and source of energy (like fructose-6-phosphate) with no dynamics associated, y is ATP concentration, $\tilde{y}$ is ADP concentration, x_i are intermediate metabolites, φ is a null state, a is the number of ATP molecules are invested in the pathway, and $a+b$ is the number of ATP molecules produced. $A \rightharpoonup B$ (sometimes $A \rightharpoonup^f B$) denotes a chemical reaction that converts the chemical species A to the chemical species B (at rate f). Most of the above reactions are catalyzed by enzymes which are proteins that speed up the chemical reactions. We do not show the enzymes in the above reactions, but note that the reaction rates depend on the concentration of the catalyzing enzymes. The first reaction is catalyzed by PFK and the rate of this reaction is modeled by $f_u(y)$. We will initially assume that a single intermediate reaction can capture the essence of all of the intermediate metabolite reactions, and denote by x the resulting "aggregate" intermediate state (Figure 2.1B). We will also assume that the last reaction, $x_n + (a+b)\tilde{y} \rightharpoonup (a+b)y + x_{n+1}$ is fast [9]. These assumptions simplify the system to the following

$$\begin{aligned} u + ay &\rightharpoonup^{f} x + az \\ x &\rightharpoonup^{g_x} (a+b)y \\ y &\rightharpoonup^{g_y} \varphi \end{aligned} \tag{2.2}$$

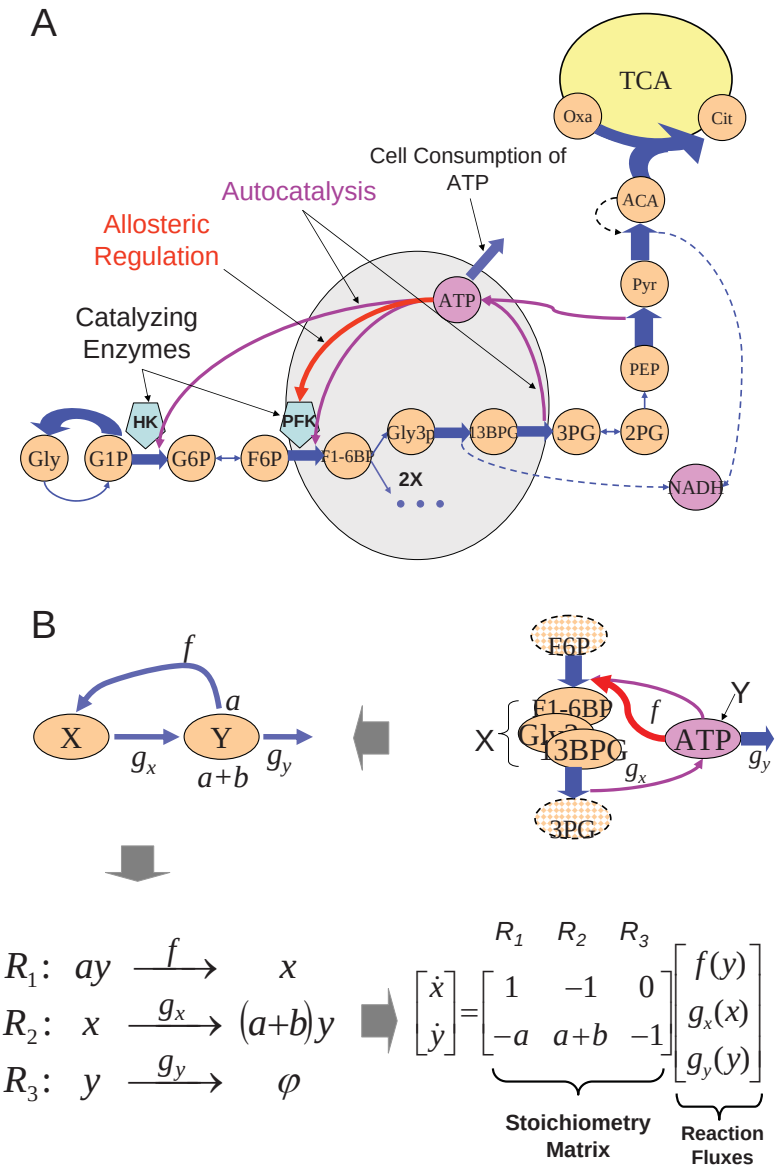

Figure 2.1: (A) Glycolysis pathway. Autocatalysis happens when two ATP molecules (energy carriers) are consumed early in the pathway through reactions catalyzed by Hexokinase (HK) and Phosphofructokinase (PFK). Four ATP molecules are generated further along the pathway (energy return). Allosteric regulation happens as ATP inhibits PFK. (B) The inner autocatalytic loop of the pathway (highlighted in blue) is reduced to a 2D system by aggregating the intermediate reactions in a single one. The resulting 2 state model is composed of 3 aggregate chemical reactions R_1, R_2 and R_3. The structure of the pathway is completely determined by the stoichiometry matrix, (where each entry $m_{i,j}$ is the net gain/loss of species i as a result of reaction R_j). The number of ATP molecules consumed and produced by the pathway are a and $a+b$ respectively (in this case $a = b = 1$).

where u is the input to the pathway. We will not keep track of u explicitly and associate no dynamics to it. We use $f(y)$ as shorthand for $f_u(y)$, noting the parameter dependence of f on u when necessary. The corresponding ordinary differential equation (ODE) is

$$\begin{bmatrix} \dot{x} \\ \dot{y} \end{bmatrix} = \begin{bmatrix} 1 & -1 & 0 \\ -a & a+b & -1 \end{bmatrix} \begin{bmatrix} f(y) \\ g_x(x) \\ g_y(y) \end{bmatrix} \tag{2.3}$$

for $x, y \geq 0$ and $g_x(0) = 0$, $g_y(0) = 0$, and $g_x(x)$ and $g_y(y)$ are continuous monotone increasing functions in the positive orthant. The constraints above on $g_x(x)$ and $g_y(y)$ are consistent with large classes of chemical kinetics models such as mass-action and Michaelis-Menten. The rate of the first reaction $f(y)$ is directly related to PFK's activity. This enzyme gets activated by AMP, and inactivated by ATP. A reasonable form for $f(y)$ that also agrees with experimental data is $f(y) = \frac{Vy^q}{1+\gamma y^h}$, where V is related to the availability of precursors such as glucose, q is the strength of autocatalysis, and γ, h are determined by the enzyme and regulate the strength of feedback inhibition [4, 9]. Finally, the ODE takes the special form

$$\begin{aligned} \dot{x} &= \frac{Vy^q}{1+\gamma y^h} - g_x(x) \\ \dot{y} &= (a+b)g_x(x) - a\frac{Vy^q}{1+\gamma y^h} - g_y(y) \end{aligned} \tag{2.4}$$

It should be noted that all the parameters are positive.

2.2.1 Other Glycolysis Models and Experimental Data

Next we examine some of the numerous glycolysis models and how the 2D model in (2.4) relates to them.

Many of the models in the literature attempt to capture the full mechanism of glycolysis [18] as it is biochemically understood. This allows for high fidelity but results in large systems that are hard to analyze. This tradeoff motivates the search for reduced or minimal models that capture the essential mechanisms and behavior.

Most reduced models are derived using reduction techniques that rely on biological intuition that leads to "lumping" several reactions and states into a single one, or eliminating fast reactions by replacing the reactions by their quasi steady state value. The parameters of such models are adjusted to fit experimental data and preserve crucial properties, such as proximity to a Hopf bifurcation, which might be the cause of oscillations in glycolysis [9, 24, 47]. Reference [9] uses two such model reduction techniques to reduce the full-scale glycolysis pathway [18] first to an eight-state model and then to a three-state model. These models are essentially derived by collapsing the two autocatalytic loops into a single one (lumping) and eliminating the fast reactions by fixing the corresponding metabolite concentrations at their steady-state values. As a result, both of them match the structure of (2.1) quite well. Additionally, the three-state model contains one additional fast reaction, shown in [9] to be several orders of magnitude faster than the other reactions. If we eliminate this reaction by fixing the corresponding species to its steady state value, we get equation (2.4) (for a particular choice of parameters and reaction rates g_x and g_y). Specifically, the three-state model in [9] is given by

$$\begin{aligned}
\dot{x}_1 &= 2\tilde{V}_2 \frac{y}{1+\frac{1}{K_i^q}y^q} - \tilde{k}_3 x_1 - \tilde{k}_8 x_1 \\
\dot{x}_2 &= \tilde{k}_3 x_1 - k_4 x_2 z \\
\dot{y} &= 2k_4 x_2 z - 2\tilde{V}_2 \frac{y}{1+\frac{1}{K_i^q}y^q} - (k_6 + \tilde{k}_7) y,
\end{aligned}$$

where x_1 is the $trioseP$ concentration, x_2 the BPG concentration, z the ADP concentration, y the ATP concentration, the parameter values are $\tilde{V}_2 = 67.7116$, $q = 2.64$, $K_i = 1.24464$, $\tilde{k}_3 = 6.65022$, $k_4 = 126519$, $k_6 = 3.2$, $\tilde{k}_7 = 9.65602$, $\tilde{k}_8 = 0.617780$, and $y + z$ is assumed to be constant. We notice that x_2 has much faster dynamics since the reaction rate k_4 is several orders of magnitude larger than the other reaction rates. Using simple perturbation theory we eliminate the fast dynamics by

setting x_2 to its (quasi) steady state value and as a result we get $\tilde{k}_3 x_1 - k_4 x_2 z$ and

$$\begin{aligned} \dot{x}_1 &= \frac{135.4232y}{1+0.56116y^{2.64}} - 7.268x_1 \\ \dot{y} &= 13.30044x_1 - \frac{135.4232y}{1+0.56116y^{2.64}} - 12.85602y, \end{aligned} \tag{2.5}$$

which is exactly (2.4) with $V = 135.4232$, $q = 1$, $h = 2.64$, $\gamma = 0.56116$, $a = 1$, $b = 0.83$ and $g_x(x) = 7.268x$, $g_y(y) = 12.85602y$. As the 3D model in [9], this 2D model has an unstable oscillatory mode ($\lambda = 0.3 \pm 14.78i$ in this case).

In addition to the above models, there are classical two-state models that differ in structure from the 2D model in (2.4) but also qualitatively capture the observed oscillations in glycolysis. For example, the model proposed in [13] focuses on the enzyme dynamics rather then the dynamics of the metabolites involved, and qualitatively captures the oscillatory behavior observed in experiments. The two-state model proposed in [35] is reduced from a larger model and uses Michaelis-Menten reaction rates. This model also exhibits hysteretic behavior and oscillations and it shows that using these reaction rates stabilization is possible.

We now examine how well the 2D model in (2.4) captures the essence of glycolysis and glycolytic oscillations. Simulations of the model using simple g_x and g_y such as $g_x(x) = k_x x$, $g_y(y) = k_y y$ (as is (2.5)), match experimental data on glycolytic oscillations. Most of these experiments on glycolytic oscillations are performed on yeast and generally fall into two categories. The first category is comprised of experiments on dense cell suspensions. Yeast is put under starving conditions and shifted to anaerobic conditions [31]. Under such conditions, glycolysis is the main source of energy in the cell. Damped oscillations are observed in the metabolites when a pulse of glucose is added. Furthermore, sustained oscillations are observed when a constant input of glucose is maintained. In our model increasing the glucose flow (u) would map to increasing the parameter V accordingly, since V is dependent on glucose availability. Increasing V in the model forces the system to go through a Hopf bifurcation, resulting in oscillations thus matching these experimental observations (Figure 2.2A).

The second type of experiment is done on yeast extracts [14, 24]. In a Continuously-

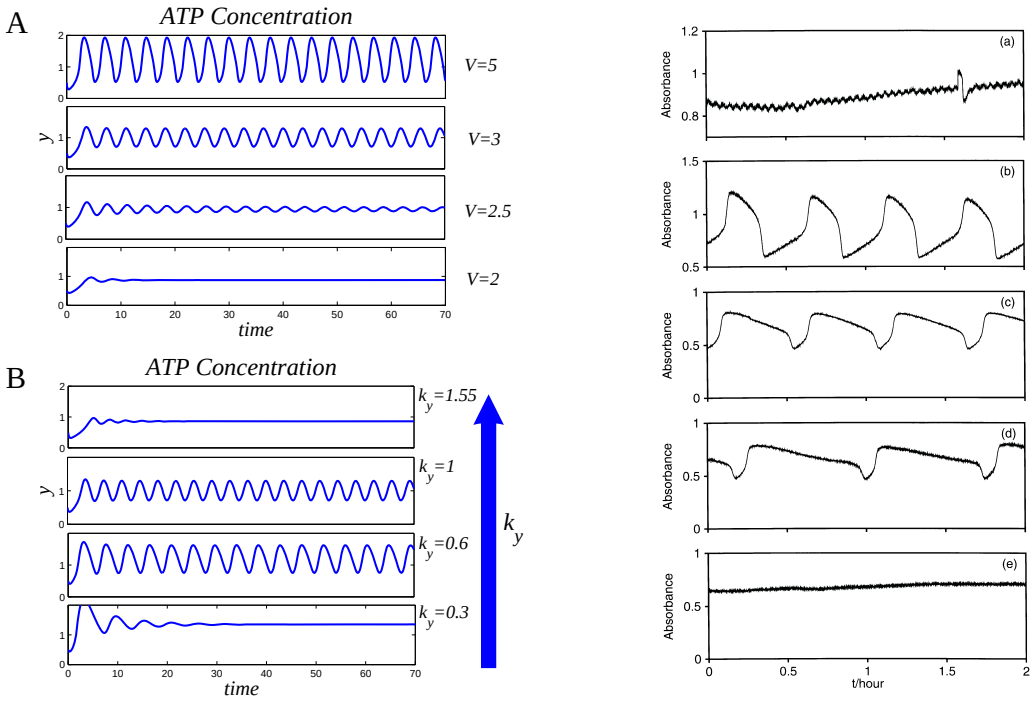

Figure 2.2: Left: Simulations of the 2D model with $h = 5$, $q = 1$, $\gamma = 2$, $a = b = 1$, $g_x(x) = x$ and $g_y(y) = k_y y$ show oscillations in ATP concentration. A) Induced oscillations by varying glucose availability ($k_y = 1$, $V = 2, 2.5, 3, 5$). B) Induced oscillations by varying ATP consumption rate ($V = 3$, $k_y = 0.3, 0.6, 1, 1.55$). Right: Experiments on yeast extracts show sustained glycolytic oscillation for intermediate flow rates in a CSTR (b-d) (figure taken from [24]).

Stirred Tank Reactor (CSTR), substrate and glucose are added at a constant rate (inflow), and the volume is kept constant by an outflow at the same rate. No oscillations are observed under high or low inflow rates, but there are oscillations at intermediate rates [24] (Figure 2.2 right) . In our model this would correspond to changes in the rate of consumption of ATP, k_y. Figure 2.2B shows that simulations of our model agree with this observation.

2.3 Control of Glycolysis

ATP is the major energy carrier in the cell. Many processes depend on ATP and drops in its concentration can be fatal to the cell. Glycolysis is the main pathway that produces ATP anaerobically and as such it is important for glycolysis to main-

tain ATP concentration close to biological standards in the presence of an uncertain environment. Uncertainty in the environment is created by fluctuations in the enzyme concentrations, variability on the demand for ATP or the supply of glucose, and intrinsic/extrinsic biological process noise. Some of the regulation needed to adjust to slow, long term changes in the cell is performed by the transcription/translation of the enzymes involved. However, for fast fluctuations and disturbances, glycolysis relies on product inhibition via the allosteric regulation of PFK by ATP. One of our goals is to understand why oscillations happen in glycolysis and how the structure of this pathway, especially autocatalysis affects how well the cell performs this task.

System (2.4) can be viewed as output feedback control of an autocatalytic plant as shown in Figure 2.3. Biology imposes hard constraints on the structure of the plant and of the controller by forcing the vector field of the open-loop plant and the controller to have the specific form of Figure 2.3. The control task is to maintain a predefined constant output in the presence of disturbances and changes in the plant dynamics. Unlike many problems in control, the controller in this case has to not only deal with unmodeled plant dynamics, but also with the fact that the plant itself is expected to change over time. The simplest way the plant changes is by fluctuations in enzyme concentrations causing changes in the intermediate reaction rates. This would be a parametric change in the plant dynamics and always happens during the lifetime of the cell. In much longer time-scale (thousands of years) there might also be structural changes in the plant, such as fundamental changes (insertion/deletion/replacement) in the nature of intermediate reactions or chemical species.

2.3.1 Linearization

We can evaluate performance based on steady-state or transient response. We will now look at linearization of the plant to get a good picture of the steady-state performance as well as to get hints about the transient response.

We will assume that PFK enzyme levels are controlled by the slow transcriptional

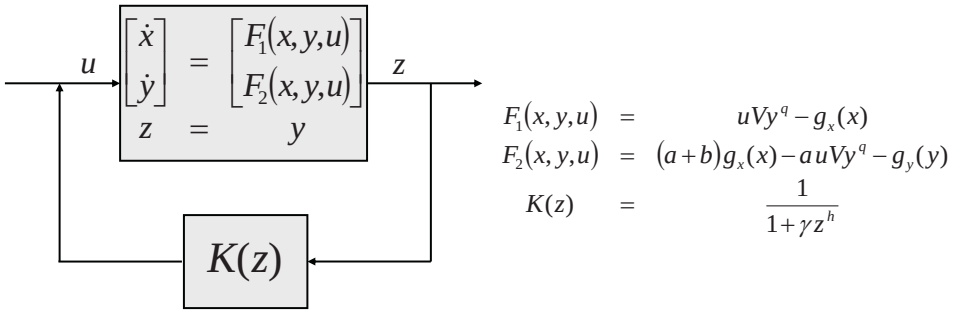

Figure 2.3: Fast regulation of glycolysis can be viewed as the output feedback control of an autocatalytic plant. Biology imposes hard constraints on the structure of the plant and the controller. This representation implies the same closed-loop system as system (2.4).

regulation. This regulates the amount of PFK (parameter V in (2.4)) to match the availability of glucose and ATP demand. Without loss of generality we will assume the equilibrium point of interest at which the cell operates is $\bar{y} = 1$. Let $g_y(1) = r_y$, $\frac{\partial}{\partial y} g_y(y)|_{y=1} = k_y$ and $\frac{\partial}{\partial x} g_x(x)|_{x=\bar{x}} = k_x$. This implies $V = r_y(1+\gamma)/b$, and the linearization of (2.4) around this point of equilibrium is

$$\begin{bmatrix}\dot{x}\\ \dot{y}\end{bmatrix} = \begin{bmatrix}-k_x & \frac{1}{b} r_y (q - \hat{h})\\ (b+a)k_x & -\frac{a}{b} r_y (q-\hat{h}) - k_y\end{bmatrix} \begin{bmatrix}x\\ y\end{bmatrix} \tag{2.6}$$

where $\hat{h} = \frac{\gamma}{\gamma+1} h$.

System (2.6) is the linearized closed-loop system as regulated by the enzyme PFK with $\hat{h}$ as the feedback gain (Figure 2.4A.) In standard output feedback control form (2.6) becomes

$$\begin{aligned}\dot{\mathbf{x}} &= A\mathbf{x} + Bu\\ z &= C\mathbf{x}\\ u &= -\hat{h}z = -\hat{h}C\mathbf{x}\end{aligned} \tag{2.7}$$

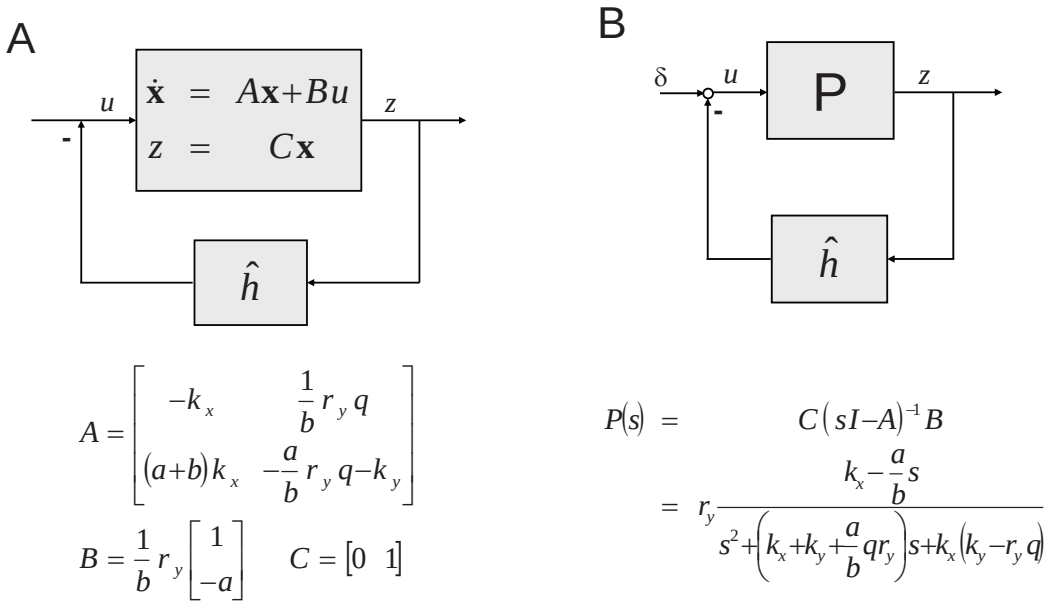

Figure 2.4: Steady state performance of glycolysis is analyzed by looking at the corresponding standard output feedback control form. A) State space model. B) Frequency domain description of the model.

where

$$
\begin{aligned}
A &= \begin{bmatrix} -k_x & \frac{1}{b} r_y q \\ (b+a)k_x & -a\frac{1}{b} r_y q - k_y \end{bmatrix} \\
B &= \frac{1}{b} r_y \begin{bmatrix} 1 \\ -a \end{bmatrix} \\
C &= \begin{bmatrix} 0 & 1 \end{bmatrix}
\end{aligned}
$$

The system above is open-loop ($\hat{h} = 0$) unstable (saddle point) but with no oscillations. Simple root locus analysis shows that it can be stabilized via output feedback control, however a high gain will destabilize the system and lead to oscillations (Figure 2.5, Table 2.1). It is the structure of autocatalysis that is responsible for causing instability (oscillations) for high feedback gain, since ATP (y) both controls and is consumed by the first reaction. Small drops in ATP concentration from the equilibrium value will be initially followed by further drops in ATP concentration before

Feedback Strength ($\hat{h}$)	Behavior
$\hat{h} < q - \frac{k_y}{r_y}$	Saddle
$\hat{h} = q - \frac{k_y}{r_y}$	Saddle-Node Bifurcation
$q - \frac{k_y}{r_y} < \hat{h} < q + \frac{b}{ar_y}(k_x + k_y)$	Stable
$\hat{h} = q + \frac{b}{ar_y}(k_x + k_y)$	Hopf Bifurcation
$\hat{h} > q + \frac{b}{ar_y}(k_x + k_y)$	Unstable Node (Oscillations)

Table 2.1: Stability of the glycolysis pathway operating point based on the closed-loop system (2.6).

the eventual increase in concentration, since it needs to consume additional ATP (y) to produce additional intermediate metabolite (x), which in turn will produce more ATP to compensate for the original drop in concentration. If the gain is high enough the initial drop might cause the system to overproduce ATP and overshoot the target concentration by a large enough margin to cause oscillations.

This suggests that the cause of oscillation in the glycolysis pathway could be aggressive control. Why might glycolysis have such an aggressive control strategy? The answer to this question will be the focus of the next few sections. A possible answer is that more aggressive control leads to better performance and the choice of a control strategy is guided by tradeoffs and hard limits on performance.

2.4 Performance and Hard Limits

2.4.1 Frequency Domain Analysis

Let

$$\begin{aligned} P(s) &= C\left(sI - A\right)^{-1} B \\ &= r_y \frac{k_x - \frac{a}{b}s}{s^2 + \left(k_x + k_y + \frac{a}{b}qr_y\right)s + k_x k_y - k_x r_y q} \end{aligned} \tag{2.8}$$

be the open-loop transfer function for (2.7) (Figure 2.4B). We first observe that the plant, in addition to the right half-plane (RHP) pole, has a RHP zero at $s = z$,

$$z = \frac{b}{a}k_x$$

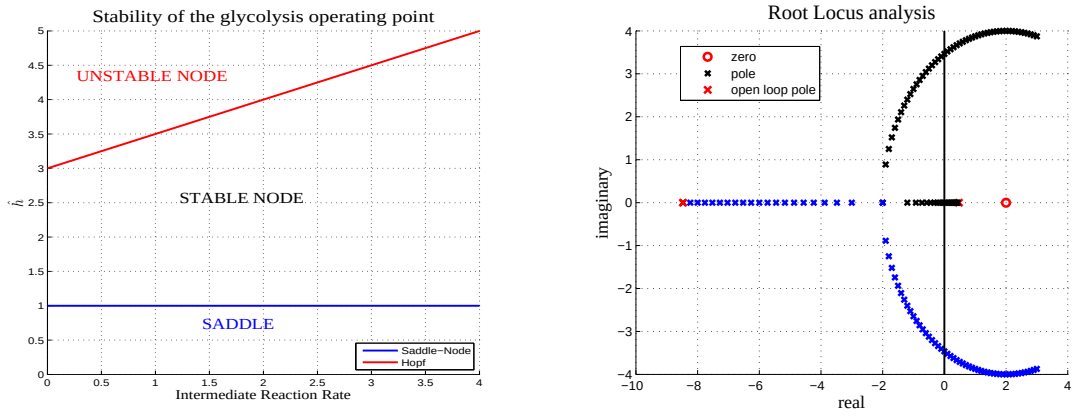

Figure 2.5: Stability diagram and root locus plots show that output feedback stabilizes glycolysis, however high gain will destabilize the system and lead to oscillations. Fast intermediate reaction rates permit higher stabilizing feedback gains.

This RHP zero depends on the intermediate reaction rate and the stoichiometry of autocatalysis, but not on the reaction rate of autocatalysis. Its existence can be shown to be a function of the structure of the autocatalysis.

We will see next that the RHP zero imposes additional hard limits on performance, by enforcing a special form of the Bode Integral formula [10]. The sensitivity function $S(s) = \frac{1}{1+\hat{h}P(s)}$ measures how sensitive the pathway is to disturbances δ in the feedback as shown in Figure 2.4B. In state space this maps to δ perturbations of (2.6), specifically

$$\begin{bmatrix} \dot{x} \\ \dot{y} \end{bmatrix} = \begin{bmatrix} -k_x & \frac{1}{b} r_y (q - \hat{h}) \\ (b+a)k_x & -\frac{a}{b} r_y (q - \hat{h}) - k_y \end{bmatrix} \begin{bmatrix} x \\ y \end{bmatrix} + \begin{bmatrix} 1 \\ -a \end{bmatrix} \delta$$

In addition weighted S measures the sensitivity to many other disturbances. One of these disturbances will be analyzed in detail in section 2.4.2.

Typically we want $|S(j\omega)|$ to be small for small steady state error in some frequency range, often around $\omega = 0$. Can we make S arbitrarily small?

2.4.1.1 Bode Integral Formula

The Bode sensitivity integral formula holds for plants of relative degree≥ 2. $P(s)$ from equation (2.8) has relative degree 1, so that formula does not apply. However the existence of a RHP zero allows the use of the following form of the Bode sensitivity integral formula

$$\frac{1}{\pi}\int_0^\infty \ln|S(j\omega)|\frac{2z}{z^2+\omega^2}d\omega = M \geq 0 \tag{2.9}$$

where $M = \ln|\frac{z+p}{z-\bar{p}}| > 0$ if the open-loop plant has a RHP pole p, and $M = 0$ otherwise. This formula can be derived easily from Lemma 3 in Chapter 6 of [10]. For completeness we show the Lemma and its application in proving (2.9) here.

Lemma 2.1: *For every point $s_0 = \sigma_0 + j\omega_0$ with $\sigma_0 > 0$,*

$$\log|S_{mp}(s_0)| = \frac{1}{\pi}\int_{-\infty}^{\infty}\log|S(s_0)|\frac{\sigma_0}{\sigma_0^2+(\omega-\omega_0)^2}d\omega \tag{2.10}$$

where S_{mp} is the minimum phase part of S.

PROOF: See [10].

Proposition 2.1: *Let z be a RHP zero of* (2.8)*. Then* (2.9) *holds.*

PROOF: In Lemma 2.1, take $s_0 = z \Rightarrow \sigma_0 = z$, $\omega_0 = 0$.

Let $S(s) = S_{ap}(s)S_{mp}(s)$, where $S_{ap}(s)$ be the all-pass part of $S(s)$ and $M = \log|S_{mp}(z)|$.

Notice that if z is a zero of the plant then $S(z) = 1$. If p is a pole of the plant, then $S(p) = 0$. Therefore, if there is no pole in the RHP, then $S_{ap}(s) = 1$ and

$$\begin{aligned} S(z) = 1 \quad &\Rightarrow \quad S_{mp}(z) = S_{ap}(z)^{-1} = 1 \\ &\Rightarrow \quad M = 0 \end{aligned}$$

If there is a pole p in the RHP, then $S_{ap}(s) = \frac{s-p}{s+p}$ and

$$\begin{aligned} S(z) = 1 \quad &\Rightarrow \quad S_{mp}(z) = S_{ap}(z)^{-1} = \frac{z+p}{z-p} \\ &\Rightarrow \quad M = \log|\frac{z+p}{z-\bar{p}}| > 0 \end{aligned}$$

So substituting into (2.10), we get

$$\begin{aligned} M &= \frac{1}{\pi}\int_{-\infty}^{\infty} \log|S(s_0)| \frac{z}{z^2+\omega^2} d\omega \\ &= \frac{1}{\pi}\int_{0}^{\infty} \log|S(s_0)| \frac{2z}{z^2+\omega^2} d\omega \end{aligned}$$

■

The formula states that the weighted area under the log of the sensitivity function is conserved (Figure 2.6). This means that pushing the low frequency response to disturbances to be small, i.e trying to obtain 'good performance', must be compensated for with a larger response in some other frequency range. Since $\frac{1}{\pi}\int_0^\infty \frac{2z}{z^2+\omega^2} d\omega = 1$, the weight puts an emphases on frequencies smaller than z, so there is a much higher price, i.e. increase in frequency response in another part of the frequency range, associated with good performance in this frequency range ($\omega < z$) (Figure 2.6). Figure 2.6 also indicates that small magnitude zeros make the price for good performance at low frequencies even steeper. Hence, since $z = \frac{b}{a}k_x$, this hard limit is aggravated by slow intermediate reactions (k_x small) or poor "efficiency" in energy production ($\frac{b}{a}$ is small, i.e. the amount of extra ATP produced per ATP invested is small).

The existence of a RHP pole and zero for the plant introduces additional hard limits on any (stable) weighted sensitivity (W_1S). It provides a lower bound on how small the peak of W_1S can be since the relation $\|W_1S\|_\infty \geq \left|W_1(z)\frac{z+p}{z-p}\right|$ (Chapter 6 of [10]) must hold.

2.4.2 Disturbances in the ATP Consumption

It is particularly important that the closed-loop system be insensitive to disturbances in the consumption of ATP. These types of disturbances might be common since a

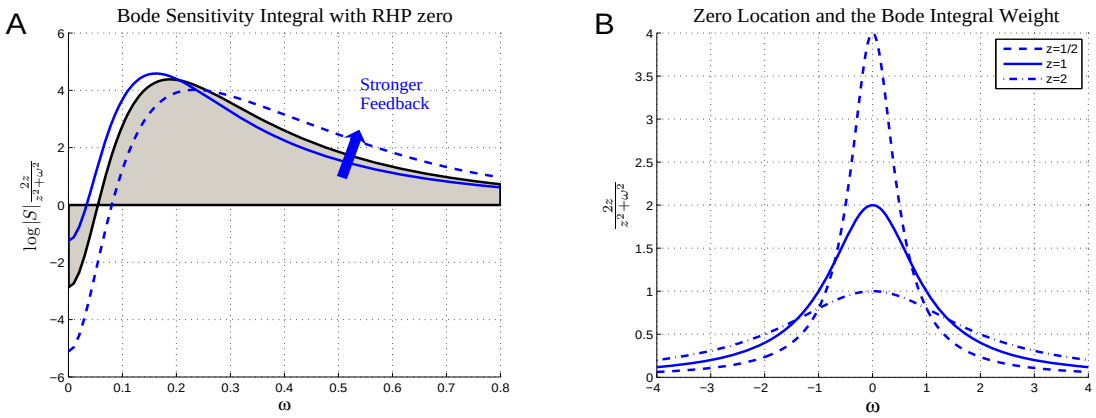

Figure 2.6: Bode Sensitivity Integral for Plants with RHP zeros. (A) The area under the curve of the (weighted) sensitivity function S is conserved. Feedback can push small frequency response to be small, but this will be compensated for with a larger response in some other frequency range. (B) The weight in the Bode integral gets tighter around 0 for smaller magnitude z. This means the price to pay for performance at small frequencies increases substantially as the RHP zero gets smaller.

number of processes, in many different parts of the cell, use ATP. In this section we quantify the ability of the control system to reject such disturbances.

The addition of disturbances of the ATP consumption to system (2.7) results in the following changes to the glycolysis model

$$\begin{aligned} \dot{\mathbf{x}} &= A\mathbf{x} + Bu + \begin{bmatrix} 0 \\ 1 \end{bmatrix} \delta \\ y &= C\mathbf{x} \\ u &= -\hat{h}y = -\hat{h}C\mathbf{x} \end{aligned} \tag{2.11}$$

Let $\Delta(s)$ be the open-loop disturbance transfer function as indicated in Figure 2.7, then the closed-loop transfer function $G_{y,\delta}$ is given by

$$G_{y,\delta} = \left(1 + \hat{h}P\right)^{-1} \Delta = W_1 S$$

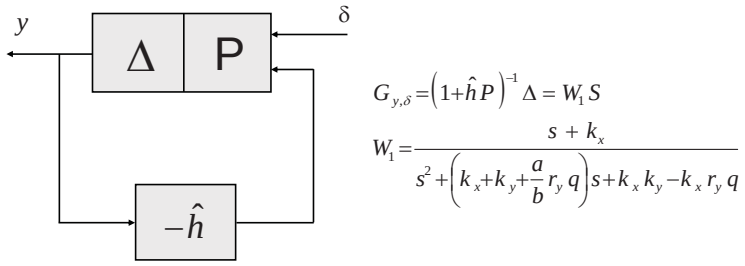

Figure 2.7: Sensitivity to disturbances in ATP consumption can be measured by W_1S using the appropriate weight function W_1.

where

$$W_1 = \Delta = \frac{s + k_x}{s^2 + \left(k_x + k_y + \frac{a}{b}qr_y\right)s + k_x k_y - k_x r_y q}$$

Small sensitivity to the disturbance δ implies that $|W_1S|$ remains small . However, since

$$\ln|W_1(j\omega)S(j\omega)| = \ln|W_1(j\omega)| + \ln|S(j\omega)|$$

(2.9) implies that we cannot make this quantity small for all frequencies, as illustrated in Figure 2.8A. More aggressive (i.e. high gain) feedback will improve the response at low frequencies, but it will make the response large at other frequencies (frequencies around $\omega = 1$ in the example plotted).

If the disturbance δ was a constant, then the value of y at the fixed point of (2.11) (ATP concentration at equilibrium) is perturbed by

$$CA^{-1}\begin{bmatrix} 0 \\ 1 \end{bmatrix}\delta = -\frac{1}{\left(\hat{h} - q\right)r_y + k_y}\delta = -\xi(\hat{h})\delta$$

where $\xi(\hat{h}) = W_1(0)S(0)$ is the DC gain of the performance function W_1S. The lower bound on the error is

$$\xi(\hat{h}) > \frac{a}{(b+a)\,k_y + k_X}$$

which can be approached arbitrarily closely by taking the maximum gain $\hat{h}$ that still keeps the system stable. However such a system will have very poor transient response as illustrated in Figure 2.8B.

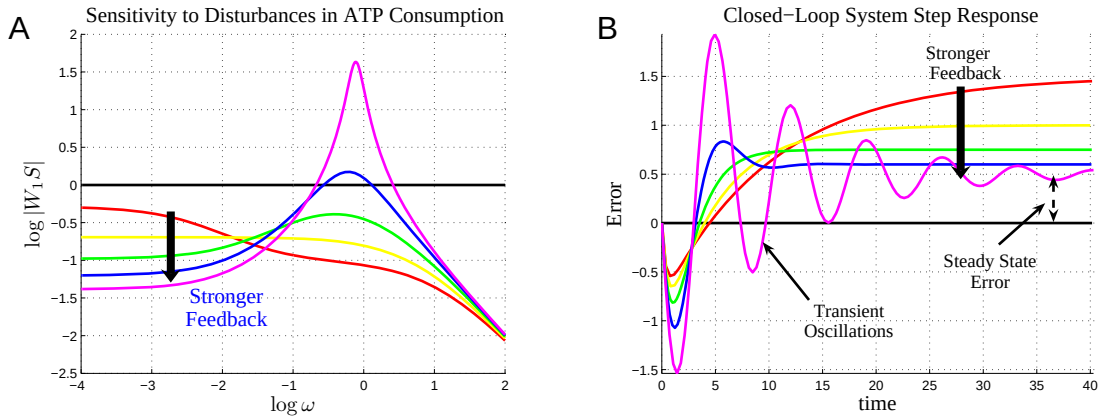

Figure 2.8: (A) Plot of $\log|W_1S|$ for different feedback gains shows that more aggressive feedback will improve the response at low frequencies, but it will make the response large at other frequencies (frequencies around $\omega = 1$ in the example plotted). (B) Plot of the output step response for different feedback gains shows that oscillations in the transient response is another price paid for improved steady state response using stronger (i.e. higher feedback gains) feedback.

In fact in general more aggressive feedback will lead to better response at low frequencies, but poorer transient response. The next section will explore tradeoffs such as this in more detail.

2.5 Tradeoffs

Glycolysis exhibits some tradeoffs that we believe to be common in biology. They appear as a result of hard constraints put on the system by the structure of the reactions/equations and the nature of control in biology. In some cases, these tradeoffs can be precisely characterized because they appear to be results of well defined "conservation laws". In other cases these tradeoffs are a result of laws that are not yet fully understood because of the complexity of the cell and/or lack of knowledge of or inability to compute what the cell is optimizing for. In these cases we use hypothesis based on existing theories or beliefs that are commonly accepted in the research community.

2.5.1 Tradeoffs in Plant Design

As previously indicated one of the reasons the plant is hard to control is the existence of the RHP zero, $z = \frac{b}{a}k_x$. This is a direct consequence of autocatalysis, since if $a = 0$ (no autocatalysis) there is no zero in the RHP. So, it is the structure of the pathway and not the parameter values (such as reaction fluxes) that dictates the existence of a RHP zero. As such, one cannot build autocatalytic plants with the topological structure of (2.2) that do not have a RHP zero. However one can build a plant that 'softens' the hard limits on performance, discussed in the section 2.4, by increasing the magnitude of the RHP zero (Figure 2.6B). There are two ways to accomplish this, increase the rate of intermediate reactions or improve autocatalysis efficiency.

Increase the rate k_x of intermediate reactions Biologically this means that either the number of enzymes that catalyze the reactions or enzyme efficiency need to be increased. There is a limit on how efficient an enzyme can be, so the only real option is to increase the number of enzymes. However this can be energetically wasteful for the cell, since it has to create and maintain a high number of proteins. So, the cell can choose big k_x for better performance but it must then pay the cost of high energy expenditure. Once the controller for the plant is designed (through selection of the proper enzyme, e.g. PFK for glycolysis) it is very hard to change it, certainly impossible over the lifetime of a cell. So if designed for good performance assuming high levels of catalyzing enzymes, these high levels need to be maintained during the lifetime of the cell, since drops in enzyme levels will decrease the rate k_x and move the system to an unstable regime.

Increase the energy efficiency $\frac{b}{a}$ of autocatalysis By increasing the extra amount of energy (ATP) attained per unit of energy invested (increasing $\frac{b}{a}$) the RHP zero can be moved further from the origin. However in addition to fundamental limits on what efficiency is achievable, more efficient systems tend to require much more complex machinery and maintenance. To illustrate this point, we look at the whole cellular respiration (simplistically glycolysis + CA Cycle + oxidative phospho-

rilation), which could produce up to 38 ATP molecules from a single glucose molecule. In this case we *might* be able to use a model similar to (2.3) but with $b = 35$ and $a = 3$. This would make the RHP zero about 12 times larger and result in a plant which is much easier to control. However, this more efficient machinery is far more biologically complex and relies on other processes (such as electron transport). This pathway also requires oxygen to proceed, which could be toxic to the cell causing oxidative stress. Oxidative stress happens when there is too much reactive oxygen that the cell cannot reduce fast enough [19]. It appears that for this example increased $\frac{b}{a}$ does not eliminate or soften the constraints or limitations, but merely trades them for other constraints and limitations.

2.5.2 Tradeoffs in Controller Design

Robust Stability As we saw in Section 2.4, better performance at low frequencies is achieved using high gain feedback, however there is a limit on how high the gain can be before the system looses stability. In order to get optimal performance, one would be tempted to use the highest gain $\hat{h}$ possible without making the system unstable. However this would mean that the system would be very sensitive to perturbations in other parameters such as k_x, i.e. if $\hat{h}$ is large then a small perturbation in the value of k_x will lead to instability. In the preceding discussion k_x was assumed to be a fixed parameter, while in reality k_x varies throughout the life of the cell, since the enzyme concentrations change continually. This leads to a tradeoff between performance and robust stability. We believe that this tradeoff is at the heart of oscillations in glycolysis. The cell might be aggressive in choosing a controller, that is stable for the most part, but in rare occasions, the parameter values fall outside the "safe" region.

This concept can be clarified through the following examples of robustness analysis for specific parameters. Consider plant uncertainty in k_x due to changes in the

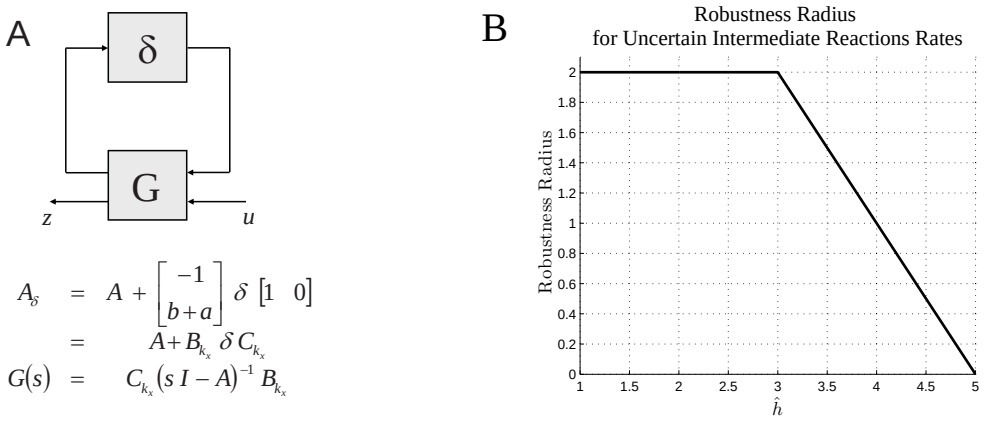

$$\begin{aligned} A_\delta &= A + \begin{bmatrix} -1 \\ b+a \end{bmatrix} \delta \begin{bmatrix} 1 & 0 \end{bmatrix} \\ &= A + B_{k_x}\, \delta\, C_{k_x} \\ G(s) &= C_{k_x} (s\, I - A)^{-1}\, B_{k_x} \end{aligned}$$

Figure 2.9: (A) Changes in the concentrations on the catalyzing enzymes create uncertainty in the parameter k_x. This uncertainty can be modeled by unstructured real perturbations to the transfer function G. (B) Robustness radius shrinks as the controller gain goes up (plotted $a = b = 1$, $k_x = 2$, $q = 2$, $k_y = r_y = 1$)

concentrations of the catalyzing enzymes. The closed-loop system is

$$\begin{aligned} \dot{\mathbf{x}} &= \begin{bmatrix} -(k_x + \delta) & \frac{1}{b} r_y (q - \hat{h}) \\ (b+a)(k_x + \delta) & -a\frac{1}{b} r_y (q - \hat{h}) - k_y \end{bmatrix} \mathbf{x} \\ &= \left(\begin{bmatrix} -k_x & \frac{1}{b} r_y (q - \hat{h}) \\ (b+a) k_x & -a\frac{1}{b} r_y (q - \hat{h}) - k_y \end{bmatrix} + \begin{bmatrix} -1 \\ b+a \end{bmatrix} \delta \begin{bmatrix} 1 & 0 \end{bmatrix} \right) \mathbf{x} \\ &= (A + B_{k_x} \delta C_{k_x})\, \mathbf{x} \end{aligned}$$

The robustness radius R_{k_x} is a measure of how much perturbation the system can tolerate before it goes unstable. For this system we can calculate R_{k_x} by examining the μ-values of the transfer function

$$G_{k_x}(s) = C_{k_x} (sI - A)^{-1} B_{k_x}$$

with scalar real perturbation δ [15] (Figure 2.9). The μ-values of a transfer function $G_{k_x}$with respect to the perturbation δ are defined by

$$\mu_\delta(G_{k_x}(j\omega)) = (\inf \{|\delta|\, | \delta \in \mathbb{R}, \det (I - \delta G_{k_x}(j\omega)) = 0\})^{-1}$$

and the robustness radius R_{k_X} is defined by

$$\begin{aligned} R_{k_x} &= \left(\sup_\omega \mu_\delta \left(G_{k_x}(j\omega)\right)\right)^{-1} \\ &= \min\left\{k_x, k_x + k_y + \tfrac{a}{b}(q-\hat{h})r_y\right\} \end{aligned} \tag{2.12}$$

Given equation (2.12) it is clear that for this perturbation, the robustness radius R_{k_x} shrinks as the controller gain increases (Figure 2.9B). In fact, in this case R_{k_x} is exactly the distance in the x direction to the instability boundary in Figure 2.5A.

Other common perturbations could be fluctuations in feedback $\hat{h}$ as a result of changes in PFK concentration by transcriptional regulation. In this case robust stability radius is exactly the distance in the y direction to the instability boundary in Figure 2.5A.

Similar results hold by looking at other plant uncertainties such as perturbations in autocatalysis q, then $R_q = \min\left\{\frac{1}{b}\left(k_y + \hat{h}r_y - qr_y\right), \frac{1}{b}\left(-\hat{h}r_y + qr_y\right) + \frac{1}{a}\left(k_y + k_x\right)\right\}$, or multiple parameter uncertainties.

Transient Response High performance via high gain will lead to "bad" transient response, as illustrated in Figure 2.8. The DC gain $CA^{-1}B_\delta$ improves with $\hat{h}$ large ($A = A_0 - \hat{h}BC$), however, as the gain $\hat{h}$ increases, the eigenvalues of the closed-loop system approach the imaginary axis. This results in poor transient response (characterized by $CA^{-1}e^{At}B_\delta$) that is characterized by oscillations and slow decay to the steady state.

2.6 Summary

Glycolysis is a prime example of an autocatalytic metabolic pathway. Such pathways are hard to control because of inherent instabilities and limitations imposed on performance by the structure of autocatalysis. Performance is defined as the ability of the control mechanisms to maintain glycolysis close to its standard biological operating point in the presence of disturbances and plant uncertainty. The existence of a RHP zero is a result of the structure of autocatalysis and controls in the pathway and is

	Parameter Choice	Pros	Cons	Comment
Plant Design	Large k_x	Hard limits on performance imposed by RHP zero at $z = \frac{b}{a}k_x$ are softened by making z big	Energetically wasteful since requires the maintenance of a high number of enzymes	RHP zero is a consequence of the structure of autocatalysis and unavoidable
	Large $\frac{b}{a}$		Requires complex machinery, high maintenance, introduces new fragilities	
Controller Design	High $\hat{h}$	Improved performance at low frequencies, smaller steady state error	Increased fragility as system is pushed close to a singularity	RHP zero forces a bound on how aggressive the control can be.
			Poor transient behavior, oscillatory and big overshoots	

Table 2.2: The structure of glycolysis imposes hard constraints on design and performance. Such constraints might manifest themselves in the form of tradeoffs. We believe these tradeoffs are not unique to glycolysis, but appear in all autocatalytic pathways.

at the core of many of the limitations imposed. This RHP zero is responsible for the existence of a conservation law, which is mathematically described by a special form of the Bode Sensitivity Integral (Equation(2.9)). This law imposes hard limits on the sensitivity function S. S is closely related to the performance objectives mentioned above, since it measures the sensitivity to a large class of disturbances. In addition, the consequences of this law are manifested in terms of the tradeoffs summarized in Table (2.2).

It is hypothesized that oscillations in glycolysis might be a result of these tradeoffs. For example, the control mechanism might operate in a regime where the pathway has close to optimal performance for the common operating conditions described by a safe set in parameter space. However, this might put the controller gain close to a set in parameter space, for which the control is too aggressive. The plant normally avoids the unsafe set, except for a few rare events. In those rare events, instabilities are exhibited in the form of oscillations in ATP concentration. This proximity to the

unsafe set for high performance feedback gains is unavoidable and a consequence of the aforementioned conservation law that arises from the structure of the autocatalytic pathways.

Chapter 3

Nonlinear Properties of the 2D Model

3.1 Introduction

In Chapter 2 the characteristics of glycolysis along with its control system near the normal operating point were studied. It is also of interest to develop an understanding of the system behavior away from that equilibrium point as well as to obtain a more global picture of the system.

It has been experimentally observed that there are oscillations of the ATP concentration in glycolysis [31, 24, 14], and it was demonstrated herein that aggressive feedback provides a plausible hypothesis for these oscillations. How big do these oscillations get?

We classify as crashes all the cases that lead to the concentration of ATP going to zero, since this would certainly lead to cell death. In this framework one can study the following questions; Do oscillations in ATP concentration lead to crashes in the pathway? Does glycolysis, as modeled in (2.3), ever crash? Does the ATP concentration ever blow up?

Linear analysis showed that negative feedback via product inhibition stabilizes glycolysis. However changes in the concentration of catalyzing enzymes during the lifetime of the cell lead to changes in the reaction rates $g_x(x)$ (Equation (2.3)), and these changes will perturb the system from the equilibrium point. With these changes in the cell's operating conditions two questions naturally arise; Can the controller restore the system to normal operating conditions from these perturbations? How big

can these perturbations from equilibrium be before the system crashes? In essence we are asking questions regarding the size of the region of attraction of the equilibrium point.

Definition 3.1: *Region of attraction of a fixed point $x^* \in \mathbb{R}^n$ with respect to the flow $\phi(x,t)$ is defined as the set $\Omega = \{x_0 \in \mathbb{R}^n \mid \lim_{t\to\infty} \phi(x_0,t) = x^*\}$.*

To address these region of attraction questions we will use the general form of the 2D model (2.3) introduced in Chapter 2, with $f(y) = \frac{Vy^q}{1+\gamma y^h}$. For simplicity we consider the case $a = b = 1$ (the results easily generalize to any $a, b > 0$). The resulting 2D model is

$$\begin{aligned} \dot{x} &= \frac{Vy^q}{1+\gamma y^h} - g_x(x) \\ \dot{y} &= 2g_x(x) - \frac{Vy^q}{1+\gamma y^h} - g_y(y) \end{aligned} \tag{3.1}$$

for $(x,y) \in \mathbb{R}^+ \times \mathbb{R}^+$, where $g_x(0) = 0$, $g_y(0) = 0$, and $g_x(x)$ and $g_y(y)$ are continuous monotone increasing functions on the positive orthant. These constraints on g_x and g_y are consistent with large classes of chemical kinetics models such as mass-action and Michaelis-Menten. The function $f(y) = \frac{Vy^q}{1+\gamma y^h}$ is the rate of the autocatalytic reaction and captures the negative feedback of ATP (y) via the inhibition of the catalyzing enzyme, PFK, of this reaction; therefore it is of particular interest. The strength of this feedback, $\hat{h} = \frac{\gamma}{\gamma+1}h$, defined in Chapter 2, is captured by the parameters γ and h and depends on the strength of chemical interaction between PFK and ATP that causes allosteric changes to PFK. Figure 3.1 illustrates both how γ and h affect the reaction rate of the autocatalytic reaction and how they change the strength of feedback at equilibrium (slope of f at y).

The fixed points for the dynamics in (3.1) are determined by the solutions of $f(y) = g_y(y)$ and $f(y) = g_x(x)$. In Chapter 2 we showed that at the equilibrium point the slope of $f(y)$ being smaller than the slope of $g_y(y)$ is necessary for stability. We will assume that such minimal feedback is present in the system and $\nu(y) := g_y(y) - f(y) > 0$ and monotone for $y > y_0$, where y_0 is the value of y at the aforementioned

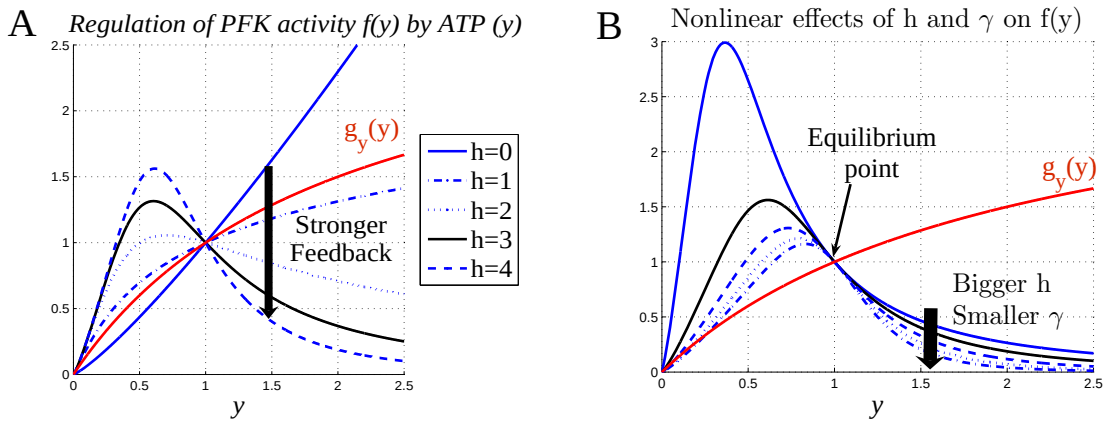

Figure 3.1: The strength of the autocatalytic reaction will depend on activity of the catalyzing enzyme $f(y)$. (A) Increasing the strength of product inhibition stabilizes the equilibrium point by shaping $f(y)$. It has been shown experimentally that PFK activity as a function of ATP has the same general features as $f(y)$ shown in black ([9], [4]). (B) Different γ and h combinations yield the same feedback strength at the equilibrium point ($\hat{h}$), but have very different global characteristics.

equilibrium point. Finally we will also assume that

$$\sup_{x>0} g_x(x) > \sup_{0<y<y_0} \frac{V y^q}{1+\gamma y^h}.$$

This condition guarantees the existence of a fixed point in the strict positive orthant if $y_0 > 0$ (i.e., $x_0 = g_x^{-1}(f(y_0))$ exists).

The special structure of continuous-time dynamical systems in $\mathbb{R}^2$, such as (3.1), enables the use of many tools, for its analysis that are not applicable to higher state dimensions. One example is the Poincare-Bendixon theorem, which coupled with uniqueness of the solutions of (3.1) allows one to rule out the existence of limit cycles through the simulation of a single solution trajectory of (3.1). In this chapter we will exploit the special nature of $\mathbb{R}^2$, but also investigate and develop tools that generalize to higher state dimensions, which is the subject of the next chapter. The purpose of the rest of this chapter is twofold.

- Investigate the 2D model, its behavior, its properties and what it teaches us about glycolysis. We use available analysis and control tools (some of them specific to 2D) for this purpose.

- Investigate the available tools. In later chapters we generalize the glycolysis model to incorporate more intermediate reactions etc, increasing the dimension of the state space in the process. We examine those tools that are generalizable to higher dimensions, and use the 2D model to illustrate their properties and limitations.

3.2 Fixed Points, Stability, and Bifurcations

First let us make a few observations. Notice that the direction of flow for (3.1) on the coordinate axes is pointing to the inside of the positive orthant

$$\begin{aligned} x = 0 \quad &\Rightarrow \quad \dot{x} = \frac{Vy^q}{1+\gamma y^h} > 0, \quad \text{for } y > 0 \\ y = 0 \quad &\Rightarrow \quad \dot{y} = 2g_x(x) > 0, \quad \text{for } x > 0 \end{aligned}$$

This means that our domain of interest (the positive orthant) is invariant with respect to the flow of (3.1). From now on we will refer to global properties as properties that hold on the entire positive orthant, unless otherwise stated. Next we prove a lemma that assures the trajectories of (3.1) do not blow up.

Lemma 3.1: *The trajectories of system* (3.1) *are bounded.*

PROOF: For a small $\epsilon > 0$, $\delta_1 > 0$ let

$$\begin{aligned} \beta_0 &:= \inf\left\{y_0 \mid g_y(y) - \tfrac{Vy^q}{1+\gamma y^h} > \delta_1,\ \forall y > y_0\right\} \\ \alpha_0 &:= \epsilon + \inf\left\{x | g_x(x) > \sup_{0<y\leq\beta_0} \tfrac{Vy^q}{1+\gamma y^h}\right\} \\ \delta_2 &:= g_x(\alpha_0) - \sup_{0<y\leq\beta_0} \tfrac{Vy^q}{1+\gamma y^h} \end{aligned}$$

Notice that $\delta_2 > 0$ (g_x is monotone increasing) and $\beta_0, \alpha_0 < \infty$. Define

$$U \ : \ \mathbb{R}^+ \times \mathbb{R}^+ \to \mathbb{R}$$

by

$$U(x,y) = \begin{cases} 2x + y - \beta_0 & y > \beta_0 \\ 2x & y \leq \beta_0 \end{cases}. \tag{3.2}$$

U is a continuous, positive, radially unbounded function on the positive orthant (Figure 3.2). For $y \neq \beta_0$,

$$\begin{aligned} \tfrac{d}{dt}U(x,y) &= \begin{cases} 2\dot{x} + \dot{y} & y > \beta_0 \\ 2\dot{x} & y < \beta_0 \end{cases} \\ &= \begin{cases} \frac{Vy^q}{1+\gamma y^h} - g_y(y) & y > \beta_0 \\ 2\left(\frac{Vy^q}{1+\gamma y^h} - g_x(x)\right) & y < \beta_0 \end{cases} \end{aligned}$$

Consider a level set of U, $U(x,y) = \eta$. For $\eta \geq 2\alpha_0$, we have that

$$y > \beta_0 \Rightarrow \frac{Vy^q}{1+\gamma y^h} - g_y(y) \leq -\delta_1 < 0$$

and

$$\begin{aligned} y < \beta_0,\ U(x,y) \geq 2\alpha_0 \quad &\Rightarrow \quad x \geq \alpha_0 \\ y < \beta_0,\ x \geq \alpha_0 \quad &\Rightarrow \quad \tfrac{Vy^q}{1+\gamma y^h} - g_x(x) \leq -\delta_2 < 0. \end{aligned}$$

So

$$\frac{d}{dt}U(x,y) \leq -\delta < 0$$

for $(x,y) \in \{(x,y) \,|\, U(x,y) \geq 2\alpha_0,\ y \neq \beta_0\}$, where $\delta = \min\{\delta_1, \delta_2\}$. The positive orthant is invariant to the flow, then for any $\eta \geq 2\alpha_0$ the trajectories cannot leave the region

$$D_\eta := \left\{(x,y) \in \mathbb{R}^2 | x \geq 0, y \geq 0, U(x,y) \leq \eta\right\},$$

illustrated by trapezoid $OABC$ in Figure 3.2. Furthermore the discontinuity of the partials of U at $y = \beta_0$ is not critical since for $y = \beta_0$,

$$\dot{y} = 2g_x(x) - f(\beta_0) - g_y(\beta_0) = 2g_x(x) - c_1$$

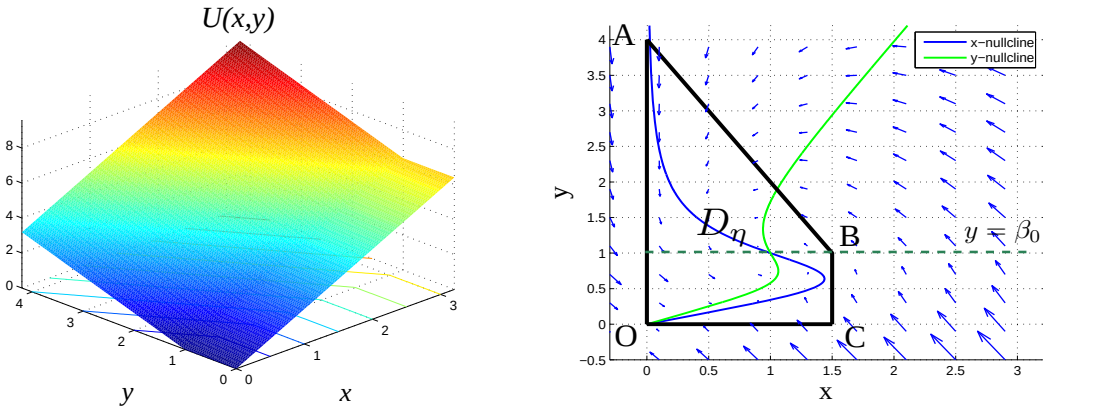

(a) Trapping function U given by (3.1).

(b) Trapping region for 2-d nonlinear glycolysis. Line ABC is the η level set of U.

Figure 3.2: Construction of the trapping region for 2-d nonlinear glycolysis.

and by monotonicity of g_x, for some κ, $\dot{y} > 0$ for $x > \kappa$ and $\dot{y} < 0$ for $x < \kappa$. Since there are no fixed points in

$$D^c_{2\alpha_0} = \{(x, y) \mid x \geq 0,\ y \geq 0,\ U(x, y) > 2\alpha_0\}$$

■

each trajectory that starts in $D^c_{2\alpha_0}$ can cross the line $y = \beta_0$ a maximum of two times (Figure 3.2). So the time the solutions spend on $y = \beta_0$ is negligible. The above argument shows that all trajectories will reach $D_{2\alpha_0}$ exponentially fast.

Remark 3.1: *Another way of constructing the set $D_{2\alpha_0}$ is by consecutive use of two Lyapunov type functions $U_1(x, y) = x$ and $U_2(x, y) = 2x + y$. U_1 will force all the trajectories to reach the invariant set*

$$D_x = \{(x, y) \mid 0 \leq x \leq \alpha_0, y \geq 0\},$$

and U_2 will force the trajectories that start in D_x to reach the invariant set $D_{2\alpha_0}$.

The vast majority of the possible instances of (3.1) are topologically equivalent to one of three instances shown in Figure 3.3, determined by the solutions to $\frac{Vy^q}{1+\gamma y^h} = g_y(y)$. The three instances A, B and C, depicted in Figures 3.3 A, B, and C respectively,

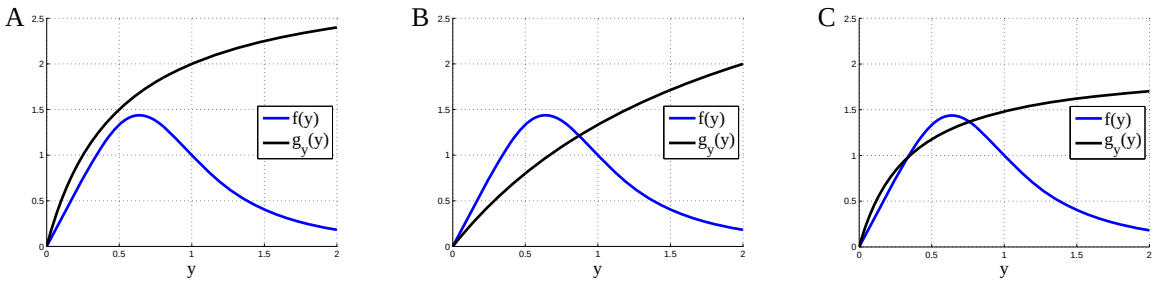

Figure 3.3: The vast majority of the possible models are topologically equivalent to one of three instances, determined by the number of fixed points in the positive orthant. This number is determined by the number of solutions to $\frac{Vy^q}{1+\gamma y^h} = g_y(y)$ as shown in (A), (B) and (C). The three instances A, B and C represent systems that have 1, 2 or 3 equilibrium points in the positive orthant respectively.

can be characterized as having 1, 2 or 3 equilibrium points in the positive orthant respectively. We will consider the case when $g_y(y)$ is tangent to $\frac{Vy^q}{1+\gamma y^h}$ as a special case of instance C, even though it has only 2 fixed points in the positive orthant.

Instance A The pathway is consuming ATP (y) faster than it can produce it, i.e. $g_y(y) > \frac{Vy^q}{1+\gamma y^h}, \forall y > 0$ (Figure 3.3A). The origin is globally asymptotically stable, i.e. all the trajectories go to the origin. This means that the pathway will crash and the cell will die. The cell can avoid this scenario by reducing ATP consumption or increasing ATP production via transcriptional regulation.

Proposition 3.1: *If* $g_y(y) > \frac{Vy^q}{1+\gamma y^h}, \forall y > 0$ *then the fixed point of* (3.1) *at the origin is globally asymptotically stable.*

PROOF: Let us consider the following function $U(x, y) = 2x + y$. U is a Lyapunov function since $U(0, 0) = 0$ and $U(x, y) > 0$ for $x, y \geq 0$, $(x, y) \neq (0, 0)$. U is unbounded and $\dot{U}(x, y) = \frac{Vy^q}{1+\gamma y^h} - g_y(y) < 0$ for $y > 0$. Invariance of the positive orthant and a simple application of LaSalle's theorem prove the asymptotic stability. ■

Instance B There are two fixed points (Figure 3.3B). The origin is a saddle point whose stable manifold not in the positive orthant. The other fixed point in the positive orthant, denoted (x_e, y_e), is a node. In Chapter 2 we discussed how this fixed point (x_e, y_e) can go through a Hopf bifurcation (by increasing the feedback gain)

and gave the conditions for its stability. The next proposition establishes that if the consumption and production of ATP fit the profile of Figure 3.3B, aggressive feedback can make the ATP concentration oscillate but the pathway will not crash.

Proposition 3.2: *If (x_e, y_e) is a linear source and the only equilibrium point of* (3.1) *in the strictly positive orthant, then there exists a globally stable limit cycle.*

PROOF: All the trajectories of (3.1) are bounded in $D_{2\alpha_0}$ (Lemma 3.1) and since no trajectories can go to either of the fixed points in the region, then by the Poincare-Bendixon theorem, there exists a globally stable limit cycle. ■

If (x_e, y_e) is linearly stable, numerical simulation of a single trajectory of (3.1) combined with Lemma 3.1 and the Poincare-Bendixon theorem show that its region of attraction is the whole positive orthant (without the origin).

Definition 3.2: *For two vectors v, $w \in \mathbb{R}^n$, $v = (v_1, \ldots, v_n)$, $w = (w_1, \ldots, w_n)$ we write $v \succ w$ if $v_i > w_i$, $\forall i$, and $v \succeq w$ if $v_i \geq w_i$, $\forall i$.*

Instance C There are three fixed points (Figure 3.3B), a saddle and two nodes. Let $(x_e, y_e) \succ (x_s, y_s) \succ (0, 0)$ be the fixed points. The origin is a stable fixed point, (x_s, y_s) is a saddle and (x_e, y_e) a node. The stability of (x_e, y_e) will depend on the strength of feedback, as discussed in Chapter 2. As the feedback gain increases, a supercritical Hopf bifurcation occurs. Numerical simulations of solutions of (3.1) combined with Lemma 3.1 and the Poincare-Bendixon theorem show the existence of a stable limit cycle in this case (i.e., when high gain destabilizes (x_e, y_e)). Numerically one can show that the stable manifold of the saddle point separates the region of attraction of the origin from the region of attraction of (x_e, y_e) (or the limit cycle when (x_e, y_e) is unstable), as illustrated in Figure 3.4.

The same Lyapunov function $U(x, y) = 2x + y$ that we used before, gives an estimate of the region of attraction of the origin as indicated in Figure 3.4. This estimate is quite conservative, however it generalizes to higher (state space) dimensions. It also highlights an important property of the model: a sufficient condition for the model

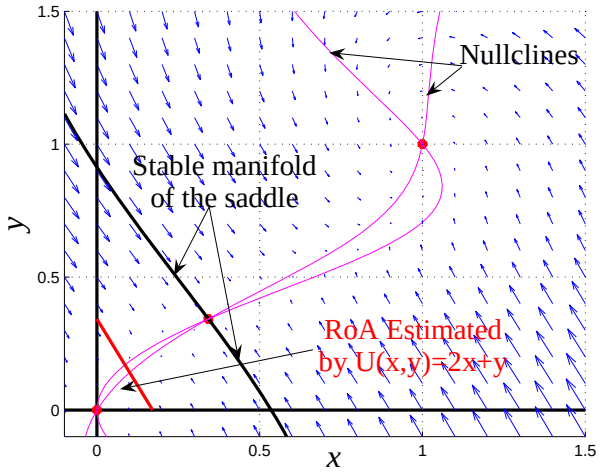

Figure 3.4: Using a simple Lyapunov function we can get an estimate for the region of attraction (RoA) of the origin. The stable manifold of the saddle separates the RoA of the origin from the RoA of $(1, 1)$.

to crash is for the initial concentrations to be in an invariant region of state space where more ATP (y) is consumed then produced by the autocatalysis.

Another important observation made via numerical simulations, is that aggressive feedback can cause crashes. This happens for certain ATP consumption functions $g_y(y)$ that are relatively flat (near saturation) near the fixed point values y_s and y_e. In this case, high feedback gain (h) could increase the size of the limit cycle to the point that it hits the saddle point (Figure 3.5). This creates a homoclinic bifurcation and causes the ATP concentration to go to 0. If this bifurcation happens, then all initial conditions (except for a set of measure zero) would cause the pathway to crash. Unlike the other types of crashes created by imbalance in the levels of consumption and production of ATP (controlled by transcriptional regulation), this type of crash is caused by aggressive allosteric regulation. The following example illustrates this case.

Example 3.1: *In equation* (3.1), *let* $h = 4$, $\gamma = 5$, $q = 2$, $V = 6$, $g_y(y) = \frac{1.2y}{0.2+y}$ *and*

$g_x(x) = kx$ (mass-action kinetics). So we get the following system

$$\begin{aligned} \dot{x} &= \frac{6y^2}{1+5y^4} - kx \\ \dot{y} &= 2kx - \frac{6y^2}{1+5y^4} - \frac{1.2y}{0.2+y} \end{aligned}$$

The equilibrium point of interest is $\left(\frac{1}{k}, 1\right)$. As discussed in Chapter 2, the strength of the negative feedback is determined by h and γ. For $k = 2$, the controller stabilizes the system as shown in Figure 3.5A. If the concentration of the intermediate catalyzing enzyme drops, the reaction rate k will drop as well. If the drop is big enough it will lead to instabilities, such as oscillations or even cause the system to crash. For example cutting the reaction rate in half at $k = 1$ will lead the ATP concentration (y) to oscillate (Figure 3.5B). If the drop is even more drastic, say $k = 0.5$ the oscillations grow much bigger and the system approaches a homoclinic bifurcation, i.e. the limit cycle is close to hitting the saddle point (Figure 3.5C). At $k = 0.4$ the pathway crashes and the cell dies. The limit cycle opens up as a result of the bifurcation and (almost) all trajectories go to the origin as shown in Figure 3.5D.

There are two ways to avoid the scenario in Example 3.1. One way is to use a less aggressive controller, which is less efficient but more robust to changes (as discussed in Chapter 2). The second is for the transcriptional regulation to adapt and adjust $g_y(y)$ (the rate of ATP consumption) and $\frac{Vy^q}{1+\gamma y^h}$ (rate of ATP production) in (3.1) accordingly. This solution requires that the transcriptional regulation act at the same timescale as the drop in enzyme concentration.

Another observation from Example 3.1 is that the equilibrium concentration of the intermediate metabolite (x) depends on the rate of the reaction (k), which depends on the concentration level of the catalyzing enzyme. As such, sudden drops to the level $\tilde{k}$ will cause a perturbation in the x-direction which moves the system a distance $\delta x = \frac{1}{k} - \frac{1}{\tilde{k}}$ from the equilibrium point. How big can this drop be if the system is to continue to converge to equilibrium? To answer this question we need to estimate the region of attraction.

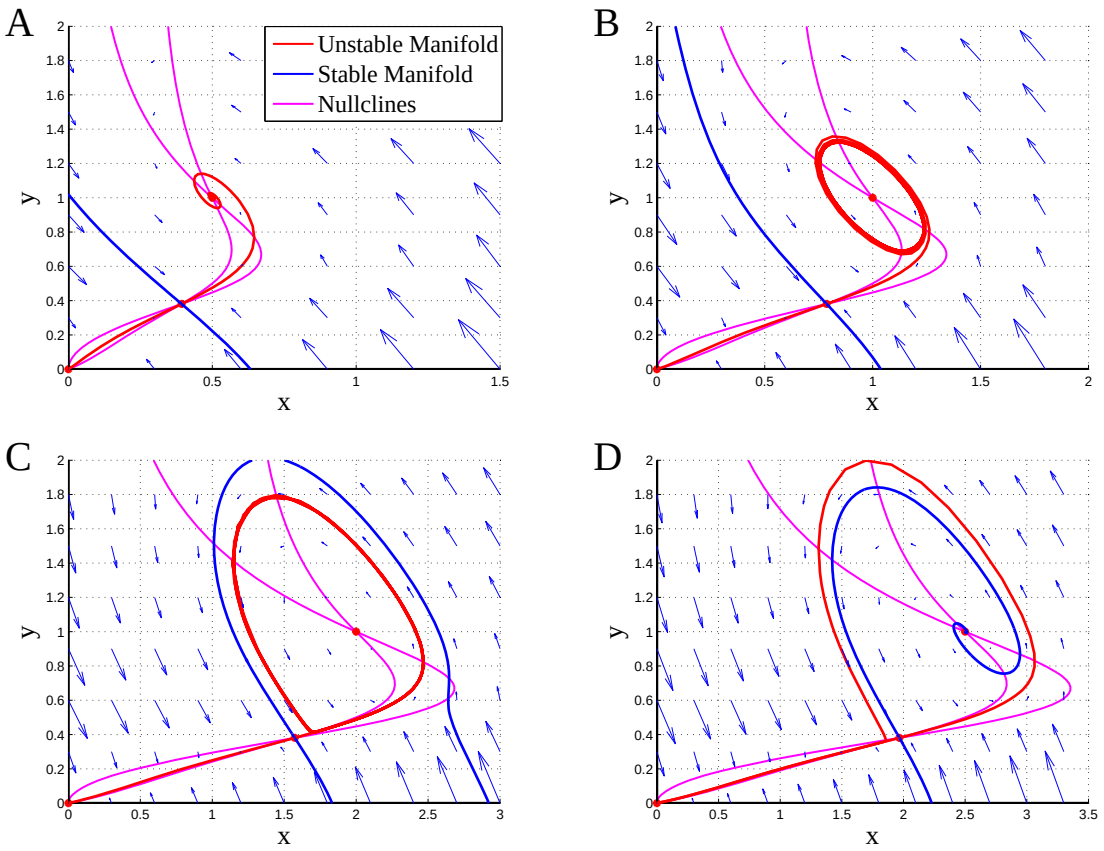

Figure 3.5: Example 3.1.The stable and unstable manifolds of the saddle point are shown in blue and red respectively. Aggressive feedback is stabilizing and efficient under some operating conditions, but fatal under some others. (A) The negative feedback stabilizes the ATP (y) production ($k = 2$). (B) A drop in enzyme concentrations could lead to slowing down the intermediate reaction ($k = 1$), causing the ATP concentration to oscillate. (C) Further slow down of the intermediate reaction ($k = 0.5$) aggravates the oscillations, pushing the system close to a homoclinic bifurcation. (D) The limit cycle grows and hits the saddle point, causing a homoclinic bifurcation. At $k = 0.4$, the system has crashed.

3.3 Region of Attraction Estimation Using Optimization-Based Formulation

If the dynamics are rational functions of the state, we can estimate the region of attraction of the origin for

$$\dot{\mathbf{x}} = F(\mathbf{x}),$$

$\mathbf{x} \in \mathbb{R}^n$ by using Lyapunov functions and Sums of Squares (SOS) programming [21, 27, 26, 44]. In this framework, we search for a polynomial function $U : \mathbb{R}^n \to \mathbb{R}$ satisfying

$$\begin{aligned} U(\mathbf{0}) &= 0 \\ U(\mathbf{x}) &> 0, \quad \mathbf{x} \in \mathcal{N}_0 \backslash \{\mathbf{0}\} \\ -\tfrac{d}{dt} U(\mathbf{x}) &> 0, \quad \mathbf{x} \in \mathcal{N}_0 \backslash \{\mathbf{0}\} \end{aligned} \tag{3.3}$$

in some neighborhood of the origin $\mathcal{N}_0$. One way to define $\mathcal{N}_0$ is by the sublevel sets of a positive definite polynomial function φ with $\varphi(\mathbf{0}) = 0$ and compact level sets, i.e $\mathcal{N}_0 = \Omega_{\varphi,\alpha} = \{\mathbf{x} \in \mathbb{R}^n \mid \varphi(\mathbf{x}) \leq \alpha\}$. Next find the maximum level set of $U(x, y)$ that lies entirely in $\mathcal{N}_0$, i.e., find maximum value of β such that

$$\{\mathbf{x} \mid U(\mathbf{x}) \leq \beta\} \subset \mathcal{N}_0 \tag{3.4}$$

Then $\Omega_{U,\beta} = \{\mathbf{x} \in \mathbb{R}^n \mid U(\mathbf{x}) \leq \beta\}$ is an invariant subset of the region of attraction of the origin [21].

We show here an outline of a procedure (similar to the one developed in [26, 40]) to estimate the region of attraction of the origin. Using generalizations of the S-procedure [7], the above problem is relaxed to a polynomial problem, translated into a semidefinite programming (SDP) problem using sums of squares (SOS) relaxations [27] and solved using SOSTOOLS [30, 34]. Given φ and degree m of U, we search U and the maximum value of α that satisfies the following SOS conditions

$$\begin{array}{rcl} U(\mathbf{x}) & \in & R_m[\mathbf{x}] \\ U(\mathbf{x}) - \epsilon \mathbf{x}^T\mathbf{x} + s_1(\mathbf{x})(\varphi(\mathbf{x}) - \alpha) & \text{is} & SOS \\ \frac{\partial}{\partial \mathbf{x}} U(\mathbf{x}) \cdot F(\mathbf{x}) - \epsilon \mathbf{x}^T\mathbf{x} + s_2(\mathbf{x})(\varphi(\mathbf{x}) - \alpha) & \text{is} & SOS \end{array} \tag{3.5}$$

where $R_m[x]$ is the set of polynomials of degree m, and s_1 and s_2 are SOS polynomials of a fixed degree. To find the maximum α, we use a line search algorithm on α and check the feasibility of (3.5) for each α. The corresponding U and α that satisfy (3.5) will satisfy (3.3) with $\mathcal{N}_0 = \Omega_{\varphi,\alpha}$.

Given U, φ, α that satisfy (3.5) we find the maximum value of β that satisfies the following SOS condition

$$s_3(\mathbf{x})(U(\mathbf{x}) - \beta) + s_4(\mathbf{x})(\alpha - \varphi(\mathbf{x})) - 1 \quad \text{is} \quad SOS \tag{3.6}$$

where s_3 and s_4 are SOS polynomials of appropriate degree. To find the maximum β, we use a line search on β and check the feasibility of (3.6) for each β. The corresponding $U, \varphi, \alpha, \beta$ that satisfy (3.6) satisfy (3.4) also, and $\Omega_{U,\beta}$ is an invariant subset of the region of attraction of the origin. To improve the estimate of the region of attraction $\Omega_{U,\beta}$, we can repeat the procedure with $\varphi = U$.

We are going to use the procedure above to estimate the region of attraction for each fixed point of the system (3.1). In this section we will use special forms of the reaction reaction rates $g_y(y) = k_y y$ and $g_x(x) = k_x x$. These types of reaction rates appear when mass-action kinetics are used to model the reaction rates. Similar treatment will apply to other types of $g_x(x)$ and $g_y(y)$. Next, we normalize the equation (3.1) so that the concentration of ATP at equilibrium point of interest is 1. *For the rest of the chapter we will assume this normalization.* Finally we shift the fixed point of interest at the the origin $(0, 0)$ by a simple change of coordinates, and after relabeling, the system of (3.1) becomes

$$\begin{array}{rcl} \dot{x} & = & F_x(x, y) \\ \dot{y} & = & F_y(x, y) \end{array} \tag{3.7}$$

for $(x,y) \in \mathcal{D}$, where

$$\begin{aligned} F_x(x,y) &:= k_y \tfrac{(1+\gamma)(y+1)^q}{1+\gamma(y+1)^h} - k_x\left(x + \tfrac{k_y}{k_x}\right) \\ F_y(x,y) &:= 2k_x\left(x + \tfrac{k_y}{k_x}\right) - k_y \tfrac{(1+\gamma)(y+1)^q}{1+\gamma(y+1)^h} - k_y\,(y+1) \\ \mathcal{D} &:= \left\{(x,y) \in \mathbb{R}^2 | (x,y) \geq (-\tfrac{k_y}{k_x}, -1)\right\} \end{aligned}$$

In the case when h, q are integers we can convert (3.7) into a polynomial vector field by the following simple transformation. Let

$$\begin{aligned} H(y) &:= 1 + \gamma\,(y+1)^h \\ G_x(x,y) &:= F_x(x,y)H(y) \\ G_y(x,y) &:= F_y(x,y)H(y) \end{aligned}$$

and define the vector field G by

$$\begin{pmatrix} \dot{x} \\ \dot{y} \end{pmatrix} = \begin{pmatrix} G_x(x,y) \\ G_y(x,y) \end{pmatrix} \tag{3.8}$$

Lemma 3.2: *Let $\Omega_{U,\beta} = \{(x,y) \mid U(x,y) \leq \beta\}$ with $U(x,y)$, β satisfying conditions* (3.3) *and* (3.4) *for* (3.8) *be an invariant subset of the region of attraction of the origin for* (3.8)*, then $\tilde{\Omega}_\beta = \Omega_\beta \bigcap \mathcal{D}$ is an invariant subset of the region of attraction of the origin for* (3.7)*.*

PROOF: Let $\mathcal{L}_F$ be the Lie derivative with respect to vector field F defined by (3.7) and $\mathcal{L}_G$ the Lie derivative with respect to vector field G defined by (3.8). Then

$$\begin{aligned} \mathcal{L}_F U(x,y) &= \frac{\partial U}{\partial x} F_x(x,y) + \frac{\partial U}{\partial y} F_y(x,y) \\ &= \frac{1}{H(y)}\left(\frac{\partial U}{\partial x} G_x(x,y) + \frac{\partial U}{\partial y} G_y(x,y)\right) \\ &= \frac{1}{H(y)} \mathcal{L}_G U(x,y) \end{aligned}$$

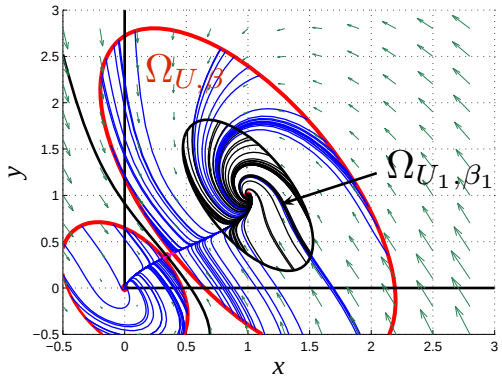

Figure 3.6: The final estimates of the region of attraction of the fixed points using a second order polynomial as a Lyapunov function are shown in red. The intermediate estimated $\mathcal{R}_{\gamma_1}$ of the region of attraction of fixed point $(1,1)$ is also shown as well as sample trajectories of the system. The stable manifold of the saddle (shown in black) separates the region of attraction's of the two fixed points.

For $(x,y) \in \mathcal{D}$, $H(y) > 1 > 0$ and

$$-\mathcal{L}_F U(x,y) = -\frac{1}{H(y)} \mathcal{L}_G U(x,y) > 0.$$

Therefore $U(x,y)$ satisfies (3.3) for system (3.7) in the domain $\Omega_{\varphi,\alpha} \bigcap \mathcal{D}$. Since $\mathcal{D}$ is invariant with respect to the flow of (3.7) then $\tilde{\Omega}_\beta = \Omega_\beta \bigcap \mathcal{D}$ is an invariant subset of the region of attraction. ■

Lemma 3.2 implies that we can get an estimate of the region of attraction of (3.7) by solving (3.3) and (3.4) for the vector field (3.8). If h and q are integers, then the constraints in (3.3) and (3.4) are polynomial constraints and as such we can use the procedure described above.

The next two examples illustrate the procedure and some of its limitations.

Example 3.2: *Let $V = 3$, $h = 4$, $q = 2$, $\gamma = 2$, $g_x(x) = x$ and $g_y(y) = y$ in (3.1). We estimate the region of attraction of the fixed points.*

Let us look at the fixed point at $(1,1)$ first. We shift this fixed point to the origin.

The resulting vector field is

$$\begin{aligned}\dot{x} &= \frac{3(y+1)^2}{1+2(y+1)^4} - 1 - x \\ \dot{y} &= 2x - \frac{3(y+1)^2}{1+2(y+1)^4} - y + 1\end{aligned}$$

for $(x,y) \in \mathcal{D} = \{(x,y) \in \mathbb{R}^2 \mid (x,y) \geq (-1,-1)\}$. *First we define*

$$\mathcal{N}_0 = \Omega_{x^2+y^2,\alpha} = \left\{(x,y) \in \mathbb{R}^2 | x^2 + y^2 \leq \alpha\right\}$$

and search for a second degree polynomial $U_1(x,y)$, *and a maximum value* α_{max} *that satisfy* (3.3) *for the corresponding polynomial vector field*

$$\begin{aligned}\dot{x} &= 3\left(y+1\right)^2 - \left(1+x\right)\left(1+2\left(y+1\right)^4\right) \\ \dot{y} &= -3\left(y+1\right)^2 + \left(2x-y+1\right)\left(1+2\left(y+1\right)^4\right).\end{aligned}$$

Next we find β_1 *by solving* (3.4) *for* $\mathcal{N}_0 = \Omega_{x^2+y^2,\alpha_{max}}$. *The resulting sublevel set* Ω_{U_1,β_1}, *with* $U_1(x,y) = 2.3842x^2 + 1.9118xy + y^2$ *and* $\beta_1 = 0.4098$, *is an estimate of the region of attraction of* $(1,1)$. *In order to improve this estimate we repeat the process with* $\mathcal{N}_0 = \Omega_{U_1,\beta_1}$. *After this iteration, the final estimate is* $\Omega_{U,\beta}$ *with* $U(x,y) = 2.3004x^2 + 2.001xy + y^2$, $\beta = 1.8463$. *Both estimates* Ω_{U_1,β_1} *and* $\Omega_{U,\beta}$ *of the region of attraction of* $(1,1)$ *as well as an estimate of the region of attraction of the origin obtained using quadratic Lyapunov functions are shown in Figure 3.6.*

We can improve the estimates on the region of attraction by using higher order polynomials as Lyapunov functions. However singularities (fixed points nearby) and the nature of the level sets near U limit how big the estimates can be.

Example 3.3: *Estimate regions of attraction of the fixed point at* $y = 1$ (3.1) *for*

(A)$V = 3$, $h = 6$, $q = 1$, $\gamma = 1$, $g_x(x) = 1.2x$ *and* $g_y(y) = y$

(B)$V = 3$, $h = 6$, $q = 2$, $\gamma = 2$, $g_x(x) = 1.1x$ *and* $g_y(y) = y$

Estimates, found using polynomial Lyapunov functions of different degree, are shown in Figure 3.7. In both cases the closest fixed point provides a limit on the maximum size of the region of attraction estimate.

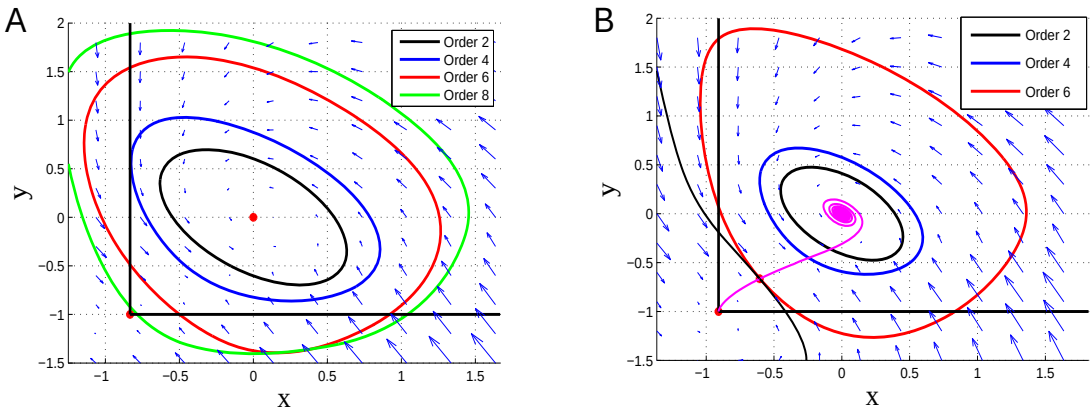

Figure 3.7: Higher degree polynomial Lyapunov functions improve the estimated region of attraction, but this improvement is limited by how close the next fixed point is.

It should be mentioned that using higher order Lyapunov functions is more computationally expensive and can be numerically unstable. Although it is not evident in the examples shown in Figure 3.7, in many cases the higher order region of attraction estimate may be worse than a lower order one, because of numerical issues and complexity associated level sets of higher order polynomials.

3.3.1 Verifying Robustness to Perturbations of Initial Conditions

Robustness to perturbation in initial conditions is closely related to the size of the region of attraction for a particular fixed point. Performance measures that capture the amount and type of perturbations from the fixed point that the system can recover from can be translated into verifying certain properties of the region of attraction of that fixed point. For instance, distance from the boundary of the region of attraction gives us a measure δ of the maximum perturbations in any direction from the fixed point that the system can tolerate and be able to recover from. An associated performance criteria would be given by requiring δ to be above a certain threshold θ. If one is interested in the fixed point $(1, 1)$, then a θ=0.3 implies we need to be able to verify that perturbations of $\delta > 0.3$ will not cause the system to crash. Given our

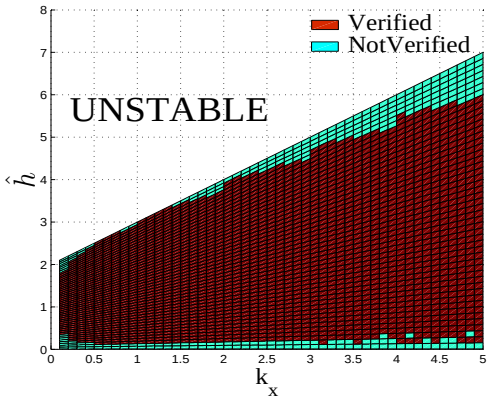

Figure 3.8: Verification of robustness to perturbations in the equilibrium concentrations using a second order polynomial as a Lyapunov function. The horizontal axis is the rate of the intermediate reaction. The vertical axis is the strength of feedback $\hat{h} = \frac{\gamma}{1+\gamma}h$ as defined in Chapter 2. In this example $q = 1$ and $k_y = 1$. $2,500$ different models were investigated and in red are shown the parameter values that define models than can recover from perturbations of 0.3 from the fixed point $(\frac{1}{k}, 1)$ (as much as 30% instantaneous change in ATP concentration.) In blue are shown the models that are stable but we cannot verify such safety margin.

normalization, $\delta > 0.3$ implies that concentration of ATP (y) can drop or increase instantaneously by as much as 30% and the system will still recover. For our glycolysis model (3.7), an invariant subset of the region of attraction with $\delta > 0.3$ can be verified using only a second degree polynomial as a Lyapunov function for most parameter values (Figure 3.8). In fact this observation holds true for many other related performance criteria that relate to the size of the verified region of attraction.

3.3.2 Complexity and Robustness

A system is considered fragile if it is sensitive to perturbations in the parameters, i.e. small perturbations in the parameters destabilize the system. In Chapter 2 we defined and calculated the robustness radius with respect to perturbations in different parameters such as k_x and $\hat{h}$. A small robustness radius with respect to a parameter means the system is fragile to perturbations in that parameter, while a large radius means the system is robust to such perturbations. As expected, calculations of the various robustness radii show that system with parameter values close to the

parameter stability boundary of the system are fragile, while systems with parameter values that fall in the middle of the parameter stability region are robust. One observation from the previous section and Figure 3.8 is that it is simple to verify the safety margins, described in terms of the size of the region of attraction of the fixed point, for these robust systems.

We will define how complex a system is by the complexity of the vector field in the neighborhood of the operating equilibrium point. One way measuring this type of complexity is by the degree of the smallest degree polynomial Lyapunov function needed to verify that a set $\mathcal{B}$ is a subset of the region of attraction. The higher the degree of that polynomial, the more complex the system is. For example we will look at the system (3.7) with $q = 1$ and time-scaled so that $k_y = 1$

$$\begin{aligned} \dot{x} &= \frac{(1+\gamma)(y+1)}{1+\gamma(y+1)^h} - 1 - k_x x \\ \dot{y} &= 2k_x x - \frac{(1+\gamma)(y+1)}{1+\gamma(y+1)^h} + 1 - y \end{aligned} \tag{3.9}$$

in the domain $\mathcal{D} = \left\{(x,y) \in \mathbb{R}^2 | (x,y) \geq (-\frac{1}{k_x}, -1)\right\}$. For a given fixed k_x, the models generated by the different choices in γ, h have the same topology in $\mathcal{D}$, i.e., they only have fixed points at $(-\frac{1}{k_x}, -1)$ and $(0,0)$. For γ, h choices that produce a linearly stable fixed point at the origin, we can show that the region of attraction is the entire domain $\mathcal{D}$ without the point $(-\frac{1}{k_x}, -1)$. For each k_x, we define the set

$$\mathcal{B}_{k_x} := \left\{ (x,y) \mid \left(x^2 + y^2\right)^{1/2} < \frac{1}{2}\sqrt{1 + \frac{1}{k_x^2}} \right\}, \tag{3.10}$$

i.e. the ball of radius half the distance to the next fixed point $(-\frac{1}{k_x}, -1)$. By fixing k_x and varying $\hat{h} = \frac{\gamma}{\gamma+1}h$ we use second and forth degree polynomial Lyapunov functions to verify $\mathcal{B}_{k_x}$ is a subset of the region of attraction. For the same k_x we use the same h and adjust γ accordingly, to make sure that the order of the vector field is not a factor. Additionally, to be more complete in the search for the appropriate Lyapunov functions, we further optimize the Lyapunov function we get from solving (3.3) and (3.4) using coordinate-wise affine iterations (CWAI) [41]. Given an initial guess U

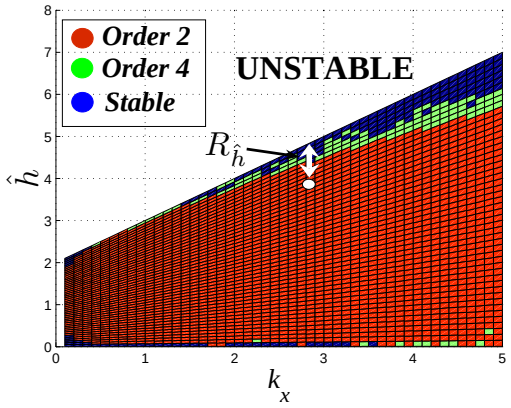

Figure 3.9: The set of parameters for which a 2nd degree polynomial can verify that the set $\mathcal{B}_{k_x}$ defined in (3.10) is a subset of the region of attraction of the origin of system (3.9), is shown in red. In green is the set that needed a 4th degree polynomial, and in blue is the set that $\mathcal{B}_{k_x}$ is still a subset of the region of attraction but could not be verified by a 2nd or 4th degree polynomial Lyapunov function.

for the Lyapunov function, CWAI solves a bilinear problem (similar to (3.3), taking $\varphi = U$) by iterating between solving for SOS multipliers and the Lyapunov function U, while maximizing the size of a compact subset of the region of attraction.

We searched for polynomial Lyapunov functions of degree two and four on 2500 different parameter combinations and the results are shown in Figure 3.9. The figure shows that the robust systems (the systems away from the fragilities at the boundaries) are simple, i.e. only need a 2nd order polynomial to verify $\mathcal{B}_{k_x}$is in the region of attraction, while higher order polynomials are required for many of the fragile systems near the boundary.

Generally we are limited by computational power and numerical errors when using higher order polynomials to verify subsets of region of attraction. An alternative way of measuring the type of complexity discussed so far is by fixing the degree of the polynomial Lyapunov function, and comparing the size of the region of attraction verified by that polynomial. The smaller that size, the more complex the system is. To do this we look at the system (3.9), and see what size estimate of region of attraction we can get using a 2nd degree polynomial as a Lyapunov function. As the measure of the size of the region of attraction verified Ω, we will use maximum value

of the radius of the the ball

$$\mathcal{B}(r) := \left\{(x, y) \mid x^2 + y^2 < r^2\right\}$$

such that $\mathcal{B}(r) \subset \Omega$.

2500 different parameter combinations were investigated and the results are shown in Figure 3.10. Again, for the same k_x we used the same h and adjusted γ accordingly, to make sure that the order of the vector field was not a factor. The main observation is that as the feedback strength goes up, and the system gets close to the Hopf bifurcation in the parameter space (small $R_{\hat{h}}$) the radius of the verified region of attraction gets very small. When the system is too close to the critical point of the Hopf bifurcation (how close depends on k) the SOS programming cannot verify anything bigger than numerical error tolerance. This numerical experiment provides evidence that high complexity of this type (characterized by the small size of the verifiable region of attraction) for the system may be an indication of how fragile the system is.

3.4 Analytic Region of Attraction Estimation

We have shown that Lyapunov-type characterizations and SOS and S-procedure based relaxations can provide good numerical estimates for a large class of glycolysis models in 2D. Much of the results could be obtained using "simple", (i.e., second order) Lyapunov functions which naturally leads one to ask whether one can analytically construct Lyapunov functions that are guaranteed to verify the existence of nontrivial region of attraction. For a specific subset of the model space such Lyapunov functions can be constructed by taking advantage of the structure of the system. We perform a change of coordinates on 3.1 so that the fixed point of interest $(x_0, 1)$ is at the origin.

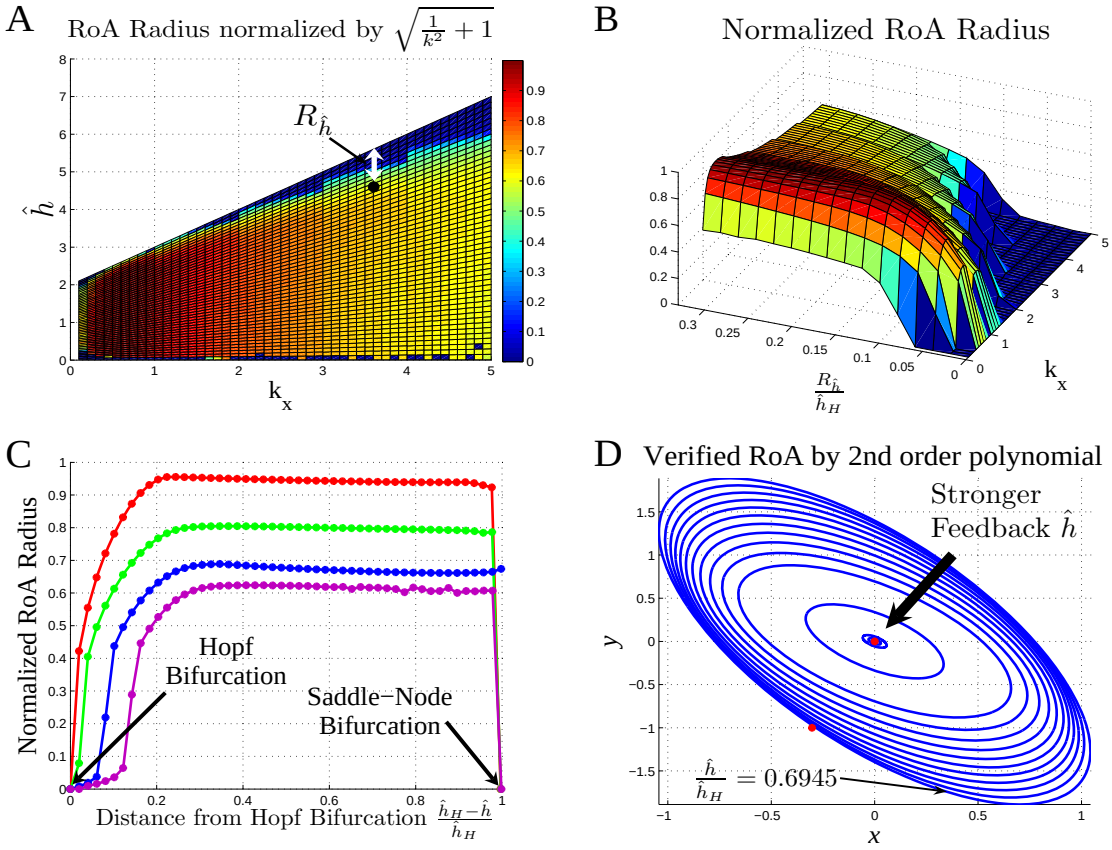

Figure 3.10: Complexity and robustness of glycolysis. (A) 2500 different parameter combinations were investigated. $R_{\hat{h}}$ is the robustness radius with respect to perturbations in the feedback parameter $\hat{h}$. Region of attraction (RoA) radius gets small as $R_{\hat{h}}$ gets small (system is fragile). For the same k_x we used the same h and adjusted γ accordingly, to make sure that the order of the vector field was not a factor. (B) 3-D representation of RoA radius as $\hat{h}$ approaches the Hopf bifurcation. (C) RoA radius normalized by $\sqrt{\frac{1}{k_x^2}+1}$ as a function of the distance of feedback strength $\hat{h}$ from the bifurcation for k_x =1, 2, 3.3, 4.7. (D) Verified RoA for $k_x = 3.3$.

Let the new system be represented by

$$\begin{aligned}\dot{\tilde{x}} &= \tilde{f}(\tilde{y}) - \tilde{g}_x(\tilde{x}) \\ \dot{\tilde{y}} &= 2\tilde{g}_x(\tilde{x}) - \tilde{f}(\tilde{y}) - \tilde{g}_y(\tilde{y})\end{aligned}$$

for $(\tilde{x}, \tilde{y}) \succeq -(x_0, y_0)$. It is easy to see that $\tilde{f}$, $\tilde{g}_x$ and $\tilde{g}_y$ are just shifted versions of f, g_x and g_y and as such preserve many of the important properties, i.e., $\tilde{g}_x$, $\tilde{g}_y$ are continuous monotone increasing functions, with $\tilde{g}_x(0) = 0$, $\tilde{g}_y(0) = 0$ and $\tilde{f}(0) = 0$. For convenience of notation we will drop the tilde for the reminder of the discussion. For this system let us define

$$\begin{aligned}U(x,y) &:= U_x(x) + U_y(y) \\ U_x(x) &:= 2\int_0^x g_x(\xi)d\xi \\ U_y(y) &:= \int_0^y g_y(\xi)d\xi\end{aligned}$$

$U(x,y)$ is positive definite since $g_x(x)$, $g_y(y)$ are monotone increasing and $U(0,0) = 0$ and satisfies

$$\begin{aligned}\tfrac{d}{dt}U(x,y) &= 2g_x(x)\dot{x} + g_y(y)\dot{y} \\ &= 2g_x(x)\left(f(y) - g_x(x)\right) + g_y(y)\left(2g_x(x) - f(y) - g_y(y)\right) \\ &= 2g_x(x)\left(g_y(y) + f(y)\right) - 2g_x^2(x) - g_y(y)\left(f(y) + g_y(y)\right) \\ &= -2\left(\tfrac{g_y(y)+f(y)}{2} - g_x(x)\right)^2 + \tfrac{1}{2}\left(g_y(y) + f(y)\right)^2 - g_y(y)\left(f(y) + g_y(y)\right) \\ &= -2\left(\tfrac{g_y(y)+f(y)}{2} - g_x(x)\right)^2 - \tfrac{1}{2}\left(g_y^2(y) - f^2(y)\right).\end{aligned}$$

Consequently, if

$$D_y := \left\{y \mid g_y^2(y) - f^2(y) > 0\right\}$$

then

$$\tfrac{d}{dt}U(x,y) < 0 \quad \text{for} \quad (x,y) \in \mathbb{R} \times D_y \backslash \left\{(0,0)\right\}.$$

Geometrically the set D_y is the set of points y for which the graph of f lies between the graph of g_y and $-g_y$ (Figure 3.11A) , since by the monotonicity of g_y we have

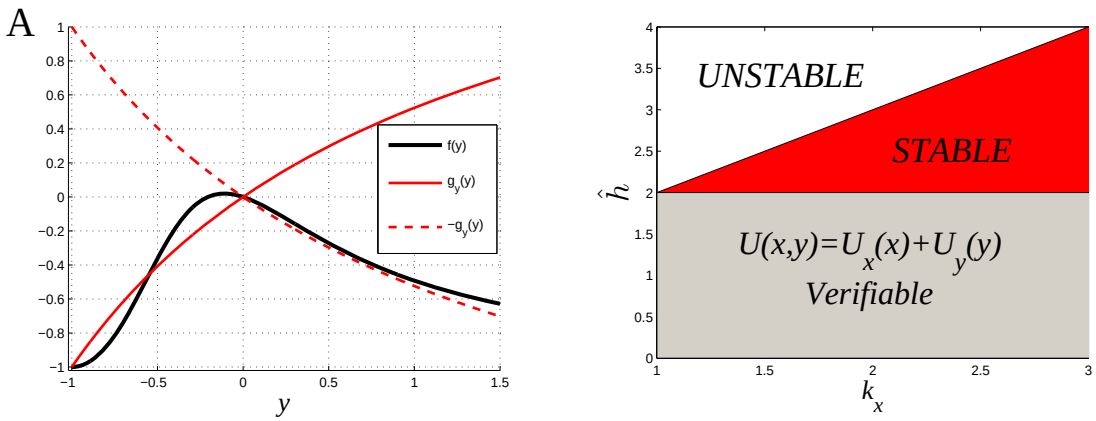

Figure 3.11: The Lyapunov function $U(x,y) = U_x(x) + U_y(y) = 2\int_0^x g_x(\xi)d\xi + \int_0^y g_y(\xi)d\xi$ is used to estimate the region of attraction. (A) $\frac{d}{dt}U < 0$ for the set of points that the graph of $f(y)$ lies between the graph of g_y and $-g_y$. (B) The systems with parameter values for which $U(x,y)$ is guaranteed to verify a nontrivial region of attraction are shown in gray. The horizontal axis is the slope of $g_x(x)$ at the fixed point, and the vertical axis is the strength of feedback $\hat{h} = q + \sigma$, where $-\sigma$ is the slope of $f(y)$ at the fixed point.

the following

$$g_y^2(y) - f^2(y) > 0 \quad \Rightarrow \quad \begin{cases} -g_y(y) < f(y) < g_y(y) & \text{for } y > 0 \\ g_y(y) < f(y) < -g_y(y) & \text{for } y < 0. \end{cases}$$

Let

$$y_M = \sup_y \left\{ y \mid g_y^2(\xi) - f^2(\xi) > 0,\ \forall \xi \text{ s.t. } 0 \le |\xi| \le y \right\}$$

and

$$\mathcal{N}_y = \{ y \mid |y| < y_M \} \subset D_y.$$

We first note that if

$$\sigma = -\frac{\partial}{\partial y} f(y)|_{y=0} < \frac{\partial}{\partial y} g_y(y)|_{y=0} \tag{3.11}$$

then $\mathcal{N}_y$ is nonempty. This class of models is shown in gray in Figure 3.11B. The β sublevel set of U , $\Omega_{U,\beta}$, is an invariant subset of the region of attraction of the origin for $\beta < U_y(y_M)$, since $\frac{d}{dt}U(x,y)$ is negative definite in $\Omega_{U,\beta} \subset \mathbb{R} \times D_y$.

We have shown that $U(x,y)$ can be used to get a nontrivial region of attraction

estimate for systems satisfying (3.11), however have not commented on how conservative this estimate is. In general, this estimate of region of attraction ($\Omega_{U,\beta}$) could be conservative since it is forced to be a subset of the "decoupled" set $\mathbb{R} \times \mathcal{N}_y$. The region of attraction estimate might be improved by solving the following for the given $U(x,y)$

$$\begin{gathered} \max \beta \\ st \\ 2\left(\frac{g_y(y)+f(y)}{2} - g_x(x)\right)^2 + \frac{1}{2}\left(g_y^2(y) - f^2(y)\right) > 0 \\ \text{for all nonzero } (x,y) \in \left\{(x,y)\,|2\int_0^x g_x(\xi)d\xi + \int_0^y g_y(\xi)d\xi \leq \beta\right\}, \end{gathered} \tag{3.12}$$

i.e., we search for the largest sublevel set $\Omega_{U,\beta}$ of the given U such that $\dot{U}(x,y) < 0$ for all nonzero $(x,y) \in \Omega_{U,\beta}$.

Example 3.4: *In* (3.1) *let* $g_x(x) = x$ *and* $g_y(y) = y$. *Let us examine how the estimate of the region of attraction changes for the following feedback/autocatalytic parameters*

A) $h = 3$, $q = 1$, $\gamma = 2$

B) $h = 4$, $q = 2$, $\gamma = 2$

The fixed point of interest is at $(1,1)$. *First we shift this point to the origin by a simple change of coordinates* $x \to x+1$, $y \to y+1$ *to obtain* (3.7), *with* $g_x(x) = x$, $g_y(y) = y$ *and* $f(y) = \frac{3(y+1)}{1+2(y+1)^3} - 1$ *for instance A and* $f(y) = \frac{3(y+1)^2}{1+2(y+1)^4} - 1$ *for instance B. Then for both instances the Lyapunov function is* $U(x,y) = x^2 + \frac{1}{2}y^2$.

In the first instance the graph of $f(y)$ *lies entirely between the graphs of* $-y$ *and* y *for* $y > -1$ *(Figure 3.12A1). This means that for* $\beta = \frac{1}{2}$ *and*

$$\mathcal{R}_\beta = \left\{(x,y)\,|x^2 + \frac{1}{2}y^2 \leq \frac{1}{2}\right\},$$

is a subset of region of attraction. Figure 3.12A2, shows this estimate of region of attraction for the corresponding glycolysis model (3.1) *as the area within the ellipsoid shown in red. Area shown in green is the area where* $\frac{d}{dt}U(x-1,y-1) \geq 0$, *which means that we can improve on* $\mathcal{R}_\beta$ *by solving* (3.12).

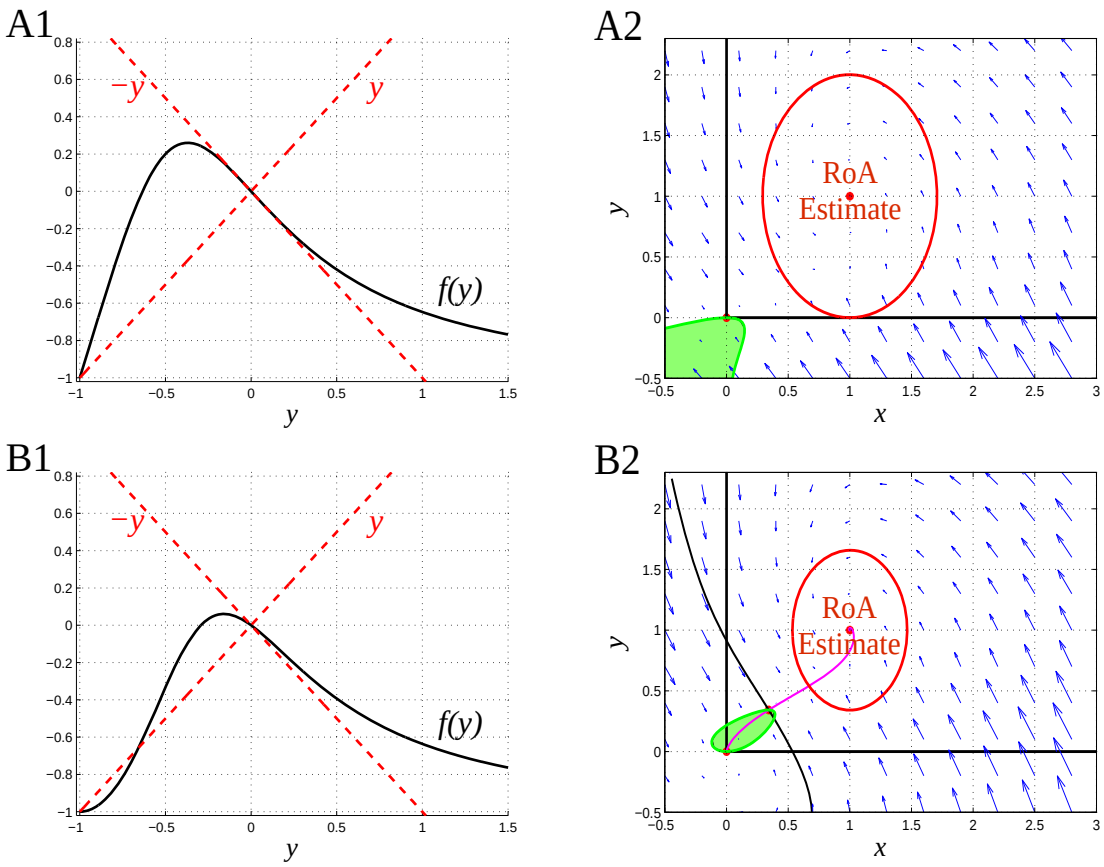

Figure 3.12: The function $U(x, y) = x^2 + \frac{1}{2}y^2$ is a Lyapunov function for both systems in Example 3.4. The sector conditions in A1 and B1 allow for the construction of region of attraction (RoA) estimates shown in red in A2 and B2. This estimates can be improved by solving (3.12), since $\dot{U} < 0$ everywhere but the region shown in green in A2 and B2.

The second case, the graph of $f(y) = \frac{3(y+1)^2}{1+2(y+1)^4} - 1$ *lies entirely between the graphs of* $-y$ *and* y *for* $y > -0.6575$ *(Figure 3.12B1). This means that* $\beta = 0.2161$ *and*

$$\mathcal{R}_\beta = \left\{ (x, y) \, | x^2 + \frac{1}{2} y^2 \leq 0.2161 \right\}.$$

Figure 3.12B2, shows this estimate of region of attraction for the corresponding glycolysis model (3.1) *as the area within the ellipsoid shown in red. Area shown in green is the area where* $\frac{d}{dt} U(x-1, y-1) \geq 0$*, which means that we can again improve on* $\mathcal{R}_\beta$ *by solving* (3.12).

3.4.1 Region of Attraction Estimates and Global Properties of f

How well $U(x, y)$ defined above performs depends not just on the local properties of f at equilibrium, but also on its global properties, specifically the shape of the graph of f. Linear analysis of the fixed point determines the strength of feedback at equilibrium, but it hides the details of how to implement this feedback for better non-local performance (i.e., away from equilibrium). In our model, the same feedback strength $\hat{h} = \frac{\gamma}{\gamma+1} h$ can be achieved by different values of the parameters γ and h, both of which depend on the catalyzing enzyme properties. Specifically $\hat{h}$ uniquely determines the slope of f at the fixed point, and all the local properties of feedback discussed in Chapter 2. However different values of γ would yield systems with more easily verifiable region of attraction than others. The values of γ, h that are the best choice for implementing the controller will depend on non-local performance criteria, like sensitivity to global changes in the curves. For example g_y may change as a result of transcriptional regulation or cell response to environmental changes. The following example illustrates the consequences of different implementations of the same feedback strength.

Example 3.5: *In* (3.1) *let* $g_x(x) = x$*,* $g_y(y) = y$*,* $q = 1$ *and the strength of feedback at the fixed point* $(1, 1)$ *is* $\hat{h} = \frac{\gamma}{\gamma+1} h = 1.8$*. Let B,C and D be three different*

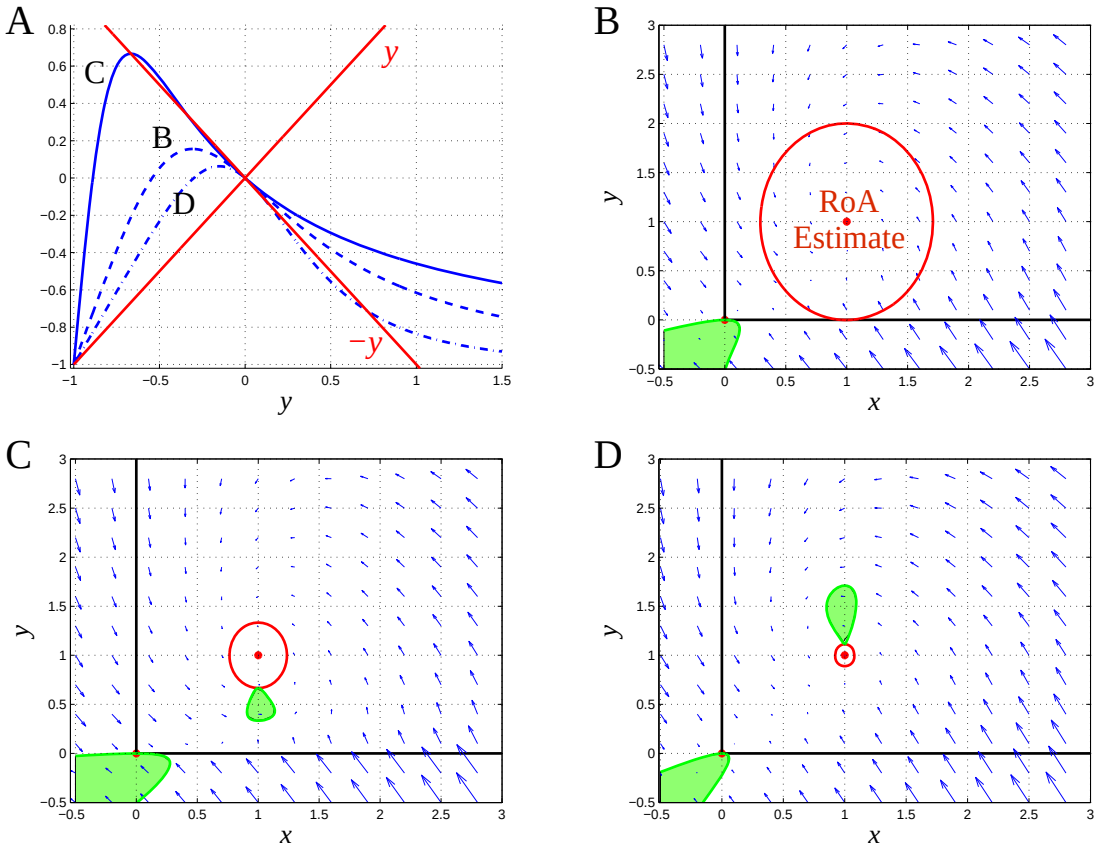

Figure 3.13: Three different implementations of the same feedback strength $\hat{h} = 1.8$ for (3.1) with $g_x(x) = x$, $g_y(y) = y$ and $q = 1$. (A) Different h's and γ's lead to different global properties of the corresponding autocatalytic reaction rate $f(y)$. (B,C,D) Different global properties of f lead to different behavior in the vicinity of the fixed point and different complexities of estimating regions of attraction (RoA) . The area shown in green is the area where the the Lyapunov function used to estimate the RoAs has non-negative time derivative ($\frac{d}{dt}U \geq 0$).

implementations of this $\hat{h}$, where $h_B = 3$, $\gamma_B = 1.5$; $h_C = 2$, $\gamma_C = 9$; and $h_D = 5$, $\gamma_B = 0.5625$. Linearly these 3 implementations are identical, however they have different global (nonlinear) properties of the corresponding autocatalytic reaction rate $f(y)$, as shown in Figure 3.13A. This leads to different behavior in the vicinity of the fixed point and harder to estimate region of attraction for implementations C and D (Figure 3.13).

3.5 Summary

The model described by Equation (3.1) suggests that there are two basic mechanisms that can cause glycolysis to crash; failure of transcriptional regulation or overly aggressive allosteric regulation. The first scenario occurs when the slow transcriptional regulation fails to prevent the system from going into a(n) (invariant) regime where the consumption of ATP (y) is faster than its production. This can be caused by a sudden drop in the input to the system (glucose) or an increase in ATP demand. Either condition causes the system to deplete all of its ATP reserves, which results in all of the concentrations going to zero and thus cell death. The overly aggressive fast allosteric feedback condition can be caused by drops in the catalyzing enzyme concentrations. Most of the time aggressive feedback leads to oscillations in ATP concentration. However, under certain circumstances, if the drops in enzyme concentrations are too severe, the magnitude of oscillations increases to the point that a homoclinic bifurcation occurs causing the pathway to crash.

Analysis of system (3.1) shows that allosteric feedback regulation can suppress the positive feedback generated by autocatalysis, thus guaranteeing both that the trajectories of the system are bounded and that the concentrations do not blow up for any initial conditions, as well as the local stability of the operating fixed point. Simulations of the system show that the region of attraction of the fixed point where the cell operates is large, which means that glycolysis is not sensitive to perturbation in the concentrations of the products and reactants (i.e., perturbation in state space).

If the dynamics of (3.1) are rational functions of the state, the size of the region

of attraction of the fixed point can be estimated by optimization-based formulations using Lyapunov functions and SOS programming. These formulations reveal that low degree polynomial Lyapunov functions can verify region of attraction related properties for a wide range of parameters. For example, systems whose operating point is robustly stable with respect to perturbations in parameter values are simple to verify, i.e., a second degree polynomial Lyapunov function verifies large invariant subsets of the region of attraction of the fixed point. In fact, polynomial Lyapunov functions of degree larger than 2 are only necessary for systems whose parameter values fall close to the stability boundary in the parameter space, which are clearly not robust as small changes in parameters may result in the instability of the fixed point.

We define the complexity of a realization of model (3.1) by the complexity of the vector field in the neighborhood of the operating equilibrium point. We then develop two related approaches of quantifying this view of complexity by using either the smallest order polynomial Lyapunov function needed to verify a specific set as an invariant subset of the region of attraction, or the size of the region of attraction verified by a specific order polynomial Lyapunov function. We compare realizations that are "topologically equivalent", i.e. realizations that have the same number and location of fixed points and the same sizes of region of attraction. This framework reveals that complex systems are fragile, i.e they are very close to instability in parameter space.

Overall, the global analysis of the model described by Equation (3.1) confirms that oscillations and crashes in glycolysis are not caused by perturbations in state space (i.e., perturbations in the concentrations of the products and reactants), but rather perturbations in the parameter space (i.e., catalytic enzyme concentrations, precursors to the pathway, ATP demand, or temperature) as observed in the literature [14, 6, 24, 31, 33, 38]. Furthermore the structure of the equations enables us to analytically construct Lyapunov functions, that are guaranteed to verify a nontrivial region of attraction for a specific subset of the model space. The size of the verified region of attraction depends on the global properties of $f(y)$ (which is the rate of the autocatalytic reaction and captures the strength of feedback), and not just on its

properties near the fixed point.

Chapter 4

Higher Dimensional Model of Autocatalytic Pathways

4.1 Introducing n-D Model

Autocatalytic pathways in general (and specifically glycolysis) are composed of a chain of enzymatically catalyzed intermediate reactions. In the previous chapters we studied the properties of such pathways through a 2D model given in (3.1), which is obtained by collapsing all the intermediate reactions (links in the chain) into a single intermediate reaction (Figure 2.1). In this chapter we consider models that explicitly account for the intermediate reactions. Consider the autocatalytic metabolic pathway with multiple intermediate metabolite reactions

$$u + ay \rightharpoonup^{f} x_1 \rightharpoonup^{g_1} x_2 \rightharpoonup \cdots \rightharpoonup x_n \rightharpoonup^{g_n} (b+a)y$$
$$y \rightharpoonup^{g_y} \varphi.$$

The corresponding ODE (in terms of the stoichiometry matrix and reaction fluxes) is

$$\begin{bmatrix} \dot{x}_1 \\ \dot{x}_2 \\ \vdots \\ \dot{x}_n \\ \dot{y} \end{bmatrix} = \begin{bmatrix} 1 & -1 & & 0 & 0 & 0 \\ 0 & 1 & \ddots & 0 & 0 & 0 \\ \vdots & & \ddots & & \ddots & \vdots \\ 0 & 0 & & 1 & -1 & 0 \\ -a & 0 & \cdots & 0 & b+a & -1 \end{bmatrix} \begin{bmatrix} f(y) \\ g_1(x_1) \\ \vdots \\ g_{n-1}(x_{n-1}) \\ g_n(x_n) \\ g_y(y) \end{bmatrix} \tag{4.1}$$

for $x_i \geq 0$, $y \geq 0$, where for all i, g_i, g_y are continuous, monotone, increasing functions, with $g_i(0) = 0$ and $g_y(0) = 0$, and $f(y) = \frac{Vy^q}{1+\gamma y^h}$ is the same as in the 2D model. As in the 2D case, it is easy to see that the positive orthant is invariant with respect to the flow since (away from the origin)

$$\begin{aligned} x_1 = 0 \quad &\Rightarrow \quad \dot{x}_1 = \frac{Vy^q}{1+\gamma y^h} \geq 0, \\ x_i = 0 \quad &\Rightarrow \quad \dot{x}_i = g_{i-1}(x_{i-1}) \geq 0, \text{ for } 2 \leq i \leq n \\ y = 0 \quad &\Rightarrow \quad \dot{y} = (a+b)\, g_n(x_n) > 0. \end{aligned}$$

Consider the case $a = b = 1$ (the results easily generalize to any $a, b > 0$). Let $0 \leq \bar{y}_1 < \cdots < \bar{y}_l$ be the solutions of $f(y) = g_y(y)$ in the positive orthant. We will assume that $\forall i$,

$$\sup_{x_i > 0} g_i(x_i) > \sup_{0 < y < \bar{y}_l} \frac{Vy^q}{1+\gamma y^h}.$$

This guarantees that there are l fixed points in the positive orthant given by

$$\left(g_1^{-1}\left(f(\bar{y}_j)\right), \ldots, g_n^{-1}\left(f(\bar{y}_j)\right), \bar{y}_j\right), \text{ for } 1 \leq j \leq l.$$

As discussed in Chapter 3 for the 2D counterpart, there are 3 main instances, $l = 1$, $l = 2$, or $l = 3$.

If $l = 1$, then

$$g_y(y) > \frac{Vy^q}{1+\gamma y^h}, \forall y > 0$$

and the only fixed point is at the origin. The behavior of the system is simple, since as in the 2D case, the origin is globally asymptotically stable.

Proposition 4.1: *If* $g_y(y) > \frac{Vy^q}{1+\gamma y^h}, \forall y > 0$ *then the fixed point of* (4.1) *at the origin is globally asymptotically stable.*

PROOF: Let us consider the following function

$$U(x_1, \ldots, x_n, y) = 2\sum_{i=1}^{n} x_i + y.$$

U is positive definite since $U(\mathbf{0}) = 0$ and $U(x_1, \ldots, x_n, y) > 0$ for $x_1, \ldots, x_n, y \geq 0$, $(x_1, \ldots, x_n, y) \neq \mathbf{0}$. U is radially unbounded and

$$\dot{U}(x_1, \ldots, x_n, y) = \frac{Vy^q}{1+\gamma y^h} - g_y(y) < 0$$

for $y > 0$. Invariance of the positive orthant and a simple application of LaSalle's theorem prove the asymptotic stability. ■

As before, this means that if $g_y(y) > \frac{Vy^q}{1+\gamma y^h}, \forall y > 0$ the pathway will crash and the cell will die. It is a consequence of the pathway consuming ATP (y) faster than it can produce. The cell can avoid this scenario by reducing ATP consumption or increasing ATP production via transcriptional regulation.

From this point on we will only consider the cases where $l > 1$. Let $(\bar{x}_1, \ldots, \bar{x}_n, \bar{y}) \succ \mathbf{0}$ be the fixed point of interest, and $k_i = \frac{\partial g_i}{\partial x_i}|_{\bar{x}} > 0$, $k_y = \frac{\partial g_y}{\partial y}|_{\bar{y}} > 0$, $r_y = g_y(\bar{y}) > 0$, $\sigma = -\frac{\partial f}{\partial y}|_{y=\bar{y}}$. *Without loss of generality, for the rest of the chapter we assume that* $\bar{y} = 1$. This implies that $V = r_y(1+\gamma)$, $\sigma = r_y(\hat{h} - q)$ where $\hat{h} = \frac{\gamma}{1+\gamma}h$, and the linearization around the equilibrium point is

$$\begin{bmatrix} \dot{x} \\ \dot{y} \end{bmatrix} = J \begin{bmatrix} x \\ y \end{bmatrix}, \tag{4.2}$$

for $x \in \mathbb{R}^n$, $y \in \mathbb{R}$, where

$$J := \begin{bmatrix} -k_1 & 0 & \cdots & 0 & 0 & r_y(q-\hat{h}) \\ k_1 & -k_2 & & 0 & 0 & 0 \\ & \ddots & \ddots & & \vdots & \vdots \\ 0 & 0 & & -k_{n-1} & 0 & 0 \\ 0 & 0 & & k_{n-1} & -k_n & 0 \\ 0 & 0 & \cdots & 0 & 2k_n & -k_y - r_y(q-\hat{h}) \end{bmatrix}.$$

4.2 Linear Stability

If $\hat{h} > q$, we can apply a secant condition as a sufficient condition for the stability of (4.2) derived by [39, 43]. For (4.2) this secant condition demonstrates that if,

$$\frac{2r_y(\hat{h}-q)}{k_y - r_y(\hat{h}-q)} \quad < \quad \left(\sec \tfrac{\pi}{n+1}\right)^{n+1} \tag{4.3}$$

then (4.2) is stable. Let

$$\theta(n) := \left(\sec \frac{\pi}{n+1}\right)^{n+1},$$

then (4.3) gives an upper bound

$$\hat{h}_d(n) = q + \frac{k_y}{r_y}\frac{\theta(n)}{2+\theta(n)}$$

on the feedback gain $\hat{h}$ that guarantees linear stability. The upper bound $\hat{h}_d(n)$ depends on the pathway size (n), ATP consumption (k_y, r_y) , and the autocatalysis parameters (q), but not on the rate k_i of the intermediate reactions. It also suggests that as the pathway size (n) increases, the maximum allowable stabilizing feedback gain decreases.

The following proposition gives tight bounds on the range of feedback gains that guarantee stability for any pathway size and intermediate reaction rates.

Proposition 4.2: *(a) Let* $\hat{h}_r := q + \frac{1}{3}\frac{k_y}{r_y}$ *and* $\hat{h}_s := q - \frac{k_y}{r_y}$. *If* $\hat{h}_s < \hat{h} \leq \hat{h}_r$, *then* (4.2) *is stable for arbitrary size (n) and arbitrary values of intermediate reaction rates* (k_i).

(b) The bounds above are tight, i.e. for any gain $\hat{h} \notin \left(\hat{h}_s, \hat{h}_r\right]$*, there exists an unstable pathway.*

PROOF: Let

$$Q := \begin{bmatrix} -k_1 & 0 & \cdots & 0 & 0 & 2r_y(q-\hat{h}) \\ k_1 & -k_2 & & 0 & 0 & 0 \\ & \ddots & \ddots & & \vdots & \vdots \\ 0 & 0 & & -k_{n-1} & 0 & 0 \\ 0 & 0 & & k_{n-1} & -k_n & 0 \\ 0 & 0 & \cdots & 0 & k_n & -k_y - r_y(q-\hat{h}) \end{bmatrix},$$

then the Jacobian given in (4.2) satisfies

$$J = \begin{bmatrix} I_n & 0 \\ 0 & 2 \end{bmatrix} Q \begin{bmatrix} I_n & 0 \\ 0 & 2 \end{bmatrix}^{-1},$$

where I_n is the $n \times n$ identity matrix. Consequently J has the same eigenvalues as Q. Since

$$\det J = (-1)^{n+1} \prod_{i=1}^{n} k_i \left(k_y - 3r_y(q-\hat{h})\right)$$

and therefore J has no zero eigenvalues for $\hat{h} \neq q - \frac{k_y}{r_y}$, the stability of Q can be easily shown using diagonal dominance [17]. There are two cases

Case 1: $\hat{h} < q$

The condition for stability is

$$k_y + r_y(q-\hat{h}) > 2r_y(q-\hat{h}) \Leftrightarrow \hat{h} > q - \frac{k_y}{r_y} = \hat{h}_s.$$

Case 2: $\hat{h} > q$

The condition for stability is

$$k_y + r_y(q-\hat{h}) \geq -2r_y(q-\hat{h}) \Leftrightarrow \hat{h} \leq q + \frac{1}{3}\frac{k_y}{r_y} = \hat{h}_r.$$

(b) For $\hat{h} \leq \hat{h}_s$, unstable systems can be constructed as in the 2D case (Chapter 2). In order to construct an unstable system for $\hat{h} > \hat{h}_r$, let $\epsilon > 0$, $\hat{h} = \hat{h}_r + \epsilon$ and for all i

$$k_i = k_y + r_y\left(q - \hat{h}\right) = \frac{2}{3}k_y - \epsilon r_y = k > 0.$$

The characteristic polynomial of (4.2) is

$$\begin{aligned} p_J(s) &= \left(s + k_y + r_y\left(q - \hat{h}\right)\right)\prod_{i=1}^{n}(s + k_i) - 2r_y\left(q - \hat{h}\right)\prod_{i=1}^{n} k_i \\ &= (s+k)^{n+1} - k^n\left(2r_y\left(-\tfrac{1}{3}\tfrac{k_y}{r_y} - \epsilon\right)\right) \\ &= (s+k)^{n+1} - k^n\left(-\tfrac{2}{3}k_y - 2\epsilon r_y\right) \\ &= (s+k)^{n+1} + k^n\left(k + 3\epsilon r_y\right) \end{aligned}$$

Eigenvalues λ_i are the roots of the polynomial $p_J(s)$, so $\lambda = k(\omega - 1)$ such that

$$\omega^{n+1} = \left(-1 - 3\epsilon\tfrac{r_y}{k}\right)^{1/(n+1)} = \left(-1 - \epsilon_1\right)^{1/(n+1)}$$

where $\epsilon_1 := 3\epsilon\frac{r_y}{k}$. The real part of the eigenvalues λ_i, $0 \leq i \leq n$ is

$$\Re(\lambda_i) = k\left(-1 + (1+\epsilon_1)^{1/(n+1)}\cos\left(\frac{\pi}{n+1} + \frac{2\pi i}{n+1}\right)\right)$$

Let

$$\begin{aligned} \gamma(n) &= (1+\epsilon_1)^{1/n}\cos\tfrac{\pi}{n} \\ &= 1 + \tfrac{1}{n}\log(1+\epsilon_1) + O(\tfrac{1}{n^2}). \end{aligned}$$

This implies that the system is unstable since for n big enough

$$\gamma(n) > 1 \;\Rightarrow\; \Re(\lambda_0) > 0.$$

■

Remark 4.1: *For general stoichiometry of autocatalysis (i.e. $a > 0$, $b > 0$ in (4.1)) $\hat{h}_r = q + \frac{b}{2a+b}\frac{k_y}{r_y}$ and $\hat{h}_s = q - \frac{k_y}{r_y}$.*

A couple of observations

- $\hat{h}_r = \lim_{n\to\infty}\hat{h}_d(n)$

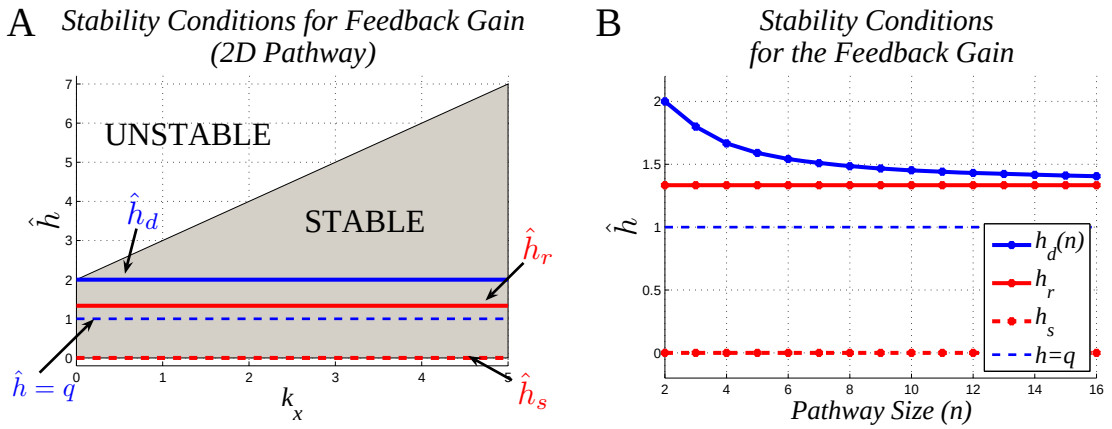

Figure 4.1: (A) The stability conditions for a 2D model with $q = 1$, $k_y = 1$ for general feedback strength $\hat{h}$ and intermediate reaction rate k_x. The gray area marks the set of parameters that define stable systems. The area between the blue lines corresponds to systems that can be verified to be stable using the secant condition (4.3). The area between the red lines corresponds to systems that can be verified using the bounds from Proposition 4.2. (B) As the pathway size increases, the upper bound on the feedback strength $\hat{h}$ given by the secant condition gets smaller.

- The bounds $\hat{h}_s$, $\hat{h}_r$ on $\hat{h}$ are robust to changes in the rate and number of intermediate reactions, since they depend on the stoichiometry and strength of autocatalysis (a, b, q), and the demand of ATP (k_y, r_y), but not on the other parameters.

Proposition 4.2 states that the goal of stability for evolvable pathways with "fixed" autocatalysis and ATP consumption curves is achievable. Both the secant condition bound $\hat{h}_d$ and $\hat{h}_r$ are conservative, especially for high intermediate reaction rates as Figure 4.1A illustrates, since they provide robustness to intermediate reaction rate fluctuations. Later in this chapter we will revisit these bounds.

4.3 Performance

As in Chapter 2, performance is defined as the ability of the control mechanisms to maintain the pathway close to its standard biological operating point in the presence of disturbances and plant uncertainty. We saw in Chapter 2 that performance as defined above can be best analyzed in the frequency domain, since many of the performance

criteria are captured by the sensitivity function S. It should be noted that comparing pathways of different sizes is possible because of the normalization of the steady state value of the output (to 1). Since we are interested in maintaining the concentration of the output of the pathway y at a desired steady state value, such normalization and performance comparison is appropriate.

In standard output feedback control form, (4.2) becomes

$$\begin{aligned} \dot{\mathbf{x}} &= A\mathbf{x} + Bu \\ z &= C\mathbf{x} \\ u &= -\hat{h}C\mathbf{x} \end{aligned}$$

where

$$\begin{aligned} A &= \begin{bmatrix} -k_1 & 0 & \cdots & 0 & r_y q \\ k_1 & -k_2 & & 0 & 0 \\ \vdots & & \cdots & & \vdots \\ 0 & 0 & & -k_n & 0 \\ 0 & 0 & \cdots & 2k_n & -k_y - r_y q \end{bmatrix} \\ B &= r_y \begin{bmatrix} 1 & 0 & \cdots & 0 & -1 \end{bmatrix}^T \\ C &= \begin{bmatrix} 0 & 0 & \cdots & 0 & 1 \end{bmatrix}. \end{aligned}$$

Then

$$\begin{aligned} P(s) &= C\left(sI - A\right)^{-1} B \\ &= r_y \frac{\prod_{i=1}^{n}(k_i+s) - 2\prod_{i=1}^{n} k_i}{(k_y+qr_y+s)\prod_{i=1}^{n}(k_i+s) - 2qr_y\prod_{i=1}^{n} k_i}. \end{aligned} \tag{4.4}$$

The coefficients of the numerator

$$\begin{aligned} n_1(s) &= \prod_{i=1}^{n}(k_i+s) - 2\prod_{i=1}^{n} k_i \\ &= s^n + (k_1 + \cdots + k_n)\, s^{n-1} + \cdots + (-\prod_{i=1}^{n} k_i) \end{aligned}$$

of $P(s)$ do not have the same sign. This means that the polynomial $n_1(s)$ is not Hurwitz stable and therefore $P(s)$ has at least one zero in the right half-plane (RHP). This implies that the special form of the Bode sensitivity integral (2.9) holds for the

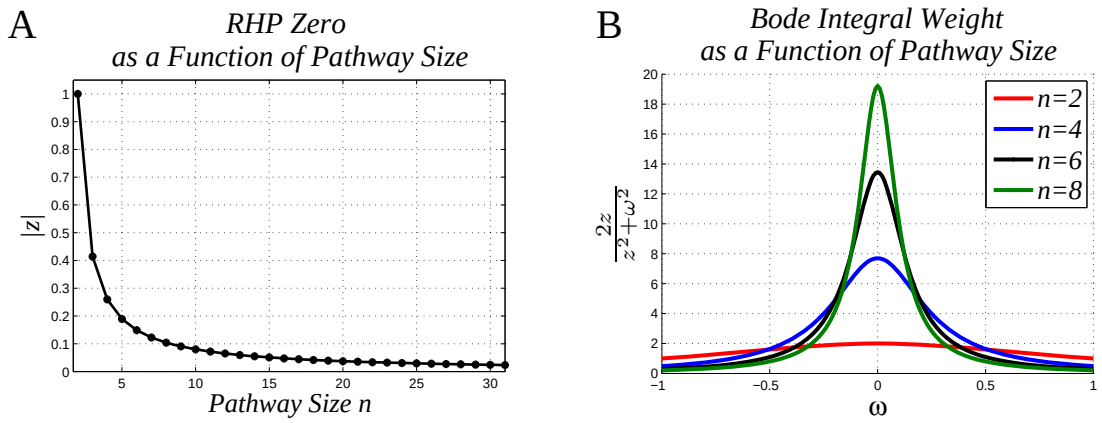

Figure 4.2: (A) The magnitude of the RHP zero decreases as pathway size increases. (B) The weight in the Bode integral gets tighter around 0 for longer pathways. This means the price paid for performance at small frequencies increases substantially as the number of intermediate reactions increases.

n-D pathway.

Let us look at the case where $k_i = k$, for all i. The zeros of $P(s)$ are at

$$\begin{aligned} s &= \left(2^{\frac{1}{n}} - 1\right) k \\ &= k\left(\left|2^{\frac{1}{n}}\right| e^{j\frac{2\pi i}{n}} - 1\right), \text{ for all } i. \end{aligned}$$

As expected, there is at least one zero in the RHP. The magnitude of this RHP zero decreases as the size of the pathway (n) increases (Figure 4.2A). This fact, coupled with the conservation law given by (2.9), implies that as the number of intermediate reactions grows the price paid for performance at small frequencies increases substantially (Figure 4.2B). Furthermore, numerical simulations confirm what (4.3) suggests, that in general as the pathway size increases, the upper bound on the feedback strength $\hat{h}$ decreases. So the increase in the intermediate metabolite reactions has two main consequences.

- The price for good performance at low frequencies increases as the magnitude of the RHP zero gets smaller.
- The upper bound on the feedback gains gets smaller, so the range of stable gains gets smaller.

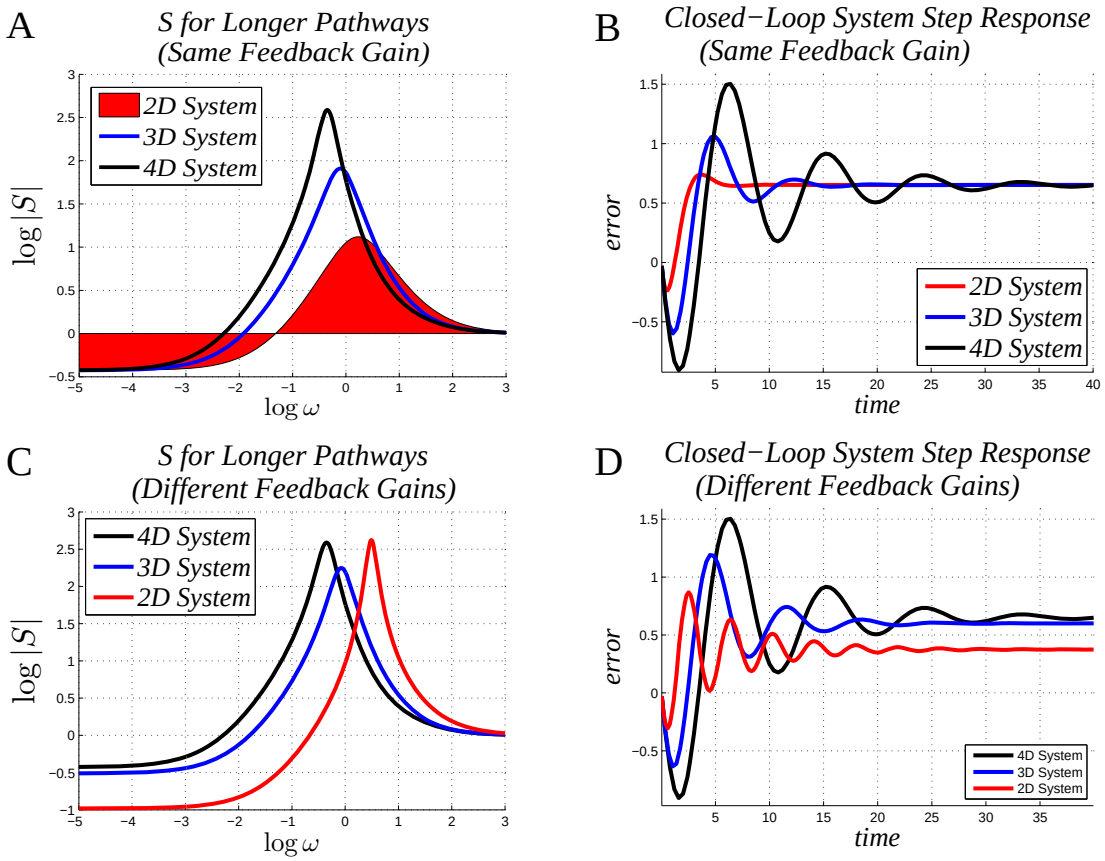

Figure 4.3: The performance of 2D, 3D and 4D systems is compared. The intermediate reaction rates are $k_1 = k_2 = k_3 = 1$ and $q = 2$, $k_y = r_y = 1$. (A) Plot of $\log|S|$ for the same feedback $\hat{h} = 3.8$, shows that the higher dimension systems pay a higher price at higher frequencies for similar performance at low frequencies (B) Closed-loop system step response shows that the same gain $\hat{h} = 3.8$ yields the same steady state error for all 3 systems. However higher dimensional systems have poorer transient response. (C) Lower dimensional systems have access to higher gains, which means that they can get better performance at low frequencies. The plot of $\log|S|$ for $\hat{h} = 5.5$, 4, 3.8 for 2D, 3D, and 4D systems respectively, illustrates the difference in performance at low frequencies, and the price paid at higher frequencies (comparable for all 3 systems). (D) Closed-loop system step response shows that access to higher gains for the low dimension systems ($\hat{h}_{2D} = 5.5$, $\hat{h}_{3D} = 4$, $\hat{h}_{4D} = 3.8$) achieves smaller steady state error and better transient response as well.

For example look at the DC gain (steady state error) of a n-D system with $q = 2$, $k_y = r_y = 1$. From (4.4) we get $P(0) = 1$ and the DC gain

$$S(0) = \frac{1}{1 + \hat{h}P(0)} = \frac{1}{1 + \hat{h}}.$$

It is clear that the DC gain improves as the gain increases, however the maximum $\hat{h}$ that still stabilizes the system gets smaller as n increases. Therefore lower dimensional systems can achieve better DC gain (steady state error). Figure 4.3 illustrates the consequences of increased pathway size on the performance of the system by looking at $\log|S|$ and the step response for comparable 2D, 3D and 4D systems.

4.4 Global Behavior

Next we prove the analogue of Lemma 3.1 for the n-D system. We will assume $\frac{Vy^q}{1+\gamma y^h}$ is bounded for all $y > 0$, (i.e. $h \geq q$) and for small $\epsilon > 0$,

$$\begin{aligned}
&\sup_{y>0} g_y(y) > \sup_{y>0} \tfrac{Vy^q}{1+\gamma y^h} + \epsilon \\
&\sup_{x_i>0} g_i(x_i) > \sup_{y>0} \tfrac{Vy^q}{1+\gamma y^h} + \epsilon, \text{ for all } i = 1, \ldots, n
\end{aligned}$$

and

$$\begin{aligned}
\delta_y &:= \sup_{y>0} \tfrac{Vy^q}{1+\gamma y^h} < \infty \\
\beta_0 &:= \inf\left\{ y_0 \mid g_y(y) - \tfrac{Vy^q}{1+\gamma y^h} > \epsilon,\ \forall y > y_0 \right\} \\
\alpha_1 &:= \inf\left\{ x_1 | g_1(x_1) > \delta_y + \epsilon \right\} \\
\alpha_i &:= \inf\left\{ x_i | g_i(x_i) > g_{i-1}(\alpha_{i-1}) + \epsilon \right\}, \text{ for all } i > 1.
\end{aligned}$$

Let

$$\begin{aligned}
U_y(x_1, \ldots, x_n, y) &:= y + \textstyle\sum_{i=1}^n 2x_i \\
\eta_0 &:= \beta_0 + \textstyle\sum_{i=1}^n 2\alpha_i \\
\Omega_{U_y,\eta_0} &:= \left\{ (x_1, \ldots, x_n, y) \in \mathbb{R}^{n+1} \mid U_y(x_1, \ldots, x_n, y) \leq \eta_0 \right\}.
\end{aligned}$$

and

$$\begin{aligned} D_1 &:= \{(x_1,\ldots,x_n,y)\in\mathbb{R}^{n+1} \mid 0\le x_1\le\alpha_1\} \\ D_i &:= \{(x_1,\ldots,x_n,y)\in\mathbb{R}^{n+1} \mid 0\le x_i\le\alpha_i\}\bigcap D_{i-1}, \quad i>1 \\ D_{\alpha,\beta_0} &:= \Omega_{U_y,\eta_0}\bigcap D_n. \end{aligned}$$

Lemma 4.1: *All the trajectories of system* (4.1) *are bounded and eventually reach* D_{α,β_0}.

PROOF: We are going to show that each of the sets D_i (Figure 4.4) are invariant with respect to the flow (4.1) and that all the trajectories of the solutions of (4.1) reach D_i, by using Lyapunov type functions

$$U_i\left(x_1,\ldots,x_n,y\right)=x_i.$$

In the positive orthant U_i are positive, $C^1(\mathbb{R}^{n+1})$ functions. For $x_1>\alpha_1$

$$\frac{d}{dt}U_1\left(x_1,\ldots,x_n,y\right)=\frac{Vy^q}{1+\gamma y^h}-g_1(x_1)<-\epsilon.$$

So the set D_1 is invariant with respect to the flow (4.1) and all the trajectories of (4.1) reach D_1. Using induction for $x_k>\alpha_k$ and $(x_1,\ldots,x_n,y)\in D_{k-1}$

$$\frac{d}{dt}U_k\left(x_1,\ldots,x_n,y\right)=g_{k-1}(x_{k-1})-g_k(x_k)\le g_{k-1}(\alpha_{k-1})-g_k(x_k)<-\epsilon.$$

So the set D_k is invariant with respect to the flow (4.1) and all the trajectories of (4.1) reach D_k, $k\le n$.

Let

$$\begin{aligned} U_y\left(x_1,\ldots,x_n,y\right) &= y+\textstyle\sum_{i=1}^n 2x_i \\ \eta_0 &= \beta_0+\textstyle\sum_{i=1}^n 2\alpha_i. \end{aligned}$$

For $(x_1,\ldots,x_n,y)\in\Omega^c_{U_y,\eta_0}\bigcap D_n$ we get

$$y>\beta_0+\sum_{i=1}^n 2\alpha_i-\sum_{i=1}^n 2x_i\ge\beta_0$$

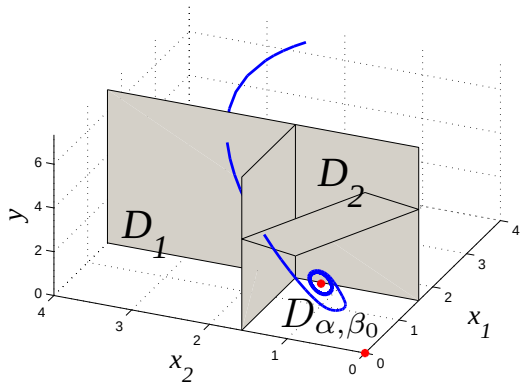

Figure 4.4: Trapping region for 3D

and

$$\begin{aligned} \frac{d}{dt}U_y\left(x_1,\ldots,x_n,y\right) &= \dot{y}+\textstyle\sum_{i=1}^{n} 2\dot{x}_i \\ &= \frac{Vy^q}{1+\gamma y^h} - g_y(y) \leq -\epsilon < 0 \end{aligned}$$

Therefore the set $D_{\alpha,\beta_0} = \Omega_{U_y,\eta_0} \bigcap D_n$ is invariant with respect to the flow (4.1) and all the solution trajectories of (4.1) reach D_{α,β_0}. ■

A consequence of Lemma 4.1 is that the system can display oscillations or chaotic behavior only inside the region D_{α,β_0}.

4.5 Region of Attraction Estimates

We perform a change of coordinates on (4.1) so that the fixed point of interest $(\bar{x}_1,\ldots,\bar{x}_n,\bar{y})$ is at the origin. Let the new system be represented by

$$\begin{aligned} \dot{\tilde{x}}_1 &= \tilde{f}(\tilde{y}) - \tilde{g}_1(\tilde{x}_1) \\ \dot{\tilde{x}}_2 &= \tilde{g}_1(\tilde{x}_1) - \tilde{g}_2(\tilde{x}_2) \\ &\vdots \\ \dot{\tilde{y}} &= 2\tilde{g}_n(\tilde{x}_n) - \tilde{f}(\tilde{y}) - \tilde{g}_y(\tilde{y}) \end{aligned}$$

for $(\tilde{x}_1,\ldots,\tilde{x}_n,\tilde{y}) \succeq -(\bar{x}_1,\ldots,\bar{x}_n,\bar{y})$. It is easy to see that $\tilde{f}$, $\tilde{g}_x$ and $\tilde{g}_y$ are just shifted versions of f, g_x and g_y and as such preserve many of their important properties. For example, for all $i = 1,\ldots,n$, $\tilde{g}_i$, $\tilde{g}_y$ are continuous, monotone, increasing functions,

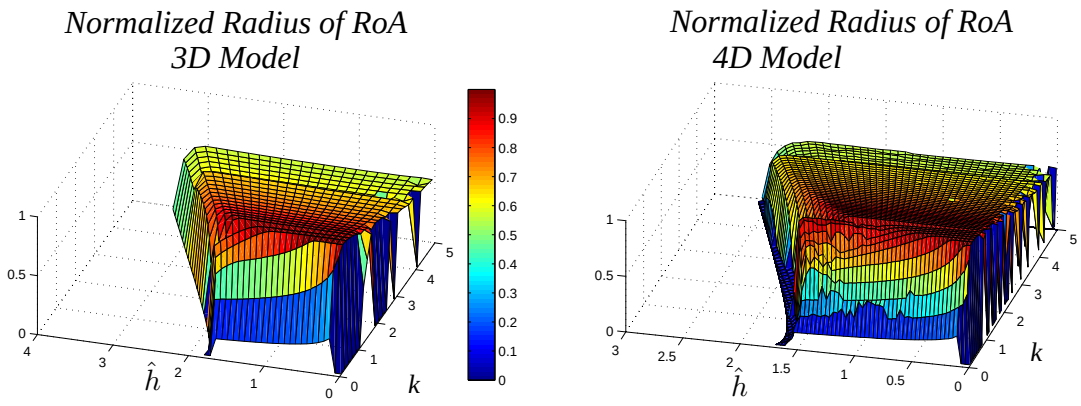

Figure 4.5: Figures show the radius of region of attraction (RoA) estimate normalized by $\sqrt{1+(n-1)/k^2}$, $n = 3, 4$ (i.e., the distance to the closest fixed point, which is the actual radius of RoA) for 3D and 4D systems with $g_i(x_i) = k$, $q = 1$, $g_y(y) = y$.

with $\tilde{g}_i(0) = 0, \tilde{g}_y(0) = 0$. For ease of notation, we will drop the tilde for the remainder of this chapter, and rewrite the system as

$$\begin{aligned} \dot{x}_1 &= f(y) - g_1(x_1) \\ \dot{x}_2 &= g_1(x_1) - g_2(x_2) \\ &\vdots \\ \dot{x}_n &= g_{n-1}(x_{n-1}) - g_n(x_n) \\ \dot{y} &= 2g_n(x_n) - f(y) - g_y(y) \end{aligned} \tag{4.5}$$

for $(x_1, \ldots, x_n, y) \succeq -(\bar{x}_1, \ldots, \bar{x}_n, \bar{y})$, where $f(y) = \frac{r_y(1+\gamma)(y+1)^q}{1+\gamma(y+1)^h} - r_y$.

For integer values of q and h, same tools discussed and used in Section 3.3 for the 2D model are used to analyze system (4.5). In the simulations we use $g_i(x_i) = k_i x_i$ (assume mass-action kinetics) but it is easy to incorporate any rational functions such as the ones derived from Michaelis-Menten kinetics. As in the 2D case, second degree polynomial Lyapunov functions verify large subsets of the region of attraction of the origin for a wide range of parameter values. Radius of region of attraction estimate is defined as the radius of the largest n-D ball centered at the origin that is contained in the estimate of the region of attraction of the origin. For 3D and 4D systems with $g_i(x_i) = k$, $q = 1$, $g_y(y) = y$, Figure 4.5 shows the radius of region of attraction

$2d \setminus n$	2	3	4	5	7	9	11	15
2	3	4	5	6	8	10	12	16
4	6	10	15	21	36	55	78	136
6	10	20	35	56	120	220	364	816
8	15	35	70	126	330	715	1365	3876
10	21	56	126	252	792	2002	4368	15504
12	28	84	210	462	1716	5005	12376	54264

Table 4.1: The size of the SDP for checking the existence of a SOS decomposition for a polynomial of degree $2d$ in n variables.

estimate normalized by $\sqrt{1+(n-1)/k^2}$ (i.e., the distance to the closest fixed point, which is the radius of actual region of attraction). It shows that for the majority of the parameter values, the region of attraction estimate radius is at least half the actual region of attraction radius. Similar to the 2D case the parameter regions where the estimate is not as good is close to the stability boundary.

Using higher degree polynomial functions becomes computationally expensive for large systems. In fact the size of the semidefinite programming (SDP) problem grows polynomially in the size of state space if the degree of the polynomials is fixed [28]. Table 4.1 shows the size of the size of the matrix in the SDP for checking the existence of a sums of squares (SOS) decomposition for a given polynomial of degree $2d$ in n variables (the corresponding expression is $\binom{n+d}{d}$). For low dimensions (short pathways) even higher degree polynomial Lyapunov functions result in SOS programs that are still manageable, but the corresponding SOS programs become prohibitively large for longer pathways even for small degree polynomial Lyapunov functions [5]. Next we propose a decomposition of high dimensional problems that takes advantage of the structure of the pathway and renders the corresponding SOS program to become computationally tractable for large subsets of the parameter space.

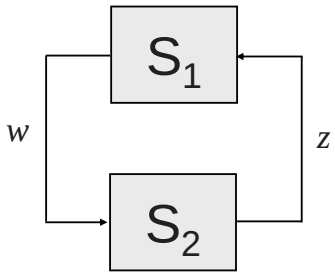

Figure 4.6: The system (4.5) is represented as feedback interconnection of 2 subsystems S_1 and S_2, given by (4.6) and (4.7).

4.6 A Simple Decomposition

The system (4.5) is represented as feedback interconnection of 2 subsystems S_1 and S_2,

$$\begin{array}{rcc} \dot{x}_1 &=& z - g_1(x_1) \\ \dot{x}_2 &=& g_1(x_1) - g_2(x_2) \\ \vdots & \vdots & \vdots \\ \dot{x}_n &=& g_{n-1}(x_{n-1}) - g_n(x_n) \\ w &=& g_n(x_n) \end{array} \tag{4.6}$$

and

$$\begin{array}{rcc} \dot{y} &=& 2w - f(y) - g_y(y) \\ z &=& f(y) \end{array} \tag{4.7}$$

where $f(y) = \frac{r_y(1+\gamma)(y+1)^q}{1+\gamma(y+1)^h} - r_y$, as shown in Figure 4.6. System S_1 is a SISO (single-input single-output) system with n states. We expect S_1 to be a "simple" well behaved system since it is composed of the chain of chemical reactions, i.e., it has a very special structure and the rates (g_i) are monotone. As such it is easy to analyze even for relatively large values of n. S_2 is a SISO system with a single state that captures the most important nonlinearity: the dynamics of ATP and its involvement in autocatalysis and feedback regulation. Using this decomposition we have separated the complexity of high dimensional states (system S_1) from the complexity of the important nonlinearity of autocatalysis control (system S_2).

Reference [42] proposes a method for computing invariant subsets of the region of

attraction of the asymptotically stable equilibrium points of systems with unmodeled dynamics, where the unmodeled dynamics are required to satisfy certain gain relations or dissipation inequalities. We apply this idea to the feedback interconnection of Figure 4.6 to compute invariant subsets of the region of attraction for (4.5).

Definition 4.1: *A continuously differentiable function* $U : \mathbb{R}^m \to \mathbb{R}$ *is positive definite in a neighborhood* $\mathcal{N}$ *of the origin if* $U(0) = 0$ *and for all nonzero* $x \in \mathcal{N}$, $U(x) > 0$.

Let $\mathcal{L}_S$, $\mathcal{L}_{S_1}$, and $\mathcal{L}_{S_2}$ denote the Lie derivatives for the systems (4.5), (4.6), and (4.7) respectively. We search for positive definite function $U_1 : \mathbb{R}^n \to \mathbb{R}$ such that

$$\mathcal{L}_{S_1} U_1(x) \leq z^2 + 2\delta wz - \kappa w^2, \quad \forall\, (x, z) \tag{4.8}$$

and $U_2 : \mathbb{R} \to \mathbb{R}$, $U_2(y)$ positive definite in some neighborhood $\mathcal{N}_0$ of the origin such that

$$\mathcal{L}_{S_2} U_2(y) \leq \kappa w^2 - 2\delta wz - z^2, \quad \forall w \text{ and } y \in \mathcal{N}_0. \tag{4.9}$$

Let $U(x, y) := U_1(x) + U_2(y)$ and β be such that

$$\Omega_{U,\beta} = \left\{(x, y) \in \mathbb{R}^{n+1} \mid U(x, y) \leq \beta\right\} \subset \mathbb{R}^n \times \mathcal{N}_0. \tag{4.10}$$

Proposition 4.3: *(a)* $\Omega_{U,\beta}$ *is an invariant subset under the flow of* (4.5).
(b) If one of the inequalities (4.8), (4.9) *is strict (i.e., equality is satisfied only at* $(0, 0)$*) then* $\Omega_{U,\beta}$ *is a subset of the region of attraction of the origin of* (4.5).

PROOF: (a) U is a Lyapunov function for (4.5), since for all nonzero $(x, y) \in \Omega_{U,\beta} \subset \mathbb{R}^n \times \mathcal{N}_0$, $U(x, y) > 0$ and

$$\mathcal{L}_S U(x, y) = \mathcal{L}_{S_1} U_1(x) + \mathcal{L}_{S_2} U_2(y) \leq 0.$$

Hence, $\Omega_{U,\beta}$ is invariant under the flow of (4.5).
(b) We examine the two cases separately. Since part (a) establishes that $\Omega_{U,\beta}$ is

invariant under the flow of (4.5), all the set mentioned below are assumed to be subsets of $\Omega_{U,\beta}$.

Case 1: If (4.8) is strict, i.e.,

$$\mathcal{L}_{S_1} U_1(x) < z^2 + 2\delta wz - \kappa w^2, \forall (x,z) \neq (0,0),$$

then

$$\Gamma_1 := \{(x,y) \mid \mathcal{L}_S U(x,y) = 0\} \subset \Gamma_2 := \{(x,y) \mid x = 0\}.$$

Since $\forall (x,y) \in \Gamma_2$

$$\dot{x}_1 = f(y) \neq 0, \quad \forall y \neq 0,$$

the only invariant subset of Γ_1 with respect to the flow of (4.5) is the origin and LaSalle's theorem shows that all trajectories in $\Omega_{U,\beta}$ go to the origin. Therefore $\Omega_{U,\beta}$ is an invariant subset of the region of attraction of the origin of (4.5).

Case 2: If (4.9) is strict, i.e.,

$$\mathcal{L}_{S_2} U_2(y) < -z^2 - 2\delta wz + \kappa w^2, \text{ for all nonzero } (y,w) \in \mathcal{N}_0 \times \mathbb{R},$$

then

$$\Gamma_1 := \{(x,y) \mid \mathcal{L}_S U(x,y) = 0\} \subset \Gamma_3 := \{(x,y) \mid y = 0\}.$$

Let $\Gamma_{inv} \subset \Gamma_3$ be a invariant set under the flow of (4.5). But $\forall (x,y) \in \Gamma_{inv}$,

$$\dot{y} = 2g_n(x_n) \neq 0, \quad \forall x_n \neq 0,$$

so $x_n = 0$. Similarly $\forall (x,y) \in \Gamma_{inv}$,

$$\dot{x}_n = g_{n-1}(x_{n-1}) \neq 0, \quad \forall x_{n-1} \neq 0,$$

so $x_{n-1} = 0$. Inductively we get that $\forall (x,y) \in \Gamma_{inv}$, $x_i = 0$, $\forall i$ and consequently the only invariant subset of Γ_3 with respect to the flow of (4.5) is the origin and LaSalle's theorem shows that all trajectories in $\Omega_{U,\beta}$ go to the origin. Therefore $\Omega_{U,\beta}$ is a subset

of the region of attraction of the origin of (4.5). ■

4.6.1 Region of Attraction Estimation via a Local Small-Gain Type Condition

Recall that $\hat{h} = \frac{\gamma}{\gamma+1}h$, $\sigma = -\frac{\partial f}{\partial y}|_{y=0} = r_y(\hat{h}-q)$, $k_y = \frac{\partial g_y}{\partial y}|_{y=0}$ and we defined $\hat{h}_r = q + \frac{1}{3}\frac{k_y}{r_y}$, $\hat{h}_s = q - \frac{k_y}{r_y}$, $\theta(n) = \left(\sec\frac{\pi}{n+1}\right)^{n+1}$ and $\hat{h}_d(n) = q + \frac{k_y}{r_y}\frac{\theta(n)}{2+\theta(n)}$. Using special forms of the inequalities (4.8) and (4.9), we show that for specific ranges of feedback gain $\hat{h}$ we can analytically find a positive definite diagonal $U(x,y)$ and β, such that $\Omega_{U,\beta}$ satisfies (4.10), i.e., $\Omega_{U,\beta}$ is an invariant subset of the region of attraction. Specifically

- if $\hat{h}_s < \hat{h} < \hat{h}_r$

$$U(x,y) := 2\sum_{i=1}^{n}\int_0^{x_i} g_i(\xi)d\xi + \frac{1}{2}\int_0^y \left(f(\xi)+g_y(\xi)\right)d\xi \tag{4.11}$$

- if $q < \hat{h} < \hat{h}_d(n)$,

$$U(x,y) := \sum_{i=1}^{n} d_i\int_0^{x_i} g_i(\xi)d\xi - \delta\int_0^y f(\xi)d\xi$$

  for some constants $d_i > 0$.

In (4.8) and (4.9), let $\delta = 0$ and $\kappa = 1$, i.e., we search for positive definite function $U_1 : \mathbb{R}^n \to \mathbb{R}$ such that

$$\mathcal{L}_{S_1}U_1(x) \le z^2 - w^2, \quad \forall\,(x,z) \tag{4.12}$$

and $U_2 : \mathbb{R} \to \mathbb{R}$, $U_2(y)$ positive definite in some neighborhood $\mathcal{N}_0$ of the origin such that

$$\mathcal{L}_{S_2}U_2(y) < w^2 - z^2, \quad \forall w \text{ and } \forall y \in \mathcal{N}_0\backslash\{0\}. \tag{4.13}$$

Definition 4.2: *A SISO system with input u and output y has gain L_2-gain at most κ if for all u,*

$$\|y\|_2 \leq \kappa \|u\|_2 .$$

The inequalities in (4.12) and (4.13) enforce that the system S_1 has L_2-gain at most 1 and system S_2 has L_2-gain less than 1 in the respective domains, and if satisfied, then the feedback interconnection meets the conditions of the local small-gain theorem [42]. Next we show that if $\hat{h}_s < \hat{h} < \hat{h}_r$ then (4.11) is a Lyapunov function for (4.5) and show how to construct a corresponding invariant subset $\Omega_{U,\beta}$ of the region of attraction.

Lemma 4.2: *System* (4.6) *has L_2-gain no more than* 1*, i.e., exists positive definite $U_1 : \mathbb{R}^n \to \mathbb{R}$ that satisfies inequality* (4.12) *$\forall\,(x, z)$.*

PROOF: Let

$$U_1(x) := \sum_{i=1}^{n} 2 \int_0^{x_i} g_i(\xi) d\xi, \tag{4.14}$$

then $U_1(0) = 0$, $U_1(x) > 0$, $\forall x \neq 0$ since $\forall i$, $g_i(x_i)$ is monotone and $g_i(0) = 0$, and for all (x, z)

$$\begin{aligned}
\mathcal{L}_{S_1} U_1(x) &= \textstyle\sum_{i=1}^{n} 2 g_i(x_i) \dot{x}_i \\
&= 2 g_1(x_1) \left(z - g_1(x_1)\right) + \textstyle\sum_{i=2}^{n} 2 g_i(x_i) \left(g_{i-1}(x_{i-1}) - g_i(x_i)\right) \\
&= 2 z g_1(x_1) - g_1^2(x_1) - g_n^2(x_n) \\
&\quad + \textstyle\sum_{i=2}^{n} \left(-g_{i-1}^2(x_{i-1}) + 2 g_i(x_i) g_{i-1}(x_{i-1}) - g_i^2(x_i)\right) \\
&= -\left(z - g_1(x_1)\right)^2 - \textstyle\sum_{i=2}^{n} \left(g_{i-1}(x_{i-1}) - g_i(x_i)\right)^2 + z^2 - w^2 \\
&\leq z^2 - w^2.
\end{aligned}$$

■

Lemma 4.3: *If $\hat{h}_s < \hat{h} < \hat{h}_r$, then there exists a nonempty neighborhood $\mathcal{N}_0$ of the origin and a function $U_2 : \mathbb{R} \to \mathbb{R}$ positive definite in $\mathcal{N}_0$ that satisfies the inequality in* (4.13) *$\forall w$ and $\forall y \in \mathcal{N}_0 \backslash \{0\}$.*

PROOF: Let

$$D_y := \left\{ y > 0 \mid -\frac{1}{3} g_y(y) < f(y) < g_y(y) \right\} \cup \left\{ y < 0 \mid g_y(y) < f(y) < -\frac{1}{3} g_y(y) \right\}.$$

Note that D_y is the set of points y for which the graph of f lies between the graph of g_y and $-\frac{1}{3} g_y$ (Figure 4.7A). Since $\frac{\partial f}{\partial y}|_{y=0} = r_y(q - \hat{h})$ and $\frac{\partial g_y}{\partial y}|_{y=0} = k_y > 0$,

$$\begin{array}{rcl} \hat{h} < \hat{h}_r = q + \frac{1}{3}\frac{k_y}{r_y} & \Rightarrow & -\frac{\partial f}{\partial y}|_{y=0} < \frac{1}{3}\frac{\partial g_y}{\partial y}|_{y=0} \\ \hat{h} > h_s = q - \frac{k_y}{r_y} & \Rightarrow & \frac{\partial f}{\partial y}|_{y=0} < \frac{\partial g_y}{\partial y}|_{y=0}. \end{array}$$

So, there is a nonempty neighborhood of the origin

$$\mathcal{N}_0 \subset D_y \cup \{0\}. \tag{4.15}$$

Furthermore,

$$U_2(y) := \frac{1}{2} \int_0^y \left(f(\xi) + g_y(\xi) \right) d\xi \tag{4.16}$$

is positive definite in $\mathcal{N}_0$ and

$$\begin{array}{rcl} \mathcal{L}_{S_2} U_2(y) - w^2 + z^2 & = & \frac{\partial U_2}{\partial y}\dot{y} - w^2 + f^2(y) \\ & = & \frac{\partial U_2}{\partial y}\left(2w - f(y) - g_y(y)\right) - w^2 + f^2(y) \\ & = & -\left(\frac{\partial U_2}{\partial y} - w\right)^2 + \left(\frac{\partial U_2}{\partial y}\right)^2 - \frac{\partial U_2}{\partial y}\left(f(y) + g_y(y)\right) + f^2(y) \\ & = & -\left(\frac{\partial U_2}{\partial y} - w\right)^2 - \frac{1}{4}\left(f(y) + g_y(y)\right)^2 + f^2(y). \end{array}$$

But, $-\frac{1}{4}\left(f(y) + g_y(y)\right)^2 + f^2(y) < 0$, $\forall y \in D_y$, and consequently

$$\mathcal{L}_{S_2} U_2(y) < w^2 - z^2, \quad \forall w,\ \forall y \in \mathcal{N}_0 \backslash \{0\} \subset D_y \ . \qquad \blacksquare$$

Remark 4.2: *If $\hat{h} > \hat{h}_r$ then the inequality in* (4.13) *cannot be satisfied by any positive definite function in any nonempty neighborhood of the origin, since the linearization of system* (4.7) *has L_2-gain greater than* 1.

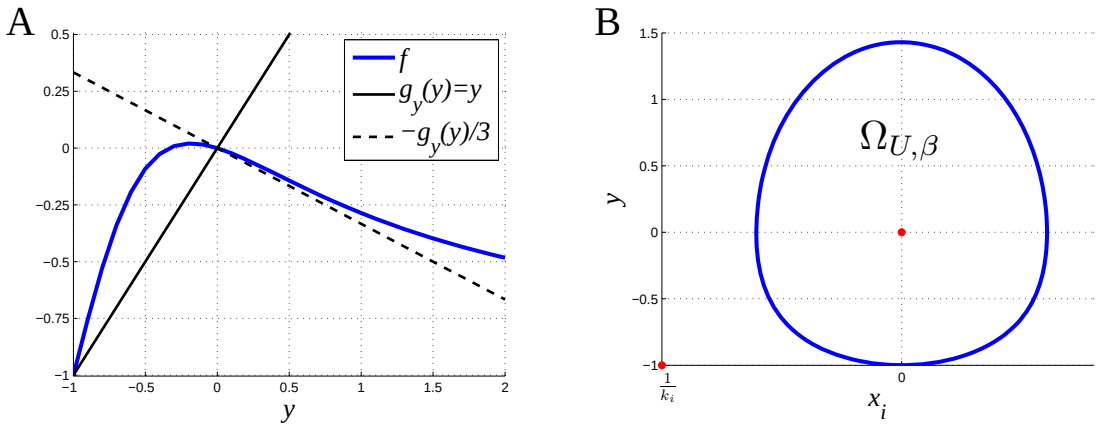

Figure 4.7: (A) $\mathcal{N}_0$ is the set of points y where the graph of f lies between g_y and $-\frac{1}{3}g_y$. In this case $\mathcal{N}_0 = \{y \mid y > -1\}$. (B) The $y - x_i$ slice of the invariant subset of region of attraction $\Omega_{U,\beta}$ ($x_j = 0$, $j \neq i$).

Notice that for U_1 and U_2 as defined in (4.14) and (4.16), if $U(x, y)$ is given by (4.11) then $U(x, y) = U_1(x) + U_2(y)$. Let $\mathcal{N}_0$ be defined as above by (4.15).

Proposition 4.4: *If $\hat{h}_s < \hat{h} < \hat{h}_r$, for any β such that $\Omega_{U,\beta} \subset \mathbb{R}^n \times \mathcal{N}_0$, $\Omega_{U,\beta}$ is an invariant subset of the region of attraction of the origin for system* (4.5).

PROOF: A direct consequence of Proposition 4.3, Lemma 4.2 and Lemma 4.3.

Example 4.1: *Let $g_i(x_i) = k_i x_i$, $g_y(y) = y$, $\gamma = \frac{3}{2}$, $q = 1$, and $h = 2$. Then $\hat{h} = \frac{6}{5}$, $\hat{h}_r = \frac{4}{3}$ and*

$$U = \sum_{i=1}^{n} k_i x_i^2 + \frac{5}{12}\log\left(5 + 6y + 3y^2\right) + \frac{1}{4}y^2 - \frac{1}{2}y - \frac{5}{12}\log 5,$$

$\mathcal{N}_0 = \{y \mid y > -1\}$ (Figure 4.7A). The maximum sublevel set β of U that satisfies (4.10) *is $\beta = 0.3682$. Figure 4.7B shows a $y - x_i$ slice of the invariant subset of region of attraction $\Omega_{U,\beta}$.*

4.6.2 Compositional Estimation of the Region of Attraction Using General Dissipation Inequalities

In the previous sections, we estimated regions of attraction of asymptotically stable equilibrium points through an application of a local small-gain type condition.

Namely, the overall system was decomposed into two input-output systems and a certificate for the estimates of the region of attraction of the overall system was assembled using certificates for the input-output gain properties of the subsystems (equations (4.12) and (4.13)). In this subsection, we consider extensions of this idea where input-output gain properties are replaced by more sophisticated so-called dissipation inequalities [46]. One diversion from the classical dissipation inequalities literature is that the inequalities devised here will be local inequalities, i.e., they are supposed to hold in certain bounded subsets (for example in certain sublevel sets of associated storage functions) of the state-space but not necessarily the whole state space [42].

In (4.8) and (4.9) let $\kappa = 0$, i.e., we search for a positive definite function $U_1 : \mathbb{R}^n \to \mathbb{R}$ such that

$$\mathcal{L}_{S_1} U_1(x) \leq z^2 + 2\delta wz, \quad \forall\, (x, z) \tag{4.17}$$

and $U_2 : \mathbb{R} \to \mathbb{R}$, $U_2(y)$ positive definite in some neighborhood $\mathcal{N}_0$ of the origin such that

$$\mathcal{L}_{S_2} U_2(y) < -z^2 - 2\delta wz, \quad \forall w \text{ and } \forall y \in \mathcal{N}_0 \backslash \{0\}. \tag{4.18}$$

Next we find U_1 and U_2 satisfying the inequalities above for $q < \hat{h} < \hat{h}_d(n)$ and a specific δ. We first show that a diagonal function U_1 exists for the linearization of (4.6) and $0 < \delta \leq \frac{1}{2}\theta(n)$, and then show that it exists for general system S_1. We treat the special case of the linearization separately since the proof outlines a procedure of finding U_1 by solving a Lyapunov inequality for the case when $g_i(x_i) = k_i x_i$ (mass-action kinetics). The linearization of system (4.6) is given by

$$\begin{aligned} \dot{x} &= Ax + Bz \\ w &= Cx \end{aligned} \tag{4.19}$$

where

$$A = \begin{bmatrix} -k_1 & 0 & \cdots & 0 & 0 \\ k_1 & -k_2 & & 0 & 0 \\ \vdots & & \cdots & & \vdots \\ 0 & 0 & & -k_{n-1} & 0 \\ 0 & 0 & \cdots & k_{n-1} & -k_n \end{bmatrix} \tag{4.20}$$

$$B = \begin{bmatrix} 1 & 0 & \cdots & 0 & 0 \end{bmatrix}^T \tag{4.21}$$

$$C = \begin{bmatrix} 0 & 0 & \cdots & 0 & k_n \end{bmatrix} \tag{4.22}$$

Definition 4.3: *A matrix A is diagonally stable if there exists a diagonal matrix $P \succ 0$ such that*

$$A^T P + PA \prec 0.$$

Lemma 4.4: *If $0 < \delta \leq \frac{1}{2}\theta(n)$, then there exists positive definite $U_1 : \mathbb{R}^n \to \mathbb{R}$ that satisfies the inequality in (4.17) $\forall\,(x, z)$ for S_1 being the linear system defined in (4.19).*

PROOF: First let $0 < \delta < \frac{1}{2}\theta(n)$ and

$$\tilde{A} = \begin{bmatrix} A & B \\ -2\delta C & -1 \end{bmatrix} \qquad G = \begin{bmatrix} A & -B \\ 2\delta C & -1 \end{bmatrix}.$$

Then

$$\tilde{A} = \begin{bmatrix} I_n & 0 \\ 0 & -1 \end{bmatrix} G \begin{bmatrix} I_n & 0 \\ 0 & -1 \end{bmatrix},$$

and so $\tilde{A}$ is diagonally stable if and only if G is diagonally stable. For $\delta > 0$, reference

[2] shows that a necessary and sufficient condition for diagonal stability of

$$G = \begin{bmatrix} -k_1 & 0 & \cdots & 0 & -1 \\ k_1 & -k_2 & & 0 & 0 \\ \vdots & & \cdots & & \vdots \\ 0 & 0 & & -k_n & 0 \\ 0 & 0 & \cdots & 2\delta k_n & -1 \end{bmatrix}$$

is

$$\delta < \frac{1}{2}\theta(n).$$

Therefore there exists a diagonal matrix $\tilde{P} \succ 0$ such that

$$\tilde{A}^T\tilde{P} + \tilde{P}\tilde{A} \prec 0. \tag{4.23}$$

Without loss of generality, let

$$\tilde{P} = \begin{bmatrix} P & 0 \\ 0 & \frac{1}{2} \end{bmatrix},$$

where P is diagonal and $P \succ 0$. Then,

$$\begin{aligned} 0 \succ \tilde{A}^T\tilde{P} + \tilde{P}\tilde{A} &= \begin{bmatrix} A^T & -2\delta C^T \\ B^T & -1 \end{bmatrix}\begin{bmatrix} P & 0 \\ 0 & \frac{1}{2} \end{bmatrix} + \begin{bmatrix} P & 0 \\ 0 & \frac{1}{2} \end{bmatrix}\begin{bmatrix} A & B \\ -2\delta C & -1 \end{bmatrix} \\ &= \begin{bmatrix} A^TP + PA & PB - \delta C^T \\ B^TP - \delta C & -1 \end{bmatrix} \end{aligned}$$

and $\forall\,(x, z) \in \mathbb{R}^n \times \mathbb{R}\backslash\{0\}$ and $0 < \delta < \frac{1}{2}\theta(n)$

$$\begin{bmatrix} x \\ z \end{bmatrix}^T \begin{bmatrix} A^TP + PA & PB - \delta C^T \\ B^TP - \delta C & -1 \end{bmatrix}\begin{bmatrix} x \\ z \end{bmatrix} < 0$$

$$\Updownarrow$$

$$\left(x^TA^T + z^TB^T\right)Px + x^TP\left(Ax + Bz\right) - 2\delta\left(Cx\right)z - z^2 < 0.$$

By continuity in δ, we get that for $0 < \delta \leq \frac{1}{2}\theta(n)$

$$\left(x^T A^T + z^T B^T\right) Px + x^T P\left(Ax + Bz\right) - 2\delta\left(Cx\right) z - z^2 \leq 0,$$

■

and therefore $U_1(x) = x^T Px$ for system (4.19) satisfies (4.17).

Remark 4.3: *We can easily find U_1 by constructing $\tilde{A}$ as shown above and solving (4.23) for a diagonal $\tilde{P}$. Inequality (4.23) is a Lyapunov inequality and can be efficiently solved as a linear matrix inequality (LMI) using many of the available solvers [23, 37].*

Lemma 4.5: *If $0 < \delta \leq \frac{1}{2}\theta(n)$, then there exists a positive definite function $U_1 : \mathbb{R}^n \to \mathbb{R}$ that satisfies the inequality in (4.17) $\forall\,(x, z)$ for S_1 being the system in (4.6).*

PROOF: Consider the system C_1 defined by

$$\begin{array}{rcl} \dot{x}_1 &=& -\tilde{z} - g_1(x_1) \\ \dot{x}_2 &=& g_1(x_1) - g_2(x_2) \\ \vdots & \vdots & \vdots \\ \dot{x}_n &=& g_{n-1}(x_{n-1}) - g_n(x_n) \\ \dot{\tilde{z}} &=& 2\delta g_n(x_n) - \tilde{z} \end{array} \tag{4.24}$$

and let $\mathcal{L}_{C_1}$ denote the corresponding Lie derivative. For $0 < \delta < \frac{1}{2}\theta(n)$, since

$$\lim_{|x_i| \to \infty} \int_0^{x_i} g_i(\xi) d\xi = \infty,$$

reference [2] (Corollary 3 and its proof) shows that for system (4.24) there exist constants $d_i > 0$, $1 \leq i \leq n+1$ such that

$$\begin{array}{rcl} \tilde{U}_1\left(x, \tilde{z}\right) &=& \sum_{i=1}^{n} d_i \int_0^{x_i} g_i(\xi) d\xi + d_{n+1} \frac{1}{2} \tilde{z}^2 \\ &=& U_1(x) + d_{n+1} \frac{1}{2} \tilde{z}^2 \end{array} \tag{4.25}$$

is a proper Lyapunov function, i.e., $\forall\,(x,\tilde{z}) \neq \mathbf{0}$

$$\frac{d}{dt}\tilde{U}_1\,(x,\tilde{z}) < 0.$$

Without loss of generality, take $d_{n+1} = 1$ and let $z = -\tilde{z}$, then $\forall\,(x,z) \neq \mathbf{0}$ and $0 < \delta < \frac{1}{2}\theta(n)$

$$\begin{aligned} 0 > \mathcal{L}_{C_1}\tilde{U}_1\,(x,-z) &= \mathcal{L}_{S_1}U_1(x) - z\,(2\delta g_n(x_n) + z) \\ &= \mathcal{L}_{S_1}U_1(x) - 2\delta wz - z^2 \end{aligned}$$

By continuity in δ, we get that for $0 < \delta \leq \frac{1}{2}\theta(n)$

$$\mathcal{L}_{S_1}U_1(x) \leq 2\delta wz + z^2.$$

■

Lemma 4.6: *If, for system in* (4.7), $q < \hat{h} < \hat{h}_d(n)$, *then there exists a nonempty neighborhood of the origin* $\mathcal{N}_0$ *and a function* $U_2 : \mathbb{R} \to \mathbb{R}$ *positive definite in* $\mathcal{N}_0$ *that satisfies inequality* (4.18) *for* $\delta = \frac{1}{2}\theta(n)$,$\forall w$ *and* $\forall y \in \mathcal{N}_0 \backslash \{0\}$.

PROOF: Let

$$D_y = \left\{ y > 0 \mid -\frac{\delta}{1+\delta} g_y(y) < f(y) < 0 \right\} \cup \left\{ y < 0 \mid 0 < f(y) < -\frac{\delta}{1+\delta} g_y(y) \right\}.$$

Note that D_y is the set of points y for which the graph of f lies between the graph of $-\frac{\delta}{1+\delta}g_y$ and the horizontal axis (Figure 4.8). Since $\frac{\partial f}{\partial y}|_{y=0} = r_y(q - \hat{h})$ and $\frac{\partial g_y}{\partial y}|_{y=0} = k_y > 0$,

$$\begin{aligned} \hat{h} < \hat{h}_d(n) = q + \tfrac{k_y}{r_y}\tfrac{\theta(n)}{2+\theta(n)} \quad &\Rightarrow \quad -\tfrac{\partial f}{\partial y}|_{y=0} < \tfrac{\delta}{1+\delta}\tfrac{\partial g_y}{\partial y}|_{y=0} \\ \hat{h} > q \quad &\Rightarrow \quad \tfrac{\partial f}{\partial y}|_{y=0} < 0. \end{aligned}$$

So there is a nonempty neighborhood of the origin $\mathcal{N}_0 \subset D_y \cup \{0\}$. Furthermore, for $y \in \mathcal{N}_0$ the function

$$U_2(y) := -\delta \int_0^y f(\xi)d\xi \tag{4.26}$$

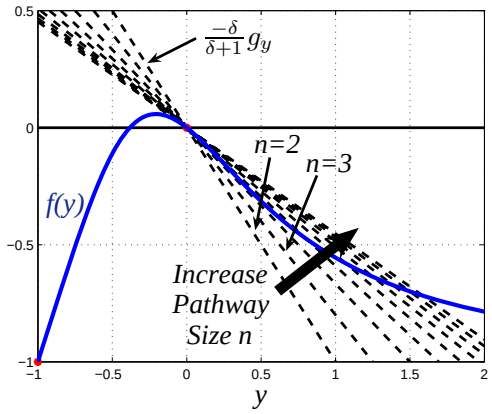

Figure 4.8: The set $\mathcal{N}_0$ is the set of points for which the graph of f lies in the area between the graph of $-\frac{\delta}{1+\delta}g_y$ and the horizontal axis. This area shrinks as the pathway size increases.

is positive definite and

$$\begin{aligned}\mathcal{L}_{S_2}U_2(y) + 2\delta wz + z^2 &= \tfrac{\partial U_2}{\partial y}\dot{y} + 2\delta w f(y) + f^2(y) \\ &= -\delta f(y)\left(2w - f(y) - g_y(y)\right) + 2\delta w f(y) + f^2(y) \\ &= (\delta+1)\, f^2(y) + \delta g(y) f(y)\end{aligned}$$

But, $(\delta+1)\, f^2(y) + \delta g(y) f(y) < 0$, $\forall y \in D_y$, and therefore

$$\mathcal{L}_{S_2}U_2(y) < -z^2 - 2\delta wz, \quad \forall w,\ \forall y \in \mathcal{N}_0 \backslash \{0\}\ .$$

■

Let $U(x,y) := U_1(x) + U_2(y)$, for U_1 and U_2 as defined in (4.25) and (4.26) for $\delta = \frac{1}{2}\theta(n)$ and let $\mathcal{N}_0$ be as constructed in the proof Lemma 4.6.

Proposition 4.5: *If $0 < \hat{h} < \hat{h}_d(n)$, for any β such that $\Omega_{U,\beta} \subset \mathbb{R}^n \times \mathcal{N}_0$, $\Omega_{U,\beta}$ is an invariant subset of the region of attraction of the origin for system* (4.5).

PROOF: A direct consequence of Proposition 4.3, Lemma 4.5, and Lemma 4.6.

Remark 4.4: *Proposition 4.2 and the secant condition establish bounds $\hat{h}_r$ and $\hat{h}_d(n)$ on $\hat{h}$ that guarantee stability of the pathway for arbitrary rates (and number in the case of $\hat{h}_r$) of intermediate reactions. Propositions 4.4 and 4.5 imply that the systems with gains that obey those bounds are simple to analyze.*

Propositions 4.4 and 4.5 establish how to construct invariant subsets of region of attraction for a family of systems, but do not offer any guarantees on how large this subsets are. In general the size of these subsets will depend on the global properties of f and g_y as illustrated in Section 3.4.1.

Remark 4.5: *There are two basic ways of improving the region of attraction estimates $\Omega_{U,\beta}$ for (4.5). Similar to 2D case (Example 3.4), given a fixed U we can solve the following problem for β:*

$$\max \beta$$
$$\mathcal{L}_S U(x,y) < 0, \quad \forall (x,y) \in \Omega_{U,\beta} \backslash \{0,0\}.$$

Another approach is to combine invariant subsets of the region of attraction, since if Ω_{U,β_1} and Ω_{W,β_2} are invariant subsets of region of attraction of the fixed point, then so is $\Omega_{U,\beta_1} \bigcup \Omega_{W,\beta_2}$. For example, if $q \leq \hat{h} \leq h_r$, then we can use $\Omega_{U,\beta}$ and the Lyapunov functions that we get from Proposition 4.4 and 4.5 to improve our estimate.

4.6.2.1 Block Diagonal Lyapunov Functions

The decomposition of (4.5) into S_1 and S_2 provides a convenient way of searching for block diagonal Lyapunov functions, i.e we search for $U(x,y) = U_1(x) + U_2(y)$, $x \in \mathbb{R}^n$, $y \in \mathbb{R}$. The next proposition examines the linearizations of S_1 and S_2 and shows that locally, if there is such a Lyapunov function for the linearization of system (4.5), then we can construct it by finding U_1 and U_2 satisfying (4.25) and(4.26) respectively. The linearization of system (4.6) is given by (4.19), and let the linearization of S_2 be

$$\begin{aligned} \dot{y} &= a_2 y + 2w \\ z &= -\sigma y \end{aligned} \tag{4.27}$$

where $\sigma = -\frac{\partial f}{\partial y}|_{y=0} = r_y(\hat{h} - q)$, $a_2 = -k_y + \sigma$. The linearization of (4.5) is given by (4.2) and we rewrite it as

$$\begin{bmatrix} \dot{x} \\ \dot{y} \end{bmatrix} = J \begin{bmatrix} x \\ y \end{bmatrix} \tag{4.28}$$

where

$$J = \begin{bmatrix} A & -\sigma B \\ 2C & a_2 \end{bmatrix}.$$

Proposition 4.6: *If there exist positive definite matrices $P_1 \in \mathbb{R}^{n\times n}$ and $p_2 \in \mathbb{R}^{1\times 1}$ such that $J^T P + PJ \prec 0$, where*

$$P := \begin{bmatrix} P_1 & 0 \\ 0 & p_2 \end{bmatrix},$$

then there exist positive definite quadratic functions $U_1 : \mathbb{R}^n \to \mathbb{R}$, $U_2 : \mathbb{R} \to \mathbb{R}$, and $\delta = \frac{\sigma}{k_y - \sigma}$ such that

$$\mathcal{L}_{S_1} U_1(x) < z^2 + 2\delta wz, \quad \forall x, z$$
$$\mathcal{L}_{S_2} U_2(y) \leq -z^2 - 2\delta wz, \quad \forall y, w$$

for systems S_1 and S_2 given by (4.19) and (4.27) respectively.

PROOF: Define

$$\tilde{U}_1(x) := x^T P_1 x \qquad \tilde{U}_2(y) := p_2 y^2$$
$$\alpha := -\tfrac{2a_2 p_2}{\sigma^2} \qquad \tilde{\delta} := \tfrac{2p_2}{\sigma}$$

and

$$\begin{aligned} Q &:= J^T P + PJ \\ &= \begin{bmatrix} A^T P_1 + P_1 A & 2p_2 C^T - \sigma P_1 B \\ 2p_2 C - \sigma B^T P_1 & 2a_2 p_2 \end{bmatrix} \prec 0. \end{aligned} \tag{4.29}$$

Notice that (4.29) implies that $a_2 < 0$, and therefore $\alpha > 0$. Then $\forall y, w$

$$\begin{aligned} \mathcal{L}_{S_2} \tilde{U}_2(y) &= 2p_2 a_2 y^2 + 4p_2 yw \\ &= -\alpha\sigma^2 y^2 + 2\tilde{\delta}\sigma yw \\ &= -\alpha z^2 - 2\tilde{\delta} zw \end{aligned} \tag{4.30}$$

and

$$\begin{aligned}\mathcal{L}_{S_1}\tilde{U}_1(x) - \alpha z^2 - 2\tilde{\delta}wz &= x^T P_1 (Ax + Bz) + \left(x^T A^T + zB^T\right) P_1 x \\ &\quad + \tfrac{2a_2p_2}{\sigma^2} z^2 - 2\tfrac{2p_2}{\sigma} zCx \\ &= \begin{bmatrix} x \\ z \end{bmatrix}^T Q_1 \begin{bmatrix} x \\ z \end{bmatrix}\end{aligned}$$

where

$$Q_1 = \begin{bmatrix} A^T P_1 + P_1 A & -\frac{1}{\sigma}\left(2p_2 C^T - \sigma P_1 B\right) \\ -\frac{1}{\sigma}\left(2p_2 C - \sigma B^T P_1\right) & \frac{1}{\sigma^2} 2a_2 p_2 \end{bmatrix}.$$

Then $Q_1 \prec 0$ since $Q \prec 0$ (the principal minors of both matrices have the same sign) and so

$$\mathcal{L}_{S_1}\tilde{U}_1(x) < \alpha z^2 + 2\tilde{\delta}wz, \quad \forall x, z. \tag{4.31}$$

Since $\alpha > 0$, inequalities (4.30) and (4.31) imply that $U_1(x) := \frac{1}{\alpha}\tilde{U}_1(x)$ and $U_2(y) := \frac{1}{\alpha}\tilde{U}_2(y)$ satisfy

$$\begin{aligned}\mathcal{L}_{S_1} U_1(x) &< z^2 + 2\delta wz, \quad \forall x, z \\ \mathcal{L}_{S_2} U_2(y) &\leq -z^2 - 2\delta wz, \quad \forall y, w\end{aligned}$$

with $\delta = \frac{1}{\alpha}\tilde{\delta} = \frac{\sigma}{k_y - \sigma}$. ■

4.6.3 Limitations of the Decomposition

Lemma 4.7: *If $k_i = k$, $\forall i$ for (4.19) and there exists a positive definite $U_1(x) = x^T P_1 x$ satisfying (4.17) with $\delta > 0$, then $\delta < \frac{1}{2}\theta(n)$ and there exists a diagonal matrix $\tilde{P}_1 \succ 0$ such that $\tilde{U}_1(x) = x^T \tilde{P}_1 x$ satisfies (4.17).*

PROOF: Let $\mathcal{L}_{L_1}$ be the Lie derivative for system (4.19) and $W(x) = kU_1(x)$, then for all x, z

$$\mathcal{L}_{L_1} W(x) < kz^2 + 2\delta kwz$$

and

$$\begin{aligned} 0 &\succ \begin{bmatrix} A^T kP_1 + kP_1 A & kP_1 B - \delta k C^T \\ B^T kP_1 - \delta kC & -k \end{bmatrix} \\ &= \begin{bmatrix} A^T & -2\delta k C^T \\ B^T & -k \end{bmatrix} \begin{bmatrix} kP_1 & 0 \\ 0 & \frac{1}{2} \end{bmatrix} + \begin{bmatrix} kP_1 & 0 \\ 0 & \frac{1}{2} \end{bmatrix} \begin{bmatrix} A & B \\ -2\delta kC & -k \end{bmatrix} \\ &= M^T P + PM, \end{aligned}$$

where

$$\begin{aligned} M &= \begin{bmatrix} -k & 0 & \cdots & 0 & 0 & 1 \\ k & -k & & 0 & 0 & 0 \\ & \ddots & \ddots & & & \vdots \\ 0 & 0 & & -k & 0 & 0 \\ 0 & 0 & & k & -k & 0 \\ 0 & 0 & \cdots & 0 & -2\delta k^2 & -k \end{bmatrix} \\ &= \begin{bmatrix} I_n & 0 \\ 0 & -1 \end{bmatrix} \begin{bmatrix} -k & 0 & \cdots & 0 & 0 & -1 \\ k & -k & & 0 & 0 & 0 \\ & \ddots & \ddots & & & \vdots \\ 0 & 0 & & -k & 0 & 0 \\ 0 & 0 & & k & -k & 0 \\ 0 & 0 & \cdots & 0 & 2\delta k^2 & -k \end{bmatrix} \begin{bmatrix} I_n & 0 \\ 0 & -1 \end{bmatrix}. \end{aligned}$$

But for $\delta > 0$, M is stable if and only if $\delta < \frac{1}{2}\theta(n)$ [43]. Furthermore, if M is stable it is diagonally stable [2]. So there exists a diagonal $\tilde{P}_1 \succ 0$ such that

$$\mathcal{L}_{L_1}\left(x^T \tilde{P}_1 x\right) < kz^2 + 2\delta kwz$$

■

Next we show that if $\frac{\partial}{\partial x_i} g_i(x_i)|_0 = k$, $\forall i$, then for $\hat{h} > \hat{h}_d(n)$ there is no quadratic block diagonal Lyapunov function $U(x, y) = U_1(x) + U_2(y)$ for system (4.28) (the linearization of system (4.5)).

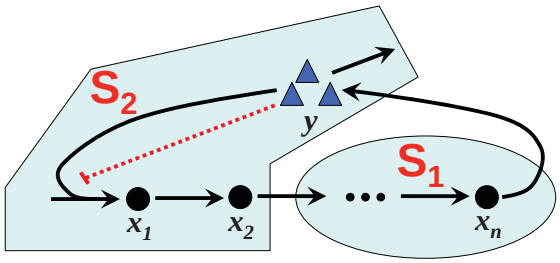

Figure 4.9: Illustration of the general decomposition for $n_2 = 3$.

Proposition 4.7: *If* $\frac{\partial}{\partial x_i} g_i(x_i)|_0 = k$, $\forall i$, *in* (4.5), *then for* $\hat{h} > \hat{h}_d(n)$ *there is no quadratic block diagonal Lyapunov function* $U(x,y) = U_1(x) + U_2(y)$ *for system* (4.28).

PROOF: Assume that for $\hat{h} > \hat{h}_d(n) > q$, and quadratic $U(x,y) = U_1(x) + U_2(y)$ exists for system (4.28). By Proposition 4.6, there exists $\tilde{U}_1 = x^T P_1 x$ and $\delta = \frac{\sigma}{k_y - \sigma}$ satisfying (4.17). On the other hand Lemma 4.7 implies $\delta < \frac{1}{2}\theta(n)$ and

$$\begin{array}{rcl} \delta = \frac{\sigma}{k_y-\sigma} = \frac{r_y(\hat{h}-q)}{k_y - r_y(\hat{h}-q)} & < & \frac{1}{2}\theta(n) = \frac{r_y(\hat{h}_d-q)}{k_y - r_y(\hat{h}_d-q)} \\ & \Downarrow & \\ \hat{h} & < & \hat{h}_d(n). \end{array}$$

Consequently, the contradiction implies that no quadratic block diagonal Lyapunov function for system (4.28) exists. ■

4.7 General Decomposition

We represent system (4.5) as feedback interconnection of 2 systems S_1 and S_2 as shown in Figure 4.6, with S_1 in $\mathbb{R}^{n_1}$ and S_2 in $\mathbb{R}^{n_2}$, $n_1 + n_2 = n + 1$ (illustrated in Figure 4.9 for $n_2 = 3$). System S_1 is given by

$$\begin{array}{rcl} \zeta & = & F_1(\zeta) + B_1 z \\ w & = & G_1(\zeta) \end{array} \qquad (4.32)$$

for $\zeta \in \mathbb{R}^{n_1}$, where

$$\begin{aligned} F_1(\zeta) &= \begin{bmatrix} -g_{m+1}(\zeta_1) \\ g_{m+1}(\zeta_1) - g_{m+2}(\zeta_2) \\ \vdots \\ g_{m+n_1-1}(\zeta_{n_1-1}) - g_{m+n_1}(\zeta_{n_1}) \end{bmatrix} \\ G_1(\zeta) &= g_{m+n_1}(\zeta_{n_1}) \\ B_1 &= \begin{bmatrix} 1 & 0 & \cdots & 0 \end{bmatrix}^T \end{aligned}$$

and $m = n_2 - 1$. System S_2 is given by

$$\begin{aligned} \psi &= F_2(\psi) + B_2 w \\ z &= G_2(\psi) \end{aligned} \tag{4.33}$$

for $\psi \in \mathbb{R}^{n_2}$, where

$$\begin{aligned} F_2(\psi) &= \begin{bmatrix} -f(\psi_1) - g_y(\psi_1) \\ f(\psi_1) - g_1(\psi_2) \\ g_1(\psi_2) - g_2(\psi_3) \\ \vdots \\ g_{n_2-2}(\psi_{n_2-1}) - g_{n_2-1}(\psi_{n_2}) \end{bmatrix} \\ G_2(\psi) &= g_{n_2-1}(\psi_{n_2}) \\ B_2 &= \begin{bmatrix} 2 & 0 & \cdots & 0 \end{bmatrix}^T. \end{aligned}$$

We will call any such feedback interconnection of systems in $\mathbb{R}^{n_1}$ and $\mathbb{R}^{n_2}$ a (n_1, n_2)-decomposition of (4.5). Let $\mathcal{L}_S$, $\mathcal{L}_{S_1}$, and $\mathcal{L}_{S_2}$ be the Lie derivatives for the systems (4.5), (4.32), and (4.33) respectively. Similar to the previous decomposition, we search for a neighborhood $\mathcal{N}_2 \subset \mathbb{R}^{n_2}$ of the origin, and positive definite function $U_1 : \mathbb{R}^{n_1} \to \mathbb{R}$ in $\mathbb{R}^{n_1}$ and positive definite function$U_2 : \mathbb{R}^{n_2} \to \mathbb{R}$ in $\mathcal{N}_2$ such that

$$\mathcal{L}_{S_1} U_1(\zeta) \leq \rho(w, z), \quad \forall\, (\zeta, z) \in \mathbb{R}^{n_1} \times \mathbb{R} \tag{4.34}$$

$$\mathcal{L}_{S_2} U_2(\psi) \leq -\rho(w, z), \quad \forall\, (\psi, w) \in \mathcal{N}_2 \times \mathbb{R}. \tag{4.35}$$

where $\rho : \mathbb{R}^2 \to \mathbb{R}$ is a supply rate parametrized by δ and κ

$$\rho(w, z) := z^2 + 2\delta wz - \kappa w^2.$$

Define

$$U(\zeta, \psi) := U_1(\zeta) + U_2(\psi), \tag{4.36}$$

and β be such that

$$\Omega_{U,\beta} \subset \mathbb{R}^{n_1} \times \mathcal{N}_0.$$

A proposition analogue to Proposition 4.3 holds.

Proposition 4.8: *$\Omega_{U,\beta}$ is invariant under the flow of* (4.5)*, and if one of the inequalities* (4.8), (4.9) *is strict then $\Omega_{U,\beta}$ is a subset of the region of attraction of the origin of* (4.5).

PROOF: Similar to proof of Proposition 4.3. ∎

As before if F_2 is rational we can search for U_1, U_2 using generalizations of the S-procedure and SOS relaxations, as in Section 3.3. Let $F_2(\psi) = \frac{n_2(\psi)}{d_2(\psi)}$, where $d_2(\psi) > 0$ for $\psi \geq 0$, and define $\mathcal{N}_2$ by using the sublevel sets of a positive definite polynomial function φ_2 with $\varphi_2(\mathbf{0}) = 0$ and compact level sets, i.e., $\mathcal{N}_2 = \Omega_{\varphi_2,R_2} = \{\mathbf{x} \in \mathbb{R}^{n_2} \mid \varphi_2(\mathbf{x}) < R_2\}$. The corresponding SOS problems for finding U_1 and U_2 are

$$\begin{aligned} U_1(\zeta) - \epsilon\zeta^T\zeta \quad &\text{is} \quad \text{SOS} \\ -\tfrac{\partial}{\partial\zeta}U_1(\zeta)\cdot(F_1(\zeta) + B_1 z) + \rho(z, G_1(\zeta)) - \epsilon\zeta^T\zeta \quad &\text{is} \quad \text{SOS} \end{aligned} \tag{4.37}$$

and

$$\begin{aligned} U_2(\psi) - \epsilon\psi^T\psi + s_1(\psi)\,(\varphi_2(\psi) - R_2) \quad &\text{is} \quad \text{SOS} \\ d_2(\psi)\left\{-\tfrac{\partial}{\partial\psi}U_2(\psi)\cdot(F_2(\psi) + B_2 w) - \rho(G_2(\psi), w)\right\} & \\ +d_2(\psi)s_2(\psi, w)\,(\varphi_2(\psi) - R_2) - \epsilon\psi^T\psi \quad &\text{is} \quad \text{SOS}, \end{aligned} \tag{4.38}$$

where s_1, s_2 are SOS polynomials. The subset Ω_{φ_2,R_2} can be further improved by taking $\varphi_2 = U_2$ and using coordinate-wise affine iterations [41]. These two problems

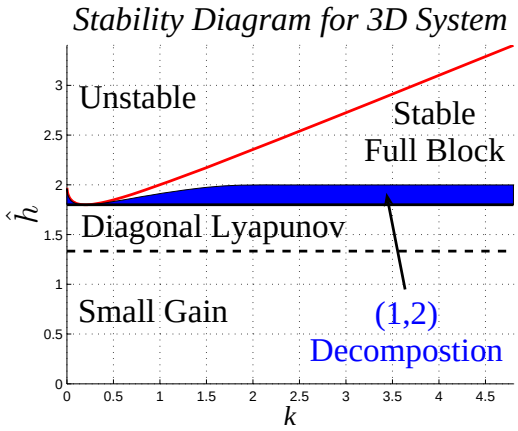

Figure 4.10: Stability diagram for the 3D system with $g_i(x_i) = kx_i$, $i = 1, 2$, $q = 1$, $\frac{\partial}{\partial y} g_y(y)|_0 = 1$. The $(2, 1)$-decomposition can only be used to construct Lyapunov functions for the parameter sets labeled Diagonal Lyapunov and Small Gain. In addition to this sets, the $(1, 2)$-decomposition only be used to construct Lyapunov functions for the set in blue also.

are coupled through the decision variables (δ, κ) in the supply rate ρ. Let us denote by $2\alpha_1$ the highest degree of the polynomials in SOS problem (4.37) and by $2\alpha_2$ the highest degree of the polynomials in SOS problem (4.38). We assume α_1 to be small since we expect system S_1 to be simple (i.e. low degree vector field, even linear if mass-action kinetics are used), and α_2 to be much larger since the degree (h) of $d_2(\psi)$ could be high.

We now focus on the special case where

$$\frac{\partial}{\partial x_i} g_i(x_i)|_0 = k, \text{ for all } i = 1, \ldots, n.$$

We have shown in the previous section that for $\hat{h}_s < \hat{h} < \hat{h}_d(n)$, we can find block diagonal Lyapunov functions that give an estimate of region of attraction for the system. For this special case Proposition 4.7 establishes that for $\hat{h} > \hat{h}_d(n)$ there is no (quadratic) block diagonal Lyapunov function of the form $U(x, y) = U_1(x) + U_2(y)$, $x \in \mathbb{R}^n$, $y \in \mathbb{R}$ exists for the linearization of (4.5), i.e., the $(n, 1)$-decomposition cannot produce even a local quadratic Lyapunov function for (4.5). To find Lyapunov functions for systems with $\hat{h} > \hat{h}_d(n)$ we increase the dimension of the system S_2. However this becomes computationally expensive since α_2 is big, i.e., we are moving

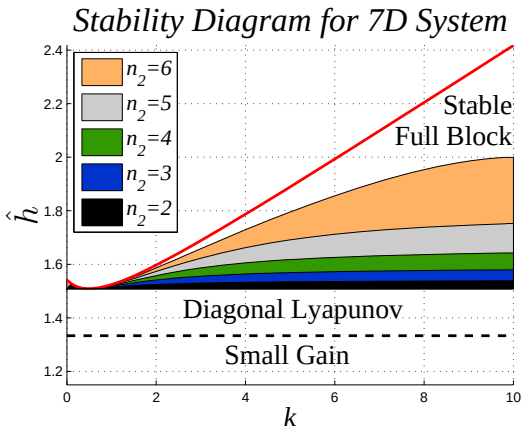

Figure 4.11: For longer pathways different (n_1, n_2)-decompositions are used to produce Lyapunov functions that verify subsets of region of attraction of the origin. For a fixed k as the feedback gain $\hat{h}$ approaches the stability boundary, it requires larger systems S_2 (increase in n_2), i.e., the computational complexity of finding a Lyapunov function increases. Figure shows the 7D system with $q = 1$, $\frac{\partial}{\partial y} g_y(y)|_0 = 1$.

toward the bottom right corner of Table 4.1. We now restrict our search to block diagonal Lyapunov functions of the form (4.36) where U_1 is diagonal, i.e. $U_1(\zeta) = \sum_{i=1}^{n_1} V_i(\zeta_i)$. As such the size of the SDP required to verify (4.34) is small, and we will approximate the size of the SDP required to find U, by the size of the SDP required to find U_2. Therefore the computational complexity of the problem (determined by the SDP size) increases as the dimension n_2 of the system S_2 increases.

Example 4.2: *Let us look at the* $(1, 2)$*-decomposition of a simple 3D pathway with* $g_i(x_i) = kx_i$, $i = 1, 2$. *Then we have the following* S_1

$$\begin{aligned} \dot{x}_1 &= z - kx_1 \\ w &= kx_1 \end{aligned}$$

and S_2

$$\begin{aligned} \dot{x}_2 &= w - kx_2 \\ \dot{y} &= 2kx_2 - f(y) - g_y(y) \\ z &= f(y) \end{aligned}$$

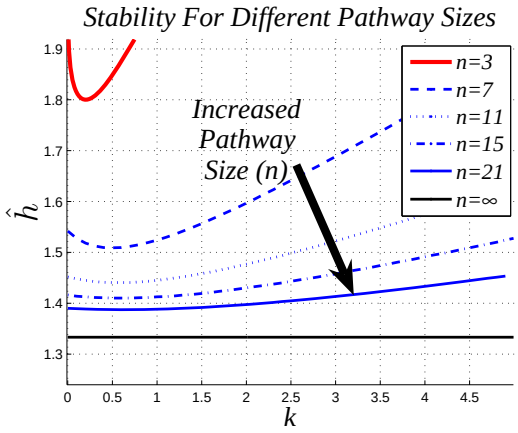

Figure 4.12: As the size of the pathway increases, the size of the stability region gets smaller. Figure shows the stability bounds for the feedback gain $\hat{h}$ as a function of k, for n-D systems with $q = 1$, $\frac{\partial}{\partial y} g_y(y)|_0 = 1$.

with $f(y) = \frac{r_y(1+\gamma)(y+1)^q}{1+\gamma(y+1)^h} - r_y$. *For* $\kappa > 0$, $\delta = \frac{\kappa-1}{2}$, $U_1(x_1) = \frac{1}{2}(1+\kappa)\, x_1^2$

$$\begin{aligned} \mathcal{L}_{S_1} U_1(x_1) - z^2 - (\kappa-1)\, wz + \kappa w^2 &= (1+\kappa)\, kx_1 (z - kx_1) - z^2 \\ &\quad - (\kappa-1)\, kx_1 z + \kappa k^2 x_1^2 \\ &= -z^2 + 2kx_1 z - k^2 x_1^2 \\ &= -(z - kx_1)^2 \end{aligned}$$

So we search for U_2 *satisfying*

$$\mathcal{L}_{S_2} U_2(x_2, y) \leq \kappa w^2 - (\kappa-1)\, wz - z^2$$

in a neighborhood of the origin. Figure 4.10 shows the set of parameters for which this decomposition can produce a Lyapunov function, for $q = 1$, $\frac{\partial}{\partial y} g_y(y)|_0 = 1$.

As the size of the pathway increases, the size of the stability region (in the parameter space) gets smaller (Figure 4.12) and range of feedback gains becomes limited. For a fixed pathway size, as feedback gains increase the corresponding systems approach the stability boundary and we need to use decompositions that require larger systems S_2, i.e., the problems become computationally more complex, as illustrated in Figure 4.11. For a fixed k as the feedback gain $\hat{h}$ approaches the stability boundary, it requires

larger systems S_2 (increase in n_2), i.e., the computational complexity of finding a Lyapunov function increases.

Let $\chi_{n_2}(k)$ be defined as the largest value of feedback gain $\hat{h}$ for which the decomposition (n_1, n_2) produces a Lyapunov function for system (4.5). Figure 4.12 and Table 2.1 show that increase in pathway size has two adverse effects. It increases the computational complexity as indicated in column 2 of Table 2.1 but also it limits the feedback gains that can be captured by the simpler decompositions, i.e. it moves the system into the lower, more complex rows of Table 2.1.

4.8 Summary

Autocatalytic metabolic networks (pathways), such as glycolysis, are composed of a chain of enzymatically catalyzed intermediate reactions. To characterize the effect of the size (n) of the chain on the stability and performance properties of the pathway, we explicitly account for the intermediate reactions in the model given by equation (4.1). As in the 2D case, allosteric feedback regulation can suppress the positive feedback generated by autocatalysis, thus guaranteeing both the boundedness of the system's trajectories, as well as the local stability of the operating fixed point. A direct application of a secant condition [2, 39, 43] gives an upper bound $\hat{h}_d(n)$ on the feedback gains $\hat{h}$, that result in stable pathways of fixed size (n) and arbitrary (fixed) intermediate reaction rates. We also establish lower and upper bounds, respectively $\hat{h}_s$ and $\hat{h}_r$, on feedback gains that result in arbitrarily large stable pathways. All of these bounds depend on the stoichiometry and strength of autocatalysis, and the demand of the pathway product (ATP in glycolysis), but not on the other parameters. These bounds are tight in the sense that unstable pathways can be constructed for gains that lie outside the ranges established by them. The bound $\hat{h}_d(n)$ suggests that the range of possible stable gains gets smaller as the pathway size (n) increases. The RHP zero, studied in detail for the 2D system, also becomes smaller with an increase in n thus making larger pathways harder to control. This means that larger chains of enzymatically catalyzed intermediate reactions in the autocatalytic pathways cause

Feedback Gain $\hat{h}$	Computational Complexity (SDP size)	Comment
$\hat{h}_r < \hat{h} < \hat{h}_s$	$O(1)$	Small Gain
$\hat{h}_s \leq \hat{h} < \hat{h}_d(n)$	$O(n)$	Diagonal Lyapunov function
$\hat{h}_d(n) \leq \hat{h} < \chi_2(k)$	$O\left(C_{\alpha_2}^{2+\alpha_2}\right) + O(n)$	Calculated by $(n-1,2)$-decomposition
$\chi_2(k) \leq \hat{h} < \chi_3(k)$	$O\left(C_{\alpha_2}^{3+\alpha_2}\right) + O(n)$	Calculated by $(n-2,3)$-decomposition
$\vdots$	$\vdots$	
$\chi_{n_2-1}(k) \leq \hat{h} < \chi_{n_2}(k)$	$O\left(C_{\alpha_2}^{n_2+\alpha_2}\right) + O(n-n_2)$	Complexity increases as the dimension n_2 of S_2 increases
$\vdots$	$\vdots$	
$\chi_n(k) \leq \hat{h} < \chi_{n+1}(k)$	$O\left(C_{\alpha_2}^{n+1+\alpha_2}\right)$	Full block Lyapunov function

Table 4.2: Computational complexity (size of the SDP) as a function of feedback gain and pathway size (n). Increase in pathway size has two adverse effects, it increases the computational complexity (column 2) and it limits the feedback gains that can be captured by the simpler decompositions, i.e., it moves the system into the lower, more complex rows of the table. α_2 is the degree of the polynomials in (4.38) and $C_j^i = \frac{i!}{j!(i-j)!}$.

two adverse effects on performance: good performance at low frequencies gets more expensive (smaller RHP zero) and, the range of stable gains available is reduced which makes the operating gains less robust and reduces the achievable performance objectives.

If the dynamics of (4.1) are rational functions of the state, the size of the region of attraction of the fixed point can be estimated by optimization-based formulations using Lyapunov functions and SOS programming. As previously discussed, these formulations reveal that low degree polynomial Lyapunov functions can verify region of attraction related properties for a wide range of parameters in three and four dimensional systems. The size of the invariant subsets of the region of attraction of the fixed point demonstrated that these pathways are not sensitive to perturbation in state space (i.e., perturbations in the concentrations of the products and reactants). We are unable to analyze systems with longer pathways because the degree of the polynomials in the corresponding SOS program is high which makes the problem computationally intractable.

A simple representation of the system (4.1) as the feedback interconnection of a n-state system S_1 given by (4.6) and a single state system S_2 given by (4.7), allows us to analytically construct diagonal Lyapunov functions via the use of local general dissipation or small-gain type inequalities for systems with feedback gain less than $\hat{h}_d(n)$. This simple decomposition allows us to construct block diagonal Lyapunov functions (i.e., functions of the type $U(x,y) = U_1(x) + U_2(y)$, $x \in \mathbb{R}^n$, $y \in \mathbb{R}$) for (4.1) if they exist. However this decomposition is not as useful for gains larger than $\hat{h}_d(n)$. In fact, we show that no quadratic block diagonal Lyapunov functions exists for the linearization of (4.1) if $\hat{h} > \hat{h}_d$ and the intermediate reaction rates are equal to each other around the fixed point.

To construct Lyapunov functions for gain $\hat{h} > \hat{h}_d$ a more general (n_1, n_2)-decomposition scheme is used. We represent (4.1) as the feedback interconnection of an n_1-state system S_1 given by (4.32) and an n_2-state system S_2 given by (4.33), with generally n_1 (much) bigger than n_2. If the vector field of system (4.1) is rational we can construct Lyapunov functions by using local dissipation inequalities and solving the correspond-

ing SOS problems (4.37) and (4.38). The first SOS problem (4.37) contains low degree ($2\alpha_1$) polynomials in many variables (n_1), and the second one contains high degree ($2\alpha_2$) polynomials in a few variables (n_2). As the size n_2 of system S_2 increases, so does the computational complexity of constructing a Lyapunov function. On the other hand, (n_1, n_2)-decomposition with the larger n_2 can be used to construct Lyapunov function for realizations of (4.1) with higher gains. This reinforces the notion that realizations that are more (computationally) complex can only arise from those realizations with high gains (i.e., gains that are close to the stability boundary, and therefore fragile to perturbations in parameter space). This framework also shows that, from the computational point of view, the increase in pathway size has two adverse effects: it makes it computationally harder to construct Lyapunov functions first by increasing the overall dimension of the problem $n = n_1 + n_2$ and second, by limiting the range of stable gains available, thus pushing current gains closer to the stability boundary, and therefore requiring (n_1, n_2)-decomposition with large n_2.

Chapter 5

Autocatalytic Networks with Reversible Reactions and Consumption of Intermediates

5.1 Introduction

Individual biological networks (pathways) within the cell do not act in isolation. They are an integral part of the whole cell activity and are coupled with other networks through the exchange of products and sharing of components. In metabolism specifically, many of the intermediate products of the pathway are used and consumed by other processes in the cell. Glycolysis for example provides many of the necessary intermediates used to produce amino acids, lipids, nucleotides, and other organic molecules essential to the function of the cell [1]. In this chapter we investigate these interactions and in particular address the following question; How does this coupling of pathways through the consumption of intermediate metabolites effect their performance? Due to the fact that many biological pathways are composed not only of irreversible chemical reactions, but also reversible ones we are also interested in understanding whether or not the reversibility of the chemical reactions make the pathways harder to control.

In order to address these questions, we investigate the role that the consumption of the intermediate resources and reversibility play in the performance of autocatalytic pathway. To carry out this study we first extend the 2D model of equation (3.1)

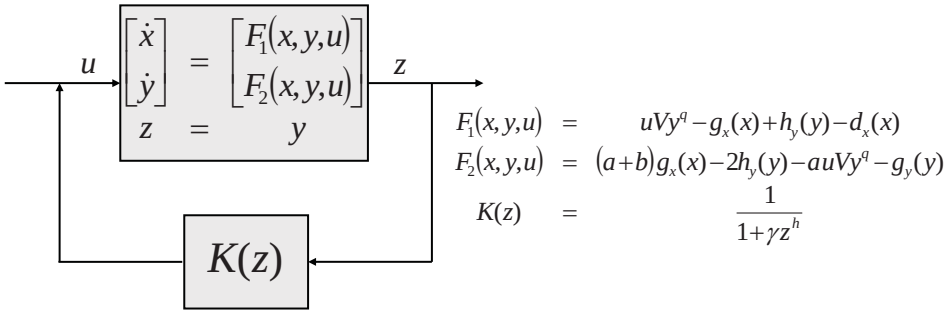

Figure 5.1: Control of autocatalytic plant with reversible reaction and intermediate consumption. This representation implies the same closed-loop system as system (5.1).

to include reversibility of the intermediate chemical reaction and consumption of the intermediate metabolite. Later in this chapter we further expand this model to incorporate large chains of intermediate (reversible) reactions. The chemical reactions that comprise the extended 2D model are given by

$$\begin{array}{ccc} u + ay \overset{f}{\rightharpoonup} x & \underset{h_y}{\overset{g_x}{\rightleftharpoons}} & (a+b)\, y \\ x \overset{d_x}{\rightharpoonup} \varphi & & y \overset{g_y}{\rightharpoonup} \varphi. \end{array}$$

We consider the case $a = b = 1$ with the corresponding ODE

$$\begin{aligned} \dot{x} &= f(y) - g_x(x) + h_y(y) - d_x(x) \\ \dot{y} &= 2g_x(x) - 2h_y(y) - f(y) - g_y(y), \end{aligned} \tag{5.1}$$

for $x, y \geq 0$ and where g_x, g_y, h_y, d_x are continuous, monotone increasing functions, with $g_x(0) = g_y(0) = d_x(0) = h_y(0) = 0$ and $f(y) = \frac{Vy^q}{1+\gamma y^h}$. In the following sections the tools and ideas developed in Chapter 2 and 3 are applied to the analysis of the model given by (5.1).

5.2 Control of Two Dimensional Model

The model (5.1) can be viewed as output feedback control of an autocatalytic plant as shown in Figure 5.1. Furthermore, if a fixed point $(x_0, y_0) \succ (0, 0)$ of (5.1) exists,

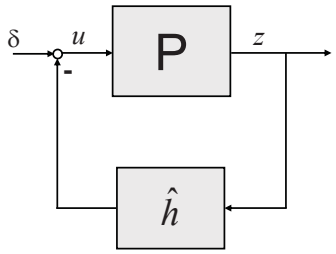

Figure 5.2: System (5.2) in output feedback control form.

then without loss of generality the system can be rescaled such that $y_0 = 1$. Then if we define

$$\begin{aligned} V_0 &:= f(1) = \tfrac{V}{1+\gamma} & \hat{h} &:= \tfrac{\gamma}{\gamma+1}h \\ k_x &:= \tfrac{\partial}{\partial x} g_x(x)|_{x_0} & \eta_x &:= \tfrac{\partial}{\partial x} d_x(x)|_{x_0} \\ k_y &:= \tfrac{\partial}{\partial y} g_y(y)|_1 & r_y &:= \tfrac{\partial}{\partial y} h_y(y)|_1 \end{aligned}$$

the dynamics near this fixed point are given by the linear system

$$\begin{bmatrix} \dot{x} \\ \dot{y} \end{bmatrix} = \begin{bmatrix} -k_x - \eta_x & V_0(q - \hat{h}) + r_y \\ 2k_x & -V_0(q - \hat{h}) - 2r_y - k_y \end{bmatrix} \begin{bmatrix} x \\ y \end{bmatrix}. \tag{5.2}$$

This system is represented by the following state space standard output linear feedback form;

$$\begin{aligned} \dot{\mathbf{x}} &= A\mathbf{x} + Bu \\ z &= C\mathbf{x} \\ u &= -\hat{h}C\mathbf{x} \end{aligned}$$

where

$$\begin{aligned} A &= \begin{bmatrix} -k_x - \eta_x & V_0 q - r_y \\ 2k_x & -V_0 q - 2r_y - k_y \end{bmatrix} \\ B &= V_0 \begin{bmatrix} 1 \\ -1 \end{bmatrix} \\ C &= \begin{bmatrix} 0 & 1 \end{bmatrix}. \end{aligned}$$

The corresponding frequency domain description is shown in Figure 5.2 with $P(s) = C\left(sI - A\right)^{-1} B$ and feedback gain $\hat{h}$. In the next section we use this formulation to first study the role of reversibility and then to investigate the role of intermediate consumption on the performance of the pathway. We are interested on how well the pathway maintains the concentration of the output y at the desired steady state y_0. Again normalizing the concentration at $y_0 = 1$, makes a comparison of the different topologies possible.

5.2.1 Effects of Reversible Reactions

If in Equation (5.1) we assume that there is no consumption of intermediate metabolite x ($d_x(x) = 0$) and consider the case $a = b = 1$, then the resulting ODE is

$$\begin{aligned} \dot{x} &= \tfrac{Vy^q}{1+\gamma y^h} - g_x(x) + h_y(y) \\ \dot{y} &= 2g_x(x) - 2h_y(y) - \tfrac{Vy^q}{1+\gamma y^h} - g_y(y). \end{aligned}$$

Similar to Equation (3.1) the fixed points are found by solving $f(y_0) = g_y(y_0)$, $x = g^{-1}\left(f(y_0) + h(y_0)\right)$. If we again set $y_0 = 1$ then the linearization around the fixed point $(x_0, 1)$ is given by

$$\begin{bmatrix} \dot{x} \\ \dot{y} \end{bmatrix} = \begin{bmatrix} -k_x & V_0(q - \hat{h}) + r_y \\ 2k_x & -V_0(q - \hat{h}) - 2r_y - k_y \end{bmatrix} \begin{bmatrix} x \\ y \end{bmatrix}. \tag{5.3}$$

Equation (5.3) shows that the fixed point is stable for

$$q - \frac{1}{V_0} k_y < \hat{h} < q + \frac{1}{V_0}\left(k_x + k_y + 2r_y\right),$$

and so the presence of the reversible reactions increases the range of stable gains $\hat{h}$. This suggests that the reversible reactions make the pathway easier to control. There

is still a RHP zero at $s = k_x$ since

$$\begin{aligned} P(s) &= C\left(sI - A\right)^{-1} B \\ &= -V_0 \tfrac{s-k_x}{p_A(s)}. \end{aligned}$$

which implies that the special form (2.9) of the Bode sensitivity integral holds for this system. However, because the range of the stable gains is larger for higher reversible reaction (RR) rates, the same feedback gain is more "robust". This suggests that systems with higher RR rates have better performance (i.e., smaller peak in the $\log|S|$, and smaller oscillations in the step response, Figure 5.3 A and B). It also means that higher gains can be used for systems with high RR rates to obtain better performance at low frequencies and better steady state error without a meaningful increase in performance losses at high frequencies and qualitatively similar oscillations in the step response, as shown in Figure 5.3 C and D.

5.2.2 Effects of the Consumption of Intermediates

Assume that there are no reversible reactions in the system (5.1), i.e., $h_y(y) = 0$, then the corresponding ODE for $a = b = 1$ is

$$\begin{aligned} \dot{x} &= \tfrac{Vy^q}{1+\gamma y^h} - g_x(x) - d_x(x) \\ \dot{y} &= 2g_x(x) - \tfrac{Vy^q}{1+\gamma y^h} - g_y(y). \end{aligned}$$

Notice that at a fixed point (x_0, y_0)

$$d_x(x_0) - g_x(x_0) = -\left(h_y(y_0) + g_y(y_0)\right),$$

so a fixed point $(x_0, y_0) \succ (0,0)$ exists only if $d_x(x_0) < g_x(x_0)$, i.e., the pathway cannot allow more intermediate metabolite consumption by other pathways than it is using. If a fixed point $(x_0, y_0) \succ (0,0)$ exists, then without loss of generality we can again

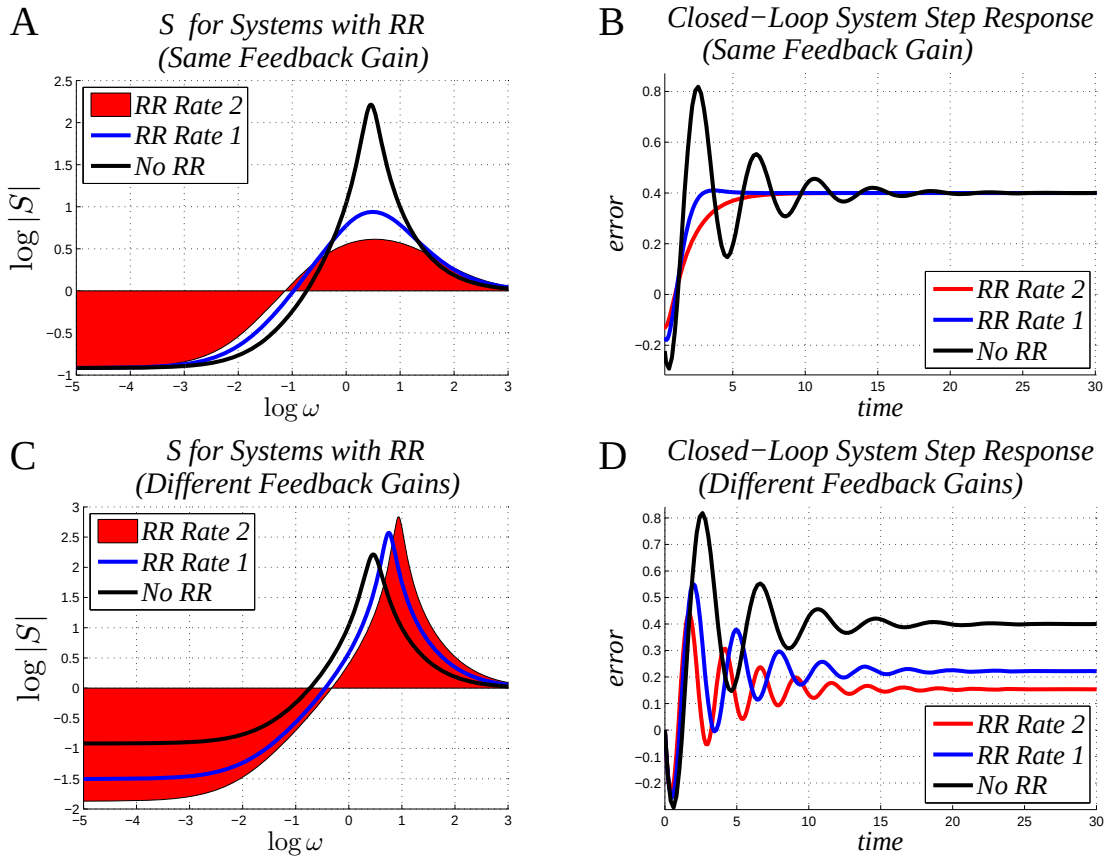

Figure 5.3: The performance of three 2D models with $k_x = 1$, $q = 2$, $k_y = 1$, $V_0 = 1$ and $r_y = 2,\ 1,\ 0$ is compared. (A)-(B) Using the same feedback gain $\hat{h} = 3.5$, the systems with higher reversible reaction (RR) rates have better performance (i.e., smaller peak in $\log|S|$, and smaller oscillations in the step response). (C)-(D) Models with higher reversible reaction rates allow for higher stabilizing gains. Using $\hat{h} = 7.5,\ 5.5,\ 3.5$ respectively, we obtain better performance at low frequencies and better steady state error (without a meaningful increase in performance losses at high frequencies and qualitatively similar oscillations in the step response) for the systems with higher RR rates.

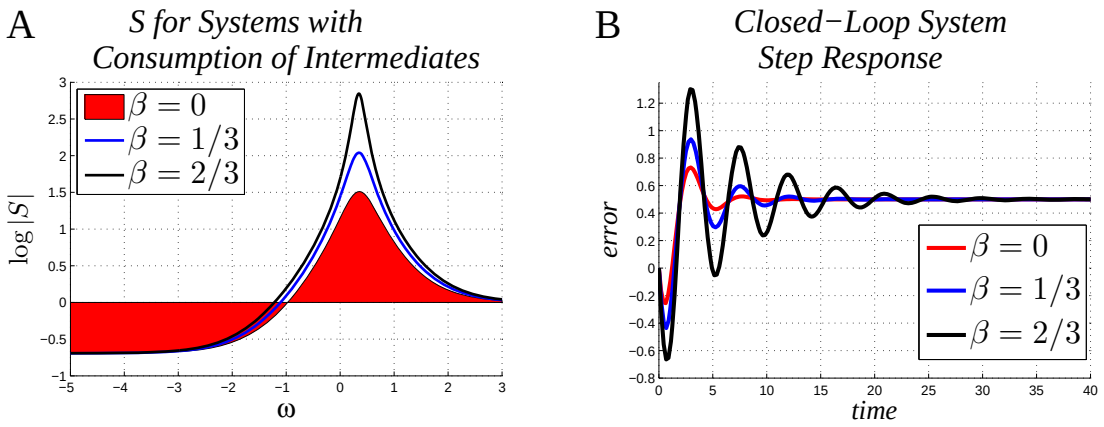

Figure 5.4: Performance of three 2D models with $k_x = 1$, $q = 2$, $k_y = 1$, and $\eta_x = \beta k_x$ with $\beta = 0$, $\frac{1}{3}$, $\frac{2}{3}$ is compared. Using the same feedback gain $\hat{h} = 3$, the systems with less consumption of intermediates have better performance, which corresponds to a smaller peak in $\log|S|$ plot, and less oscillations in the step response.

set $y_0 = 1$ and the linearization around the fixed point $(x_0, 1)$ is given by

$$\begin{bmatrix} \dot{x} \\ \dot{y} \end{bmatrix} = \begin{bmatrix} -k_x - \eta_x & V_0(q - \hat{h}) \\ 2k_x & -V_0(q - \hat{h}) - k_y \end{bmatrix} \begin{bmatrix} x \\ y \end{bmatrix}. \tag{5.4}$$

The point $(x_0, 1)$ is stable for

$$q - \frac{1}{V_0} k_y \frac{k_x + \eta_x}{k_x - \eta_x} < \hat{h} < q + \frac{1}{V_0}(k_x + k_y + \eta_x)$$

and, as it can be shown that it is open-loop ($\hat{h} = 0$) stable when η_x is close enough to k_x. Notice that η_x cannot be larger than k_x, since for $\delta := \eta_x - k_x > 0$ and $\delta < k_y \frac{\eta_x + k_x}{\eta_x + k_x + k_y}$, the system is not stabilizable.

Under the above conditions, the consumption of the intermediate increases the range of stable gains $\hat{h}$. Similar to the RR case, this suggests that the consumption of the intermediate might make the pathway easier to control. However, the plant has a RHP zero at $s = k_x - \eta_x$ since

$$\begin{aligned} P(s) &= C(sI - A)^{-1} B \\ &= -V_0 \frac{s - k_x + \eta_x}{p_A(s)}, \end{aligned}$$

which implies that as η_x increases the magnitude of the RHP zero gets smaller, which puts harder constrains on performance. It appears that this is another performance tradeoff and it is not clear whether or not the consumption of intermediates helps the performance of the system.

We can further investigate the effect of the intermediate consumption on the system by defining $m(x) := g_x(x) + d_x(x)$ and $\alpha(x)$ such that $d(x) = \alpha(x)m(x)$ which results in a system of the form;

$$\begin{aligned} \dot{x} &= \frac{Vy^q}{1+\gamma y^h} - m(x) \\ \dot{y} &= (2-\alpha(x))\, m(x) - \frac{Vy^q}{1+\gamma y^h} - g_y(y). \end{aligned}$$

These equations show that consumption of intermediates has the same effect as reducing the efficiency of the pathway. For example, if $g_x(x) = kx$ and $d_x(x) = \beta kx$, then $\alpha = \frac{\beta}{\beta-1}$ and this pathway is equivalent to a pathway with $g_x(x) = (1+\beta)kx$ that produces $(2-\alpha)$ molecules of y for each molecule y invested. As Figure 5.4 shows, larger β leads to a higher price paid for good performance at low frequencies and more oscillations for the same steady state error.

5.3 Nonlinear Characterization for the Extended 2D Model

The global nonlinear characteristics of the 2D system of Equation (3.1) are similar to the case with no RR or consumption of intermediates described by system (3.1) in Chapter 3. In addition the positive orthant remains invariant with respect to the flow of (5.1) since

$$\begin{aligned} x = 0 \;&\Rightarrow\; \dot{x} = \frac{Vy^q}{1+\gamma y^h} + g_y(y) > 0, \quad \text{for } y > 0 \\ y = 0 \;&\Rightarrow\; \dot{y} = 2g_x(x) > 0, \quad \text{for } x > 0. \end{aligned}$$

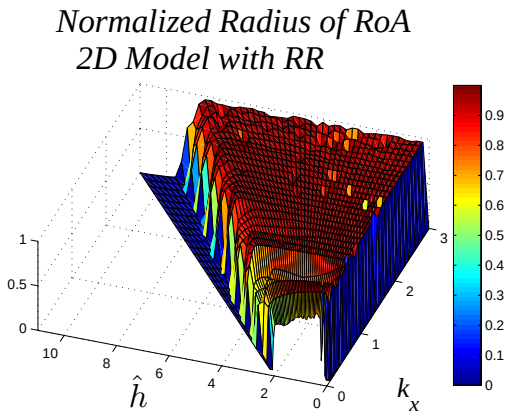

Figure 5.5: The normalized radius of the invariant subset of region of attraction (RoA) for the nominal operating point for a 2D systems with reversible reactions (RR), computed using second degree polynomial Lyapunov functions ($g_x(x) = k_x x$, $h_y(y) = k_x y$, $q = 1$, $g_y(y) = y$, $d_x(x) = 0$). The normalized radius of RoA is the radius of RoA estimate normalized by the distance to the nearest fixed point.

Also under some similar mild assumptions, an analogue of Lemma 3.1 holds as well, which assures that the trajectories of (5.1) are bounded.

Using the same optimization-based formulation as in Section 3.3, we can compute invariant subsets of the region of attraction for each of the fixed points. Figure 5.5 shows that for most parameter values, large invariant subsets of region of attraction can again be verified using second degree polynomial Lyapunov functions. Similar to the case with irreversible reactions (Equation (3.1)), the systems with parameter values close to the parameter stability boundary are harder to verify. This provides further evidence that the observation of Chapter 3 that robust realization have simple proofs (i.e., low degree polynomial Lyapunov functions can verify large invariant subset of region of attraction) is a property of these autocatalytic pathways.

5.4 Higher Dimensional Model of Autocatalytic Pathways with Reversible Reactions and Consumption of Intermediates

In this section we combine the ideas of Section 5.2 to analyze a general autocatalytic metabolic pathway composed of both reversible reactions and consumption of intermediate metabolites. The chemical reactions that comprise this general pathway are given by

$$\begin{array}{lccccccccc} u + ay \rightharpoonup^{f} & x_1 & \rightleftharpoons_{h_2}^{g_1} & x_2 & \rightleftharpoons_{h_3}^{g_2} & \cdots & \rightleftharpoons_{h_n}^{g_{n-1}} & x_n & \rightleftharpoons_{h_y}^{g_n} & (a+b)\,y \rightharpoonup^{g_y} \varphi \\ & \downarrow_{d_1} & & \downarrow_{d_2} & & & & \downarrow_{d_n} & & \\ & \varphi & & \varphi & & & & \varphi & & \end{array}$$

We consider the case where $a = b = 1$ with the corresponding ODE given by

$$\begin{array}{rcl} \dot{x}_1 & = & f(y) + h_2(x_2) - g_1(x_1) - d_1(x_1) \\ \dot{x}_2 & = & g_1(x_1) + h_3(x_3) - g_2(x_2) - h_2(x_2) - d_2(x_2) \\ \vdots & \vdots & \vdots \\ \dot{x}_{n-1} & = & g_{n-2}(x_{n-2}) + h_n(x_n) - g_{n-1}(x_{n-1}) - h_{n-1}(x_{n-1}) - d_n(x_{n-1}) \\ \dot{x}_n & = & g_{n-1}(x_{n-1}) + h_y(y) - g_n(x_n) - h_n(x_n) - d_n(x_n) \\ \dot{y} & = & 2g_n(x_n) - f(y) - 2h_y(y) - g_y(y), \end{array} \tag{5.5}$$

for $x_i \geq 0$, $y \geq 0$, and where $f(y) = \frac{Vy^q}{1+\gamma y^h}$ and for all i, g_i, h_i, d_i, g_y, h_y are continuous, monotone increasing functions that take the value 0 at 0.

5.4.1 Existence of the Fixed Point

Here we present a necessary conditions for the existence of a nonzero fixed point and provide a probabilistic interpretation for this condition. Let $h_y = 0$, $h_i = 0$ for all $i = 1, \ldots n$, i.e., no reversible reactions. Assume that the fixed point $(\bar{x}, \bar{y}) \succ (0, 0)$

exists, then

$$\begin{cases} f(\bar{y}) = g_1(\bar{x}_1) + d_1(\bar{x}_1) \\ g_1(\bar{x}_2) = g_2(\bar{x}_2) + d_2(\bar{x}_2) \\ \vdots \\ g_{n-1}(\bar{x}_{n-1}) = g_n(\bar{x}_n) + d_n(\bar{x}_n) \\ 2g_n(\bar{x}_n) = f(\bar{y}) + g_y(\bar{y}) \end{cases} \Rightarrow \left(2\prod_{i=1}^{n} \frac{g_i(\bar{x}_i)}{g_i(\bar{x}_i)+d_i(\bar{x}_i)} - 1\right) f(\bar{y}) = g_y(\bar{y}).$$

This implies that the fixed point $(\bar{x}, \bar{y}) \succ (0, 0)$ exists only if

$$2\prod_{i=1}^{n} p_i(\bar{x}_i) - 1 > 0 \tag{5.6}$$

where $p_i(\bar{x}_i) := \frac{g_i(\bar{x}_i)}{g_i(\bar{x}_i)+d_i(\bar{x}_i)}$. We can think of $p_i(\bar{x}_i)$ as the probability that a molecule x_i will continue to the next step of the pathway (i.e., will be converted into x_{i+1}), and $1 - p_i(\bar{x}_i) = \frac{d_i(\bar{x}_i)}{g_i(\bar{x}_i)+d_i(\bar{x}_i)}$ the probability that it will be used by another pathway. Then the probability that a molecule x_1 (produced by the first reaction through the investment of 1 molecule of y) will ultimately be converted into 2 molecules of y and not be used by other pathways is given by $\prod_{i=1}^{n} p_i(\bar{x}_i)$. So for each investment of 1 molecule of y at the start, the pathway expects a return of $E_p[y] = 2\left(\prod_{i=1}^{n} p_i(\bar{x}_i)\right)$ molecules of y at the end.

Condition (5.6) states that for a fixed point to exist, the expected return $E_p[y]$ should exceed the value of the investment, i.e., each molecule y invested must produce at least one molecule of y ($E_p[y] > 1$). So in order for the pathway to have a stable operating fixed point it must not allow excessive consumption of the intermediate metabolites. For example, let $d_i(x_i) = \alpha_i g_i(x_i)$, then condition (5.6) becomes

$$\prod_{i=1}^{n} \frac{1}{1+\alpha_i} > \frac{1}{2}.$$

If $\alpha_i = \alpha$ for all $i = 1, \ldots, n$ then $\alpha < \sqrt[n]{2} - 1$. So for a pathway of size 10, α has to be less than 0.072, i.e., only a small percentage of the intermediate metabolites can

be consumed at each step.

Remark 5.1: *If there are reversible reactions, we can get a similar condition to* (5.6) *by considering the "net flow"* $g_i(x_i) - h_{i+1}(x_{i+1})$ *through the pathway.*

5.4.2 Stability of the Fixed Point

If a nonzero fixed point $(\bar{x}, \bar{y}) \succ (0,0)$ of (5.5) exists, then without loss of generality we can set $\bar{y} = 1$. *For the rest of the chapter we will assume* $\bar{y} = 1$. If $\hat{h} := \frac{\gamma}{\gamma+1} h$, and

$$\begin{aligned} V_0 &:= f(1) = \tfrac{V}{1+\gamma} & r_i &:= \tfrac{\partial}{\partial x_i} h_i(x_i)|_{\bar{x}} \\ k_i &:= \tfrac{\partial}{\partial x_i} g_i(x_i)|_{\bar{x}} & \eta_i &:= \tfrac{\partial}{\partial x_i} d_i(x_i)|_{\bar{x}} \\ k_y &:= \tfrac{\partial}{\partial y} g_y(y_i)|_1 & r_y &:= \tfrac{\partial}{\partial y} h_y(y)|_1, \end{aligned}$$

then the dynamics of (5.5) near the fixed point are given by the following linear system

$$\begin{bmatrix} \dot{x} \\ \dot{y} \end{bmatrix} = J \begin{bmatrix} x \\ y \end{bmatrix} \tag{5.7}$$

for $x \in \mathbb{R}^n$, $y \in \mathbb{R}$ and where

$$J := \begin{bmatrix} -m_1 & r_2 & 0 & \cdots & 0 & 0 & V_0(q-\hat{h}) \\ k_1 & -m_2 & r_3 & & 0 & 0 & 0 \\ 0 & k_2 & -m_3 & \ddots & 0 & 0 & 0 \\ & & \ddots & \ddots & & & \vdots \\ 0 & 0 & 0 & & -m_{n-1} & r_n & 0 \\ 0 & 0 & 0 & & k_{n-1} & -m_n & r_y \\ 0 & 0 & 0 & \cdots & 0 & 2k_n & -k_y - V_0(q-\hat{h}) - 2r_y \end{bmatrix},$$

and for all i, $m_i := k_i + r_i + \eta_i$, $r_1 := 0$. Notice that all of the parameter in J are non-negative and k_i are strictly positive. This allows us to prove that the following analogue to Proposition 4.2 holds for this more general pathway.

Proposition 5.1: *(a) Let* $\hat{h}_r := q + \frac{1}{3}\frac{k_y}{V_0}$ *and* $\hat{h}_s := q - \frac{k_y}{V_0}$. *If* $\hat{h}_s < \hat{h} \leq \hat{h}_r$, *then*

(5.7) *is stable for arbitrary size (n) and arbitrary values of intermediate reaction rates (k_i,η_i,r_i, r_y).*

(b) The bounds above are tight, i.e. for any gain $\hat{h} \notin \left(\hat{h}_s, \hat{h}_r\right]$, there exists an unstable pathway.

PROOF: (a) Define

$$\begin{aligned} D &:= \operatorname{diag}\{\eta_1, \ldots, \eta_n, 0\} \succeq 0 \\ J_0 &:= J - D \end{aligned}$$

and

$$Q_0 := \begin{bmatrix} -k_1 & r_2 & 0 & \cdots & 0 & 2V_0(q-\hat{h}) \\ k_1 & -k_2 - r_2 & r_3 & & 0 & 0 \\ 0 & k_2 & -k_3 - r_3 & & 0 & 0 \\ \vdots & & \ddots & \ddots & & \\ 0 & 0 & 0 & & -k_n - r_n & 2r_y \\ 0 & 0 & 0 & & k_n & -k_y - V_0(q-\hat{h}) - 2r_y \end{bmatrix},$$

then

$$J_0 = \begin{bmatrix} I_n & 0 \\ 0 & 2 \end{bmatrix} Q_0 \begin{bmatrix} I_n & 0 \\ 0 & 2 \end{bmatrix}^{-1},$$

Consequently J_0 has the same eigenvalues as Q_0. Also by adding all of the preceding rows to row i of Q_0 one can easily compute the determinant of Q_0 as

$$\det Q_0 = (-1)^{n+1} k_1 \prod_{i=2}^{n} (k_i + r_i) \left(k_y - V_0(q-\hat{h})\right).$$

Consequently if $\hat{h} \neq q - \frac{k_y}{V_0} = \hat{h}_s$, then $\det Q_0 \neq 0$, and using diagonal dominance we can conclude that for $\hat{h}_s < \hat{h} \leq \hat{h}_r$, Q_0 is Hurwitz, and therefore J_0 is Hurwitz. This means that there exists a matrix $P \succ 0$ such that

$$J_0^T P + P J_0 = -I_{n+1}$$

[20]. Then

$$\begin{aligned} J^T P + PJ &= (J_0 - D)^T P + P(J_0 - D) \\ &= J_0^T P + PJ_0 - D^T P - PD \\ &= -I_{n+1} - (D^T P + PD) \end{aligned}$$

But $D^T P + PD \succeq 0$ since $P \succ 0$, $D \succeq 0$ and D is diagonal, so

$$J^T P + PJ \prec 0$$

and therefore J is Hurwitz for $\hat{h}_s < \hat{h} \leq \hat{h}_r$, and (5.7) is stable.

(b) This follows from direct application of Proposition 4.2 with $r_y = 0$, $\eta_i = 0$, $r_i = 0$ for all i. ■

5.5 Compositional Analysis

We showed in Section 5.3 that we can use optimization-based formulations to compute invariant subsets of the regions of attraction of the fixed points for the 2D version of (5.5). However, as the dimension of the pathway grows, the corresponding SOS programs become prohibitively large. To ameliorate this effect we propose a decomposition scheme for high dimensional problems that is similar to the decomposition of Chapter 4. This method takes advantage of the structure of the pathway and thus creates an SOS program that is computationally tractable for large subsets of the parameter space.

To begin the procedure we perform a change of coordinates for (5.5) so that the fixed point of interest, $(\bar{x}, 1)$, is at the origin. As before, all of the functions $g_i, h_i, d_i, g_y, h_y, f$ are just shifted versions of themselves. After relabeling we get

$$\begin{aligned} \dot{x} &= F(x) + B \begin{bmatrix} f(y) \\ r(y) \end{bmatrix} \\ \dot{y} &= 2g_n(x_n) - 2h_y(y) - f(y) - g_y(y) \end{aligned} \tag{5.8}$$

where $x \in \mathbb{R}^n$, $y \in \mathbb{R}$,

$$F(x) = \begin{bmatrix} h_2(x_2) - g_1(x_1) - d_1(x_1) \\ g_1(x_1) + h_3(x_3) - g_2(x_2) - h_2(x_2) - d_2(x_2) \\ \vdots \\ g_{n-1}(x_{n-1}) + h_y(y) - g_n(x_n) - h_n(x_n) - d_n(x_n) \end{bmatrix},$$

$$B = \begin{bmatrix} 1 & 0 & \cdots & 0 & 0 \\ 0 & 0 & \cdots & 0 & 1 \end{bmatrix}^T,$$

for all i, g_i, h_i, d_i, g_y, h_y are continuous, monotone increasing functions and take the value 0 at 0, and

$$f(y) = \frac{V(y+1)^q}{1+\gamma(y+1)^h} - \frac{V}{1+\gamma}.$$

System (5.8) can be decomposed into the feedback interconnection of two systems S_1 and S_2. System S_1 is a "simple" n-dimensional input-output system defined as

$$\begin{aligned} \dot{x} &= F(x) + Bz \\ w &= g_n(x_n) \end{aligned}$$

where $x \in \mathbb{R}^n$, $z \in \mathbb{R}^2$. System S_2 is a one dimensional nonlinear input-output system that captures the most important nonlinearity and has the form

$$\begin{aligned} \dot{y} &= 2w - 2h_y(y) - f(y) - g_y(y) \\ z &= \begin{bmatrix} f(y) \\ h_y(y) \end{bmatrix} \end{aligned}$$

where $y \in \mathbb{R}$.

If one considers the supply rate $\rho : \mathbb{R}^3 \to \mathbb{R}$, parametrized by δ_1, δ_2,κ_1, and κ_2

$$\rho(w, z_1, z_2) := w^2 - 2\delta_1 w z_1 - 2\delta_2 w z_2 - \kappa_1 z_1^2 - \kappa_2 z_2^2$$

and defines

$$\begin{aligned}
C_1(\delta_1,\delta_2) &:= 2\delta_1\sigma - 2\delta_2 c_2 + (2c_2 - \sigma + c_1) \\
C_2(\delta_1,\delta_2,\kappa_1,\kappa_2) &:= c_1^2 + 4c_1c_2 + 4c_2^2 - 2c_1\sigma - 4c_2\sigma + \sigma^2 \\
&\quad -4\kappa_1\sigma^2 - 4\kappa_2 c_2^2 \\
&\quad +4\delta_1\left(c_1\sigma + 2c_2\sigma - \sigma^2\right) \\
&\quad +4\delta_2\left(c_2\sigma - 2c_2^2 - c_1c_2\right) \\
v_1(y) &:= 2\left(\delta_1 f(y) + \delta_2 h_y(y)\right) - \left(2h_y(y) + f(y) + g_y(y)\right) \\
v_0(y) &:= \left(\delta_1 f(y) + \delta_2 h_y(y)\right)^2 + \kappa_1 f^2(y) + \kappa_2 r_y^2(y)
\end{aligned}$$

where $c_1 = k_y$, $c_2 = r_y$ and $\kappa_1, \kappa_2 > 0$, then one obtains the following lemmas.

Lemma 5.1: *(a) There exists a nonempty neighborhood $\mathcal{N}_0$ of the origin and a positive definite function $U_2 : \mathbb{R} \to \mathbb{R}$ in $\mathcal{N}_0$, such that for all nonzero $y \in \mathcal{N}_0$ and $w \in \mathbb{R}$, $U_2(y) > 0$ and*

$$\frac{\partial U_2}{\partial y}\left(2w - 2h_y(y) - f(y) - g_y(y)\right) < \rho(w, f(y), h_y(y)) \tag{5.9}$$

if and only if

$$C_1(\delta_1,\delta_2) > 0, \text{ and } C_2(\delta_1,\delta_2,\kappa_1,\kappa_2) > 0 \tag{5.10}$$

(b) Define

$$U_2(y) := -\int_0^y \frac{1}{2} v_1(\xi) d\xi \tag{5.11}$$

and

$$\mathcal{D}_y := \left\{ y \in \mathbb{R} \mid -v_1(y)y > 0 \text{ and } v_1^2(y) - 4v_0(y) > 0 \right\}. \tag{5.12}$$

If inequality (5.10) is satisfied, then there exists a nonempty neighborhood $\mathcal{N}_0$ of the origin, $\mathcal{N}_0 \subset \mathcal{D}_y \bigcup \{0\}$ such that U_2 is positive definite in $\mathcal{N}_0$ and for all nonzero $y \in \mathcal{N}_0$ and $w \in \mathbb{R}$, U_2 satisfies (5.9).

PROOF: (a) Let

$$M_1(y,w) := \frac{\partial U_2}{\partial y}\left(2w - 2h_y(y) - f(y) - g_y(y)\right) - \rho(w, f(y), h_y(y))$$

then

$$\begin{aligned} M_1(y,w) &= \tfrac{\partial U_2}{\partial y}\left(2w - 2h_y(y) - f(y) - g_y(y)\right) \\ &\quad -w^2 + 2\delta_1 w f(y) + 2\delta_2 w h_y(y) + \kappa_1 f^2(y) + \kappa_2 r_y^2(y) \\ &= -\left(w - \left(\tfrac{\partial U_2}{\partial y} + \delta_1 f(y) + \delta_2 h_y(y)\right)\right)^2 + \left(\tfrac{\partial U_2}{\partial y} + \delta_1 f(y) + \delta_2 h_y(y)\right)^2 \\ &\quad -\tfrac{\partial U_2}{\partial y}\left(2h_y(y) + f(y) + g_y(y)\right) + \kappa_1 f^2(y) + \kappa_2 r_y^2(y) \end{aligned}$$

Let

$$\begin{aligned} M_2(y) &:= \left(\tfrac{\partial U_2}{\partial y} + \delta_1 f(y) + \delta_2 h_y(y)\right)^2 \\ &\quad -\tfrac{\partial U_2}{\partial y}\left(2h_y(y) + f(y) + g_y(y)\right) + \kappa_1 f^2(y) + \kappa_2 r_y^2(y) \\ &= \left(\tfrac{\partial U_2}{\partial y}\right)^2 + v_1(y)\tfrac{\partial U_2}{\partial y} + v_0(y). \end{aligned}$$

Notice that

$$\frac{\partial}{\partial y} v_1(y)|_0 = -C_1\left(\delta_1, \delta_2\right)$$

The first order term of the Taylor expansion of $M_2(y)$ is 0. Let the second order term in the expansion be M_3 and

$$p := \tfrac{\partial^2 U_2}{\partial y^2}|_0 \qquad a_0 := \tfrac{\partial^2 v_0}{\partial y^2}|_0$$

then

$$\tfrac{1}{2} M_3 = p^2 - C_1\left(\delta_1, \delta_2\right) p + a_0,$$

where $a_0 := \left(\delta_1\sigma + \delta_2 c_2\right)^2 + \kappa_1\sigma^2 + \kappa_2 c_2^2 > 0$. Notice that

$$C_2(\delta_1, \delta_2, \kappa_1, \kappa_2) = \left(C_1\left(\delta_1, \delta_2\right)\right)^2 - 4a_0.$$

$\Rightarrow$ direction:

Assume such U_2 exists. We will show that if either $C_2 \leq 0$ or $C_1 \leq 0$ then there is no nonempty neighborhood of the origin where U_2 is positive definite and satisfies (5.9).

If $C_2(\delta_1, \delta_2, \kappa_1, \kappa_2) \leq 0$ then $M_3 \geq 0$ and in every neighborhood of the origin, there exists a $y_0 \neq 0$ such that $M_2(y_0) \geq 0$, and for $w = \left(\frac{\partial U_2}{\partial y} + \delta_1 f(y_0) + \delta_2 h_y(y_0)\right)$, $M_1 \geq 0$.

If $C_2(\delta_1, \delta_2, \kappa_1, \kappa_2) > 0$ and $C_1(\delta_1, \delta_2) \leq 0$, then the roots of $M_3 = 0$ are negative and therefore $M_3 > 0$ for all $p \geq 0$. So in every neighborhood of the origin, there exists a $y_0 \neq 0$ such that either $M_2(y_0) \geq 0 \Rightarrow M_1 \geq 0$, or $U_2(y_0) < 0$.

$\Leftarrow$ direction:

If $C_2(\delta_1, \delta_2, \kappa_1, \kappa_2) > 0$ and $C_1(\delta_1, \delta_2) > 0$. Pick U_2 such that

$$\frac{\partial^2 U_2}{\partial y^2}|_0 = \frac{1}{2} C_1(\delta_1, \delta_2).$$

Then $M_3 < 0$ and therefore there exists a neighborhood of the origin $\mathcal{N}_0$ such that for all nonzero $y \in \mathcal{N}_0$, $w \in \mathbb{R}$, $U_2(y) > 0$ and $M_2 < 0 \Rightarrow M_1 < 0$.

(b) Notice that for $y \in \mathcal{D}_y$ and $U_2(y)$ defined as in (5.11), $U_2(y) > 0$ $(-v_1(y)y > 0$) and $M_2(y) > 0$ since

$$M_2(y) = \frac{1}{4} v_1^2(y) - \frac{1}{2} v_1^2(y) + v_0(y) = -\frac{1}{4} v_1^2(y) + v_0(y).$$

But

$$\begin{aligned} -v_1(y) &= C_1(\delta_1, \delta_2)\, y^2 + O(y^3) \\ v_1^2(y) - 4v_0(y) &= C_2(\delta_1, \delta_2, \kappa_1, \kappa_2) y^2 + O(y^3) \end{aligned}$$

■

and therefore there exists nonempty neighborhood of the origin $\mathcal{N}_0 \subset \mathcal{D}_y \bigcup \{0\}$.

Lemma 5.2: *Let $U_1 : \mathbb{R}^n \to \mathbb{R}$ be a solution to the following SOS feasibility problem*

$$\begin{aligned} U_1(x) &\quad is \quad SOS \\ -\tfrac{\partial U_1}{\partial x}(F(x) + Bz) - \rho(g_n(x_n), z_1, z_2) &\quad is \quad SOS \\ C_1(\delta_1, \delta_2) &\quad is \quad SOS \\ C_2(\delta_1, \delta_2, \kappa_1, \kappa_2) &\quad is \quad SOS \\ \kappa_1, \kappa_2 &> 0. \end{aligned} \tag{5.13}$$

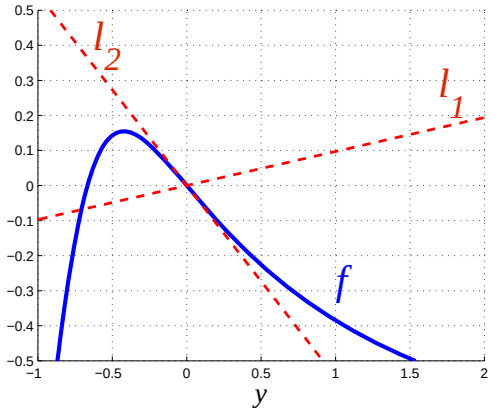

Figure 5.6: The restrictions $C_1(\delta_1, \delta_2) > 0$, $C_2(\delta_1, \delta_2, \kappa_1, \kappa_2) > 0$ imposed on the supply parameters, result in sector conditions for f in Example 5.1. In this case $\dot{U}(x, y) < 0$ for $(x, y) \in \mathbb{R}^n \times \mathcal{D}_y$ where $\mathcal{D}_y$ is the set of points y for which the graph of f lies in the area between the lines $l_1(y) = 0.0971y$ and $l_2(y) = -0.5464y$.

Then for U_2 defined as in (5.11), *D_y defined as in* (5.12)

$$U(x, y) := U_1(x) + U_2(y)$$

there exists $\beta > 0$ such that

$$\Omega_{U,\beta} = \{(x, y) \mid U(x, y) < \beta\} \subset \mathbb{R}^n \times D_y$$

is an invariant subset of the region of attraction of the origin of (5.8).

PROOF: Direct consequence of Lemma 5.1.

Remark 5.2: *Lemma 5.2 gives us a way to compute a Lyapunov function for* (5.8) *by solving* (5.13). *Since we expect $F(x)$ to be "simple", the degrees of SOS polynomial in the SOS program* (5.13) *are expected to be low, and thus computationally tractable.*

Example 5.1: *Let $n = 11$, $g_y(y) = y$, $h_y(y) = y$, $f(y) = \frac{4(y+1)}{1+3(y+1)^2} - 1$, $g_i(x_i) = 2x_i$, $h_i(x_i) = x_i$, and $d_i(x_i) = 0$. Solving* (5.13) *returns*

$$\delta_1 = 2.2046 \qquad \delta_2 = -0.6424$$
$$\kappa_1 = 7.9964 \qquad \kappa_2 = 3.6494.$$

Consequently,

$$\begin{aligned} v_1(y) &= 2\left(\delta_1 f(y) + \delta_2 h_y(y)\right) - \left(2h_y(y) + f(y) + g_y(y)\right) \\ &= 3.4093\, f(y) - 4.2848\, y, \end{aligned}$$

and

$$U_2(y) = 1.0712y^2 + 3.4093y + 3.15086 - 2.27287 \log\left(1 + 3(1+y)^2\right)$$

and $\mathcal{D}_y$ is the set of points y for which the graph of f lies in the area between the lines $l_1(y) = 0.0971y$ and $l_2(y) = -0.5464y$ (Figure 5.6), which gives $\beta = 0.7073$.

5.6 Summary

Autocatalytic metabolic pathways, such as glycolysis, provide many of the necessary intermediates used to produce organic molecules that are essential to the function of the cell. For glycolysis, as a model pathway, this means that there are less resources to produce energy (ATP) from, which effectively reduces the efficiency of the pathway (i.e., how much energy (ATP) is produced per energy invested in the autocatalytic step). This effective reduction in efficiency makes the pathway harder to control because it corresponds with the RHP zero getting smaller, and thus good performance at low frequencies gets more expensive. Additionally, glycolysis must enforce a positive return in the energy investment, i.e., for each unit of energy invested at the beginning, it must produce at least that much energy produced by the end of the pathway. The loss of the intermediates to the other pathways must be only a fraction of the available resources, otherwise excessive consumption of these intermediates causes the pathway to crash.

On the other hand, the presence of reversible reactions makes the autocatalytic pathways easier to control. They function as "release valves" by making higher stable gains available, thus providing more robustness and better achievable performance objectives.

High feedback gains can cause instability and lead to oscillation in autocatalytic

pathways with both reversible reactions and intermediate consumption. However, as in the case with no reversible reactions or consumption of intermediates, if a fixed point exists, then there are tight lower and upper bounds, respectively $\hat{h}_s$, $\hat{h}_r$, on the feedback gain $\hat{h}$ that guarantee stability for arbitrary size pathway as well as arbitrary values of both the (reversible) reaction rates and intermediate consumption rates.

Nonlinear global analysis of the model given by Equation (5.1), as before shows that allosteric feedback regulation can suppress the positive feedback generated by autocatalysis, thus guaranteeing both that the trajectories of the system are bounded, as well as the local stability of the operating fixed point. Region of attraction analysis using optimization-based formulation using Lyapunov functions and SOS programming specifically reveals that although the system is robust to perturbations in state space, its stability can be susceptible to perturbations in the parameter space.

Estimation of the region of attraction for the higher dimensional model described by equation (5.5) is a hard nonlinear problem, that is not amenable to a direct brute force application of optimization-based formulations. However the underlying structure of the system allows for compositional analysis of the system using the feedback interconnection of two systems and local dissipation inequalities, similar to the framework developed in Chapter 4. We use a simple decomposition to show that for a subset of the models we can find Lyapunov functions by solving a computationally tractable SOS feasibility problem.

Chapter 6

Conclusions

6.1 Summary

Stability of the Glycolytic Pathway Glycolysis is a prime example of an autocatalytic metabolic network (pathway). The task of the control system in glycolysis is to maintain the pathway close to its standard biological fixed point where the cell operates in the presence of disturbances and plant uncertainty. A simple 2D model described by Equation (3.1) captures the essential dynamics of the glycolytic pathway. This model reveals that the existence of a right half-plane (RHP) zero, which is a result of the structure of autocatalysis and controls in the pathway, is at the core of many of the limitations that constrain pathway performance. This RHP zero is responsible for the existence of a conservation law, which is mathematically described by a special form of the Bode Sensitivity Integral (Equation(2.9)). It is hypothesized that oscillations in glycolysis might be a result of tradeoffs that stem from this conservation law. For example, the control mechanism might operate in a regime where the pathway has close to optimal performance for the common operating conditions described by a safe set in parameter space. However, this might put the controller gain close to a set in parameter space, for which the control is too aggressive. The plant normally avoids the unsafe set, except for a few rare events. In those rare events, instabilities are exhibited in the form of oscillations in ATP concentration. This proximity to the unsafe set for high performance feedback gains is unavoidable and a consequence of the aforementioned conservation law that arises

from the structure of the autocatalytic pathways.

The 2D model described by Equation (3.1) suggests that there are two basic mechanisms that can cause glycolysis to crash (i.e., ATP concentration approach zero); failure of transcriptional regulation or overly aggressive allosteric regulation. The first scenario occurs when the slow transcriptional regulation fails to prevent the system from going into a(n) (invariant) regime where the consumption of ATP is faster than its production. This can be caused by a sudden drop in the input to the system (glucose) or an increase in ATP demand. Either condition causes the system to deplete all of its ATP reserves, which results in all of the concentrations going to zero and thus cell death. The overly aggressive fast allosteric feedback condition can be caused by drops in the catalyzing enzyme concentrations. Most of the time aggressive feedback leads to oscillations in ATP concentration. However, under certain circumstances, if the drops in enzyme concentrations are too severe, the magnitude of oscillations increases to the point that a homoclinic bifurcation occurs causing the pathway to crash.

Simulations of the system (3.1) show that the region of attraction of the fixed point where the cell operates is large. This means glycolysis as modeled by (3.1) is not sensitive to perturbations in the concentration of the reactants. In fact, the analysis of the glycolysis model confirms that oscillations and crashes in glycolysis are not caused by perturbations in state space (i.e., perturbations in the concentrations of the products and reactants), but rather perturbations in the parameter space (i.e., catalytic enzyme concentrations, precursors to the pathway, ATP demand, or temperature) as observed in the literature [14, 6, 24, 31, 33, 38].

Stability and Performance of Autocatalytic Pathways Autocatalytic networks (pathways) are hard to control because of inherent instabilities and limitations imposed on their performance by the structure of autocatalysis. Performance of an autocatalytic pathway is defined as the ability of the control mechanisms to maintain the pathway close to its standard biological operating point in the presence of disturbances and plant uncertainty. These metabolic pathways are composed of large chains

of both irreversible and reversible reactions, that interact with other components in the cell. In fact, they are an integral part of the whole cell activity and are coupled with other networks through the exchange of products and sharing of components, as many of their intermediate products are used by other processes in the cell. We analyze these autocatalytic metabolic networks (pathways) using the different models described by Equations (5.1), (4.1) and (5.5) that incorporate multiple intermediate reactions (Equations (4.1) and (5.5)), and reversible reactions and consumption of the intermediate metabolites (Equations (5.1) and (5.5)).

Output feedback regulation of autocatalytic pathways can suppress the positive feedback generated by autocatalysis, thus guaranteeing both that the trajectories of the system remain bounded, as well as the local stability of the operating fixed point. However the structure of autocatalysis limits the range of stable feedback gains $\hat{h}$, because the product of the pathway both controls and is consumed by the first reaction. A direct application of a secant condition [2, 39, 43] to the n-dimensional model described by (4.1) (no reversible reactions and no consumption of intermediates) gives an upper bound $\hat{h}_d(n)$ on the feedback gains $\hat{h}$, that result in stability of pathways of fixed size (n) and arbitrary (fixed) intermediate reaction rates. The bound $\hat{h}_d(n)$ suggests that the range of available stable gains gets smaller as the pathway size (n) increases. On the other hand, consumption of intermediate metabolites and the presence of reversible reactions increases the range of stable gains. For the more general model described by (5.5) there are tight lower and upper bounds, respectively $\hat{h}_s$, $\hat{h}_r$, on the feedback gain $\hat{h}$ that guarantee stability for arbitrary pathway size as well as arbitrary values of both the (reversible) reaction rates and the intermediate consumption rates. These bounds are tight in the sense that unstable pathways can be constructed for gains that lie outside the ranges established by these bounds.

Similar to the 2D model of glycolysis described by Equation (3.1), the existence of a RHP zero z is at the core of many of the limitations imposed on the performance of these pathways. The special form of the Bode Sensitivity Integral (Equation(2.9)) imposes hard limits on the sensitivity function S, requiring the conservation of the area under the curve of the "weighted" $\log|S|$. S is closely related to many perfor-

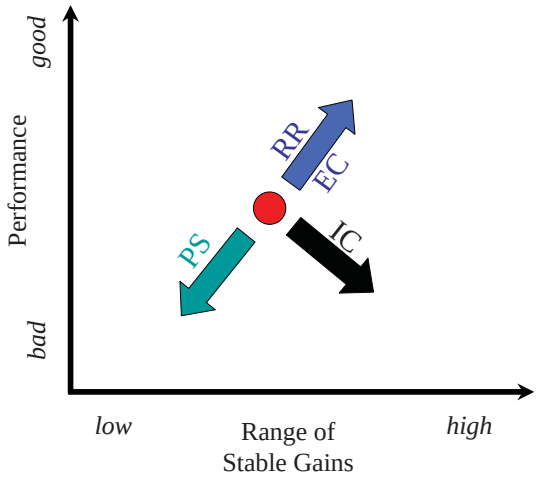

Figure 6.1: The effect of increases in enzyme concentrations (EC), pathways size (PS), intermediate consumptions (IC), and reversible reactions (RR) on the performance and range of stable feedback gains.

mance objectives, since it measures the sensitivity to a large class of disturbances. The weight on S in Equation (2.9) depends on the magnitude of z and emphasizes the frequencies smaller than z, thus making better performance (small S) at low frequencies more expensive (i.e., large S) in higher frequency ranges.

High concentration of catalyzing enzymes leads to an increase in the rates of the intermediate reactions, which makes the pathway more stable (i.e., there is a larger range of stable gains available) and increase the magnitude of z (i.e., "softens" the hard limits on performance).

Pathway size has the opposite effect of increasing the enzyme concentrations on pathway performance. An increase in the size of the chain of enzymatically catalyzed intermediate reactions in the autocatalytic pathways causes two adverse effects on performance: good performance at low frequencies gets more expensive (i.e., z becomes smaller) and the range of available stable gains is reduced which makes the operating gains less robust and reduces the achievable performance objectives.

Consumption of intermediates in autocatalytic metabolic pathways results in less resources available to convert to the product of the pathway, which effectively reduces the efficiency of the pathway. This effective reduction in efficiency makes the pathway harder to control because it again corresponds to the RHP zero(s) getting smaller, and

thus good performance at low frequencies gets more expensive. Another constraint on these pathways is that the loss of the intermediates to the other pathways must be only a fraction of the available resources because excessive consumption of these intermediates causes the pathway to crash.

On the other hand, the presence of reversible reactions makes the autocatalytic pathways easier to control, as they function as "release valves" by making higher stable gains available, thus providing more robustness and better achievable performance objectives. Figure 6.1 shows a summary of the role of concentration of catalyzing enzymes, pathway size, consumption of intermediate metabolites, and reversible reactions in determining the stability and performance of the pathway.

Nonlinear Analysis and Region of Attraction Estimations If the dynamics of the systems given by (3.1),(5.1), (4.1) and (5.5) are rational functions of the state, then the size of the region of attraction of the fixed point can be estimated by optimization-based formulations using Lyapunov functions and SOS programming. These formulations reveal that low degree polynomial Lyapunov functions can verify region of attraction related properties for a wide range of parameters. For example extensive experiments run on 2D, 3D and 4D systems reveal that systems whose operating point is robustly stable with respect to perturbations in parameter values are simple to verify, i.e., a second degree polynomial Lyapunov function verifies large invariant subsets of the region of attraction of the fixed point. In fact, polynomial Lyapunov functions of degree larger than 2 are only necessary for systems whose parameter values fall close to the stability boundary in the parameter space. These points are clearly not robust as small changes in parameters may result in the instability of the fixed point. Computing and characterizing the invariant subsets of region of attraction for larger pathways is not possible because the degree of the polynomials in the corresponding SOS program is high (even when searching for quadratic polynomial Lyapunov functions) and the problem becomes computationally intractable.

The underlying structure of the system (4.1) allows for compositional analysis of the system using the feedback interconnection of two systems and local dissipation

inequalities. The system given by (4.1) is represented as the feedback interconnection of an n_1-state system S_1 given by (4.32) and an n_2-state system S_2 given by (4.33), with n_1 generally (much) bigger than n_2. If the vector field of system (4.1) is rational we can construct Lyapunov functions using local dissipation inequalities and solving the corresponding SOS problems (4.37) and (4.38). The first SOS problem (4.37) contains low degree ($2\alpha_1$) polynomials in many (n_1) variables, and the second one contains high degree ($2\alpha_2$) polynomials in a few (n_2) variables. As the size (n_2) of system S_2 increases, so does the computational complexity of constructing a Lyapunov function. However if computing resources are available, (n_1, n_2)-decompositions with the larger n_2 can be used to construct Lyapunov function for realizations of (4.1) with higher the gains. Notably, the $(n, 1)$-decomposition specifically allows us to analytically construct diagonal Lyapunov functions for system with feedback gain less than $\hat{h}_d(n)$.

The structure of the system described by Equation (5.5) similarly allows for compositional analysis of (5.5) using the feedback interconnection of two systems and local dissipation inequalities. We use a simple $(n, 1)$-decomposition to show that for a subset of the models we can find Lyapunov functions by solving a computationally tractable SOS feasibility problem. Figure 6.2a shows a summary of the role of concentration of catalyzing enzymes, pathway size, consumption of intermediate metabolites, and reversible reactions in determining the computational complexity of the pathway and how they each relate to performance.

Tradeoffs The investigation of the autocatalytic pathways reveals a few fundamental performance tradeoffs which can be classified in the following manner.

- Overall cell energy efficiency vs. performance. Performance and stability of the pathway improves with increases in the catalyzing enzyme concentrations (i.e., faster reaction rates). However maintaining high enzyme concentrations in the cell is energetically wasteful.

- Multi-purposeness of the pathway vs. performance. Autocatalytic pathways

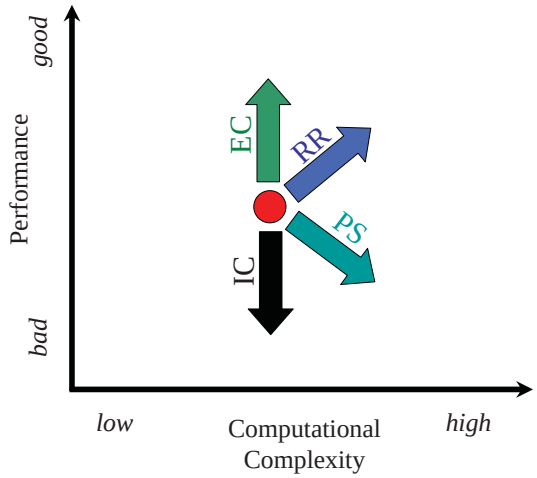

Figure 6.2: The effect of increases in enzyme concentrations (EC), pathways size (PS), intermediate consumptions (IC), and reversible reactions (RR) on the performance and computational complexity of the pathways.

provide many of their intermediate products to other processes in the cell. These intermediates are essential to the cell, however their consumption reduces the efficiency of the pathway which causes its performance to suffer.

- Robustness vs. performance. Higher feedback gains generally lead to better performance at the low frequencies, but this makes the operating point less robust because these high gains could be close to the stability boundary. In this case a change in the nominal parameter values (for example a drop in the catalyzing enzyme concentrations) could lead to oscillations in the ATP concentration and instability of the operating point.

- Evolvability vs. performance. For feedback gains smaller than $\hat{h}_r$, the pathway is robustly stable with respect to the insertion or removal of intermediate reactions. However the pathway sacrifices performance by using smaller gains to have this additional flexibility.

- Computational complexity vs. performance. Higher feedback gains (i.e., better performance) make the system harder to analyze. Specifically, as discussed in the previous paragraph, in order to construct Lyapunov functions for realizations with high gains we need to use we need to use (n_1, n_2)-decomposition with

the large n_2. However as the n_2 increases, so does the computational complexity of the corresponding SOS problem.

Complexity and Robustness We define the complexity of a realization of model (3.1) by the complexity of the vector field in the neighborhood of the operating equilibrium point. We then develop two related approaches to quantify this view; the smallest order polynomial Lyapunov function needed to verify a specific set as an invariant subset of the region of attraction, or the size of the region of attraction verified by a specific order polynomial Lyapunov function. To evaluate the complexity of system realizations we compare realizations that are "topologically equivalent", i.e. realizations that have the same number and location of fixed points and the same size region of attraction. This framework in 2, 3, and 4D reveals that robust systems (systems whose parameter values are in the middle of the stability region) have simple proofs (i.e. second degree polynomial can verify large invariant subsets of region of attraction). In higher dimensions, using (n_1, n_2)-decompositions, we again observe that realizations that are more (computationally) complex can only arise from those realizations with high gains (i.e., gains that are close to the stability boundary, and therefore fragile to perturbations in parameter space). This is derived from the fact that (n_1, n_2)-decompositions with large n_2 are necessary only for gains that are close to the instability boundary (Table 2.1).

6.2 Future Research Directions

The work done up to this point covers networks that contain one autocatalytic loop. This topology is applicable to many glycolysis models that "lump" the two ATP autocatalytic loops of glycolysis into a single one. It would be of interest to investigate more general networks composed of multiple autocatalytic loops. These pathways could be controlled by allosteric feedback at different points in the pathway. A first step toward such pathways would be the study of the network shown in Figure 6.3. This network better captures the topology of the real glycolysis pathway, as it models

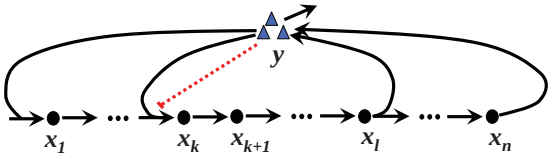

Figure 6.3: Pathway with two autocatalytic loops.

the two ATP autocatalytic loops explicitly. Even though the presence of these loops breaks down some of the nice structure of the networks discussed so far, enough special structure remains that the results of this thesis might generalize for these networks.

Another direction of research is to determine where in parameter space the real biology lies. Applying tools from areas such as optimal control, one can determine the optimal parameter value for specific performance measures. Alternately, by using parameter values obtained experimentally one can determine the performance measures that are being optimized.

Many methods proposed in this thesis, such as the decomposition and the construction of Lyapunov functions, are quite general and can be applied to many other biological networks that exhibit similar structure. More generally one can investigate if the various tradeoffs and results in this thesis are generalizable to other classes of biological networks.

Bibliography

[1] B. Alberts, A. Johnson, J. Lewis, M. Raff, K. Roberts, and P. Walter. *Molecular Biology of the Cell, Fourth Edition*. Garland, 2002.

[2] M. Arcak and E. D. Sontag. Diagonal stability of a class of cyclic systems and its connection with the secant criterion. *Automatica*, 42(9):1531–1537, 2006.

[3] M. Arcak and E. D. Sontag. A passivity-based stability criterion for a class of biochemical reaction networks. *Mathematical Biosciences and Engineering*, 5(1):1–19, 2008.

[4] M. Banuelos, C. Gancedo, and J. M. Gancedo. Activation by phosphate of yeast phosphofructokinase. *Journal of Biological Chemistry*, 252(18):6394–6398, 1977.

[5] A. Ben-Tal and A. Nemirovski. *Lectures on Modern Convex Optimization: Analysis, Algorithms, and Engineering Applications*. MPS-SIAM Series on Optimization, 2001.

[6] M. Bier, B. Teusink, B. N. Kholodenko, and H. V. Westerhoff. Control analysis of glycolytic oscillations. *Biophysical Chemistry*, 62(1-3):15–24, Nov 1996.

[7] S. Boyd and L. Vandenberghe. *Convex Optimization*. Cambridge Univ. Press, 2004.

[8] F.A. Chandra, G. Buzi, and J.C. Doyle. Linear control analysis of the autocatalytic glycolysis system. In *American Control Conference*, pages 319–324, June 2009.

[9] S. Danø, M. F. Madsen, H. Schmidt, and G. Cedersund. Reduction of a biochemical model with preservation of its basic dynamic properties. *FEBS Journal*, 273(21), 2006.

[10] J. Doyle, B. Francis, and A. Tannenbaum. *Feedback Control Theory*. Macmillan Publishing Co, 1990.

[11] M. Feinberg. Chemical reaction network structure and the stability of complex isothermal reactors: II multiple steady states for networks of deficiency one. *Chemical Engineering Science*, (43):1–25, 1988.

[12] M. Feinberg. The existence and uniqueness of steady states for a class of chemical reaction networks. *Archive for Rational Mechanics Analysis*, (132):311–370, 1995.

[13] A. Goldbeter. *Biochemical Oscillations and Cellular Rhythms*. Cambridge University Press, Cambridge, 1996.

[14] B. Hess and A. Boiteux. Substrate control of glycolytic oscillations. In B. Chance, E. K. Pye, A. A.K. Ghosh, and B. Hess, editors, *Biological and Biochemical Oscillators*, pages 229–241. Academic Press, 1973.

[15] D. Hinrichsen and A. J. Pritchard. *Mathematical Systems Theory I*. Springer-Verlag Berlin, 2005.

[16] F. Horn and R. Jackson. General mass action kinetics. *Arch. Rational Mech. Anal*, 47(2):81–116, 1972.

[17] R. A. Horn and C. R. Johnson. *Matrix Analysis*. Cambridge University Press, February 1990.

[18] F. Hynne, S. Danø, and P. G. Sørensen. Full-scale model of glycolysis in saccharomyces cerevisiae. *Biophysical Chemistry*, 94(1-2):121 – 163, 2001.

[19] J. A. Imlay. Pathways of oxidative damage. *Annual Review of Microbiology*, 57(1):395–418, 2003.

[20] R. E. Kalman and J. E. Bertram. Control system analysis and design via the "second method" of lyapunov: Parts I and II. *Journal of Basic Engineering*, 82:371–400, 1960.

[21] H. K. Khalil. *Nonlinear Systems*. Prentice Hall, 3^{rd} edition, 2002.

[22] P. De Leenheer, D. Angeli, and E. D. Sontag. Monotone chemical reaction networks. *Journal of Mathematical Chemistry*, 41(3):295–314, April 2007.

[23] J. Lofberg. Yalmip : A toolbox for modeling and optimization in MATLAB. In *Proceedings of the CACSD Conference*, Taipei, Taiwan, 2004.

[24] K. Nielsen, P. G. Sorensen, F. Hynne, and H. G. Busse. Sustained oscillations in glycolysis: an experimental and theoretical study of chaotic and complex periodic behavior and quenching of simple oscillations. *Biophysical Chemistry*, 72:49–62, 1998.

[25] B. O'Rourke, B. Ramza, and E. Marban. Oscillations of membrane current and excitability driven by metabolic oscillations in heart cells. *Science*, 265(5174):962–966, 1994.

[26] A. Papachristodoulou. *Scalable analysis of nonlinear systems using convex optimization*. Ph.D. dissertation, Caltech, January 2005.

[27] P. A. Parrilo. *Structured semidefinite programs and semialgebraic geometry methods in robustness and optimization*. Ph.D. dissertation, California Institute of Technology, May 2000.

[28] P. A. Parrilo. Semidefinite programming relaxations for semialgebraic problems. *Mathematical Programming Series B*, 96(2):293–320, 2003.

[29] J. R. Pomerening, S. Y. Kim, and J. E. Ferrell. Systems-level dissection of the cell-cycle oscillator: bypassing positive feedback produces damped oscillations. *Cell*, 122(4):565–578, August 2005.

[30] S. Prajna, A. Papachristodoulou, P. Seiler, and P. A. Parrilo. *SOSTOOLS: Sum of squares optimization toolbox for MATLAB*, 2004.

[31] P. Richard. The rhythm of yeast. *FEMS Microbiology Reviews*, 27:547–557, 2003.

[32] P. H. Richter and J. Ross. Concentration oscillations and efficiency: glycolysis. *Science*, 211(4483):715–717, 1981.

[33] P. Ruoff, M. Christensen, J. Wolf, and R. Heinrich. Temperature dependency and temperature compensation in a model of yeast glycolytic oscillations. *Biophysical Chemistry*, 106:179–192, 2003.

[34] P. Seiler. *Multipoly and SOSOpt: Matlab packages to represent multivariate polynomials and for sum-of-squares optimization.* available at http://jagger.me.berkeley.edu/software/acc09/.

[35] E. E. Selk̀ov. Stabilization of energy charge, generation of oscillations and multiple steady states in energy metabolism as a result of purely stoichiometric regulation. *European Journal of Biochemistry*, 59(1):151–157, 1975.

[36] E. D. Sontag. Monotone and near-monotone biochemical networks. *Systems Synthetic Biology*, 1(2):59–87, Apr 2007.

[37] J. F. Sturm. Using SeDuMi 1.02, a MATLAB toolbox for optimization over symmetric cones. *Optimization Methods and Software*, 11–12:625–653, 1999. Available at `http://sedumi.mcmaster.ca/`.

[38] B. Teusink, B. M. Bakker, and H. V. Westerhoff. Control of frequency and amplitudes is shared by all enzymes in three models for yeast glycolytic oscillations. *Biochimica et Biophysica Acta*, 1275(3):204–212, Jul 1996.

[39] C. D. Thron. The secant condition for instability in biochemical feedback control – Parts I and II. *Bulletin of Mathematical Biology*, 53:383–424, 1991.

[40] U. Topcu. *Quantitative local analysis of nonlinear systems*. Ph.D. dissertation, UC, Berkeley, 2008. available at `http://jagger.me.berkeley.edu/~utopcu/dissertation`.

[41] U. Topcu, A. Packard, and P. Seiler. Local stability analysis using simulations and sum-of-squares programming. *Automatica*, 44:2669 – 2675, 2008.

[42] U. Topcu, A. Packard, P. Seiler, and G. Balas. Stability region estimation for systems with unmodeled dynamics. In *Proceedings of the European Control Conference*, 2009.

[43] J. J. Tyson and H. G. Othmer. The dynamics of feedback control circuits in biochemical pathways. In R. Rosen and F. M. Snell, editors, *Progress in Theoretical Biology*, volume 5, pages 1–62. Academic Press, New York, NY, USA, 1978.

[44] M. Vidyasagar. *Nonlinear Systems Analysis*. Prentice Hall, 2^{nd} edition, 1993.

[45] L. Wang and E. D. Sontag. Singularly perturbed monotone systems and an application to double phosphorylation cycles. *Journal of Nonlinear Science*, 18(5):527–550, October 2008.

[46] J. C. Willems. Dissipative dynamical systems I: General theory. *Archive for Rational Mechanics and Analysis*, 45:321–343, 1972.

[47] J. Wolf, J. Passarge, O. J. G. Somsen, J. L. Snoep, R. Heinrich, and H. V. Westerhoff. Transduction of intracellular and intercellular dynamics in yeast glycolytic oscillations. *Biophysical Journal*, 78(3):1145 – 1153, 2000.